Jagiellonian University

Doctoral Thesis

Determining topological order with tensor networks

Author:
Anna Francuz

Supervisor:
Prof. Jacek Dziarmaga

A thesis submitted in fulfilment of the requirements for the degree of Doctor of Philosophy

in the

Quantum Many Body Theory Group
Institute of Theoretical Physics

Kraków, November 2021

2:9787526056

Wydział Fizyki, Astronomii i Informatyki Stosowanej
Uniwerystetu Jagiellońskiego

Oświadczenie

Ja, niżej podpisana, Anna Francuz, (nr indeksu: 1090316), doktorantka Wydziału Fizyki, Astronomii i Informatyki Stosowanej Uniwersytetu Jagiellońskiego oświadczam, że przedłożona przeze mnie rozprawa doktorska pt. "Determining topological order with tensor networks" jest oryginalna i przedstawia wyniki badań wykonanych przeze mnie osobiście, pod kierunkiem prof. dra hab. Jacka Dziarmagi. Pracę napisałam samodzielnie.

Oświadczam, że moja rozprawa doktorska została opracowana zgodnie z Ustawą o prawie autorskim i prawach pokrewnych z dnia 4 lutego 1994 r. (Dziennik Ustaw 1994 nr 24 poz. 83 wraz z późniejszymi zmianami).

Jestem świadoma, że niezgodność niniejszego oświadczenia z prawdą ujawniona w dowolnym czasie, niezależnie od skutków prawnych wynikających z ww. ustawy, może spowodować unieważnienie stopnia nabytego na podstawie tej rozprawy.

Kraków, ...
(data) (podpis doktorantki)

JAGIELLONIAN UNIVERSITY

Abstract

Faculty of Physics
Institute of Theoretical Physics

Doctor of Philosophy

Determining topological order with tensor networks

by Anna Francuz

Exotic phases of matter, which fall beyond the Landau paradigm of phases and phase transitions, emerged as one of the main directions of research in the field of condensed matter physics in the last few decades. This lead to both advancement in their experimental realizations and progress in their analysis, thanks to powerful numerical methods like tensor networks. Among those exotic phases there are topologically ordered phases, the analysis of which is especially hard due to degeneracy of the ground state and no local order parameter. Topological order gained recognition after it was realized, thanks to Alexei Kitaev, that quantum computational models can be written in the language of condensed matter systems. However, apart from few exactly solvable models, the analysis of lattice Hamiltonians for the occurrence of topological order was considered a very hard problem.

This thesis provides a basic overview of theories aiming at classifying topologically ordered states and novel numerical approaches to determine both Abelian and non-Abelian topological order starting from a lattice Hamiltonian. The numerical method of choice in the study of strongly correlated two-dimensional systems, like topologically ordered systems, is projected entangled pair states (PEPS), as it allows analysing states which were not achievable by the state-of-the-art 2D DMRG algorithms due to long correlation length.

In this thesis, numerical methods of analysing the optimized infinite PEPS (iPEPS) are presented, allowing to extract the information about the topological order. The key idea is to find the infinite matrix product operator (iMPO) symmetries of the iPEPS, whose existence is a necessary condition for the TN state to exhibit topological order. The iMPO symmetries can be later used to obtain topological S and T matrices, which (in most known cases) can be considered as a non-local order parameter of topologically ordered phases, in the sense that they give us unambiguous information about the model along with its excitations and their statistics. The method is immune to any small perturbations of the tensors, which had been a long feared problem due to numerical inaccuracies which may arise during the ground state optimization. Furthermore, finding iMPO symmetries enables an elegant description of the model in terms of the mathematical structure underlying the topologically ordered phases of matter – modular tensor category.

Acknowledgements

First and foremost, I would like to express my deepest gratitude to my supervisor Prof. Jacek Dziarmaga for his guidance, patience during many long discussions, as well as joint winter expeditions to four-thousanders and other trips. I am very thankful for introducing me to the scientific world, both pioneering research and the possibility to meet world-renowned physicists. I am greatly indebted also to Dr Łukasz Cincio, for his help with my first steps in the field of topological order and tensor networks. Many thanks to my colleagues from the department, Aritra Sinha, Gabriela Wójtowicz and Anna Dziubyna, for interesting discussions during our meetings and to Dr Marek Rams and Dr Piotr Czarnik, whom I could always turn to with my questions.

I would also like to thank Prof. Frank Verstraete for his ideas and the possibility to visit his group in Ghent, which resulted in one of the articles published together. I am very grateful to Laurens Lootens for sharing his in-depth knowledge of the mathematical structures behind topological order, and to Dr Bram Vanhecke for explaining to me the VUMPS algorithm.

Finally, nothing would be possible without the support of my family, especially towards the completion of this thesis. I am very grateful to my parents, who were my first teachers and supported me in every part and aspect of my life. Last, but not least, I would like to thank my dearest husband, Dániel Németh, for his patience and constant support, for believing in me, listening to my talks before every conference and reading this thesis.

This research was supported by the Polish Ministry of Science and Education under Grant No. DI2015 021345 and by Narodowe Centrum Nauki (NCN) under Grants No. 2016/23/B/ST3/00830 and No. 2019/35/B/ST3/01028 and Etiuda Grant No. 2020/36/T/ST3/00451.

Contents

Oświadczenie **iii**

Abstract **v**

Acknowledgements **vii**

1 Introduction **1**

2 Topological order **3**
2.1 Long range entanglement 4
2.2 Quantum statistics 5
2.3 String-nets and fusion category 10

3 Tensor networks **15**
3.1 Variational ansatz 15
3.2 Algorithms 22
3.3 Entanglement 26
3.4 Gauge transformations and symmetries 30
3.5 Topological order with tensor networks 34

4 Articles **39**

10:1038458673

List of Abbreviations

CFT	**C**onformal **F**ield **T**heory
CP	**C**ompletely **P**ositive
DMRG	**D**ensity **M**atrix **R**enormalization **G**roup
iDMRG	**i**nfinite **D**ensity **M**atrix **R**enormalization **G**roup
iMPS	**i**nfinite **M**atrix **P**roduct **S**tate
iPEPS	**i**nfinite **P**rojected **E**ntangled **P**air **S**tates
LU	**L**ocal **U**nitary
MERA	**M**ultiscale **E**ntanglement **R**enormalization **A**nsatz
MES	**M**inimally **E**ntangled **S**tates
MPO	**M**atrix **P**roduct **O**perator
MPS	**M**atrix **P**roduct **S**tate
NN	**N**earest **N**eighbour
PEPS	**P**rojected **E**ntangled **P**air **S**tates
RG	**R**enormalization **G**roup
QMC	**Q**uantum **M**onte **C**arlo
QSL	**Q**uantum **S**pin **L**iquid
SL	**S**pin **L**iquid
SPT	**S**ymmetry **P**rotected **T**opological
TEE	**T**opological **E**ntanglement **E**ntropy
TM	**T**ransfer **M**atrix
TN	**T**ensor **N**etworks
TO	**T**opological **O**rder
VUMPS	**V**ariational **U**niform **M**atrix **P**roduct **S**tate

To my daughter, Eszter...

Chapter 1

Introduction

One of the most successful theories in classifying different gapped phases used to be Landau-Ginzburg theory [4, 5] of symmetry breaking, according to which all condensed matter systems could be classified by a pair of groups $(G_H,\ G_{gs})$ describing the symmetry of the Hamiltonian – G_H and the symmetry of the ground state – G_{gs}, with $G_{gs} \subseteq G_H$. In particular, for symmetry breaking phases $G_{gs} \subset G_H$. Despite its success it failed to describe many new exotic phases of matter which appeared in the experiments starting from prominent example of Fractional Quantum Hall Effect[6], for which a 1998 Nobel Prize in Physics was awarded (to Robert B. Laughlin, Horst L. Störmer and Daniel C. Tsui "for their discovery of a new form of quantum fluid with fractionally charged excitations") [7], and finishing with recent observations of quantized thermal Hall conductance in $\alpha-RuCl_3$[8]. It turns out that those exotic phases of matter fall beyond the Landau paradigm and also exhibit some kind of order, which is not a symmetry-breaking order but a topological order.

Topological order proved to be very elusive, both from the perspective of theoretical description and from the experiments. Gapped, as well as, gapless phases without any sign of long-range order were therefore put into one box with label – *spin liquids* (SL). Quantum spin liquids (QSL) are very highly entangled ground states, where strong quantum fluctuations prevent ordering at low or at zero temperature [9]. This definition is still very evasive, because it tries to capture extremely many of those exotic phases of matter, a set, which is much more rich in different structures than the symmetry breaking phases. The formal description of topological order can be grasped by fusion theory and category theory [10]. The only numerical methods capable of providing such description seems to be tensor networks, due to their ability to encode long-range entanglement and a very specific construction, which enables access to these entanglement properties directly, at the level of virtual degrees of freedom of tensor networks. Therefore, they are the methods of choice in the study of topological order.

The thesis is based on three articles:

- [1] *Determining topological order from infinite projected entangled pair states*,
  Anna Francuz, Jacek Dziarmaga, Guifre Vidal, and Lukasz Cincio,
  Phys. Rev. B **101**, 041108(R)

- [2] *Determining non-Abelian topological order from infinite projected entangled pair states*,
  Anna Francuz and Jacek Dziarmaga, Phys. Rev. B **102**, 235112

- [3] *Variational methods for characterizing matrix product operator symmetries*,
  Anna Francuz, Laurens Lootens, Frank Verstraete, Jacek Dziarmaga, accepted for publication in Phys. Rev. B

In the articles, we propose a numerical method for analysing topologically ordered states, which are beyond the standard description in terms of local order parameter and symmetry breaking. Therefore, Chapters 2 and 3 constitute an introduction into the topics

covered in the articles. Chapter 2 approaches the theory of topological order and classification of topologically ordered phases, which cannot be captured by the Landau paradigm of phases and phase transitions. Finally, Chapter 3 introduces the numerical methods – tensor networks used in the articles. The use of tensor networks has grown extensively in the last two decades and finds applications in the fields ranging from condensed matter systems to neural networks and AdS/CFT correspondence. However, this introduction is focused primarily on those aspects of tensor networks that are related to strongly correlated systems in two spatial dimensions exhibiting topological order and underlines the importance of entanglement degrees of freedom, in contrast to physical degrees of freedom, in the description of these exotic phases of matter.

Chapter 2

Topological order

Topological order is a phase of matter beyond the Landau paradigm of phases and phase transitions. While the Landau description captures extremely well many short-range entangled states, which are related via local unitary transformations to product states (see Sec. 2.1), topologically ordered states are described by different types of long range entanglement. The following summarizes the known characteristic features of 2D topologically ordered phases:

- they belong to the class of insulators – there is an energy gap between the subspace of degenerate ground states and excited states – Fig. 2.1(A),
- they are characterized by different patterns of long range entanglement – Fig. 2.1(B),
- there is a ground state degeneracy, which depends on the genus of the manifold, on which the system is defined, and no local order parameter exists, that could distinguish between different (orthogonal) degenerate ground states – Fig. 2.1(C),
- an amazing feature of some systems is the emergence of elementary quasiparticle excitations with fractional statistics – anyons.

To be precise, anyons appear in non-invertible topological orders[11], which are of the focus in this thesis. Among non-invertible topological orders we also distinguish non-chiral topological orders, when both the bulk and the boundary are insulating, and the chiral ones, characterized by the gap in the bulk and gapless chiral edge modes. In general, two same chiral TO, but with opposite chiralities, produce a non-chiral TO when stacked together. Last but not least, among all non-chiral topological orders, there still exist many distinct ones. Thus, a new way of classifying different phases of matter is needed that would grasp all these new kinds of phases and assign some universal labels to topological

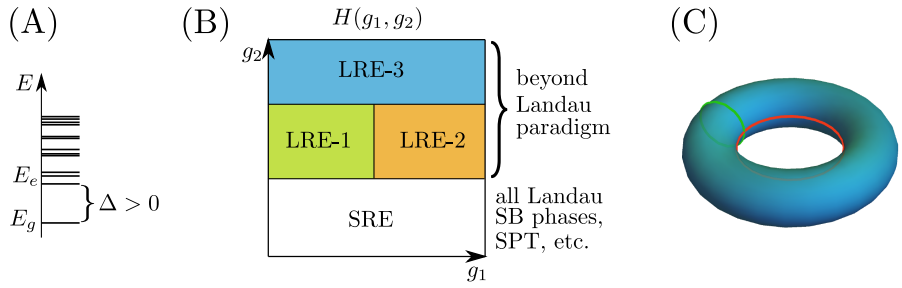

FIGURE 2.1: The known characteristic features of 2D topologically ordered states are: (A) gap between ground states and excited states, they are insulating, (B) long range entanglement, (C) topological ground state degeneracy, that depends on the topology of the manifold the system is defined on.

orders within the same universality class. There were a few attempts to achieve that goal, including:

- topological S and T matrices encoding mutual and self-statistics of the emergent anyons,
- F-symbols defining a fusion category – a mathematical structure underlying topologically ordered phases analogous to symmetry group for symmetry breaking phases.

Both approaches have its advantages and short-comings, and they are more broadly discussed in the Sec. 2.2 and Sec. 2.3 respectively. It should be noted at this point that from F-symbols one can obtain unique topological S and T matrices, while the other way round it is not always the case, which we also elaborate more later in this chapter.

2.1 Long range entanglement

Among the gapped phases of matter all ground states described by Landau symmetry breaking are actually short range entangled, while topologically non-trivial phases are characterized by long range entanglement, a term introduced by Xiao Gang Wen in Ref.[12]. Moreover, among the so-called topological phases of matter, many of them are actually topologically trivial in a sense of being short range entangled, with the best example of the SPT - symmetry protected topological phases, where the slightest symmetry-breaking perturbation already destroys the protected edge modes[13]. Therefore, the distinguishing factor of the topological order is long range entanglement and different topological orders posses different pattern of long range entanglement. In order to define those entanglement patterns let us first divide gapped quantum phases of matter into distinct universality classes (see Fig 2.1(B)), hence below we present several definitions of this equivalence relations [12].

Definition 2.1.1. Let $H(g)$ be a Hamiltonian of a local quantum system with smooth dependence on the parameter $g \in [0,1]$ with gapped ground states $|\psi(0)\rangle$ and $|\psi(1)\rangle$ at $H(0)$ and $H(1)$ respectively. If there exist such a smooth path $H(g)$ (family of Hamiltonians) that $H(g)$ is gapped[1] for all g then there is no phase transition along $0 \leq g \leq 1$ and two states belong to the same phase.

With the paradigmatic example of the transverse-field Ising model:

$$H = -J \sum_{<ij>} \sigma_i^z \sigma_j^z - g \sum_i \sigma_i^x, \tag{2.1}$$

it can be realized that ground states of the Hamiltonian at both limits $J \gg g$ and $J \ll g$ are adiabatically connected, without undergoing a phase transition, to the gapped ground states at $g = 0$ and $J = 0$ respectively. In both limits $g = 0$ and $J = 0$ the ground states are exact product states: $|\psi(g = 0)\rangle = \otimes_i |\uparrow\rangle_i$ or $|\psi(g = 0)\rangle = \otimes_i |\downarrow\rangle_i$ and $|\psi(J = 0)\rangle = \otimes_i (|\uparrow\rangle_i + |\downarrow\rangle_i) \propto \otimes_i |+\rangle_i$, where $|\uparrow\rangle$, $|\downarrow\rangle$ are the σ^z eigenstates and $|+\rangle$ is the σ^x eigenstate to eigenvalue $+1$, hence they are short range entangled.

However, in general, finding a path along which there is no phase transition is not a computationally feasible task, therefore the next two definitions provide more insight from the computational point of view.

[1] The energy gap in context of phase transitions is defined in the limit of infinite system size.

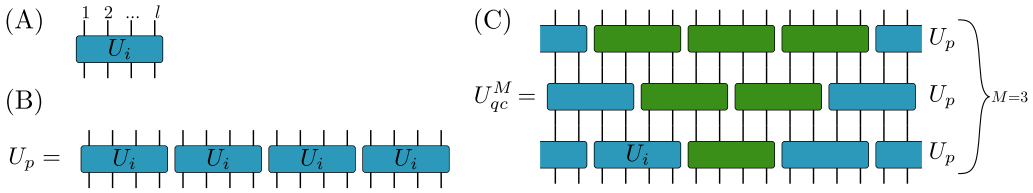

FIGURE 2.2: In (A) local unitary operator U_i acting on l sites. In (B) a piecewise local unitary operator U_p defined as a product of local unitary operators U_i acting on disjoint regions. In (C) finite depth quantum circuit U_{qc}^M with depth $M = 3$ and a causal cone denoted with green colour.

Definition 2.1.2. Two gapped states $|\psi(0)\rangle$ and $|\psi(1)\rangle$ are in the same phase if and only if they are related by a local unitary (LU) evolution:

$$|\psi(0)\rangle \sim |\psi(1)\rangle \text{ iff } |\psi(1)\rangle = \mathcal{T}\left(\mathrm{e}^{-i\int_0^1 dg\tilde{H}(g)}\right)|\psi(0)\rangle, \tag{2.2}$$

where $\mathcal{T}$ denotes the path ordering and $\tilde{H}(g)$ is a sum of local hermitian operators.

The Hamiltonian $\tilde{H}(g)$ in general is not the same as $H(g)$, however one can show, using the Lieb-Robinson bound, that a local operator evolved with a local Hamiltonian in a finite time remains local (with some larger range) determined by the maximal velocity of spreading of the quasiparticle excitations. Even more direct causal structure can be seen in the definition using quantum circuits.

Definition 2.1.3. Let $U_p = \prod_i U_i$ be a piecewise local unitary operator, with U_i being a set of unitary operators acting on disjoint regions of maximal finite size l. A quantum circuit with depth M $U_{qc}^M = U_p^{(1)}U_p^{(2)}...U_p^{(M)}$ is a product of M piecewise local unitary operators, U_p as shown in Fig.2.2. Then the equivalence relation between two gapped states is:

$$|\psi(0)\rangle \sim |\psi(1)\rangle \text{ iff } |\psi(1)\rangle = U_{qc}^M|\psi(0)\rangle. \tag{2.3}$$

Two gapped states $|\psi(0)\rangle$, $|\psi(1)\rangle$ belong to the same phase if they are related by a finite depth quantum circuit.

In the last two definitions, the LU evolution and constant depth quantum circuit can be considered together under the common label of LU transformations. With these definitions at hand, it can be stated that all gapped states which are related to product states via LU transformation are short range entangled and can be transformed into each other by LU transformation, while different topological orders correspond to different long range entanglement patterns and form equivalence classes under LU transformations. Different Landau symmetry-breaking phases or different SPT phases can be recovered when considering equivalence classes under symmetric LU transformations, but they still remain short range entangled. Also, long range entangled phases can exhibit more phases under symmetric LU transformations.

Having introduced the way of determining whether two states belong to the same or different phase (universality class) we need to assign them certain characteristic and unequivocal properties, which we approach in the following sections.

2.2 Quantum statistics

The relation between spin and quantum statistics of particles, commonly known as spin statistics theorem[14] originally distinguishes between particles with intrinsic half-integer

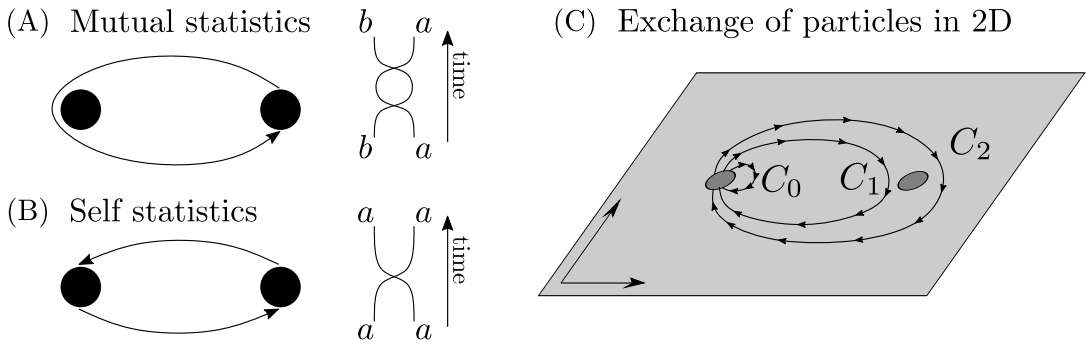

FIGURE 2.3: In (A) mutual statistics of 2 types of point-like particles a and b and in (B) self statistics of a particle a. Self statistics is an interaction involving a single swap of two same particles a, while the mutual statistics encodes the change in the system after double swap, so that in the final state the particles appear in the same place as in the initial state. In (C) on a 2D plane the particles can be represented as holes and their winding as loops denoted by C_i with C_0 being the trivial loop. The loop C_2 enclosing another particle is not homotopic to the trivial one, whereas in 3D it could be smoothly transformed into C_1 homotopic to C_0 by lifting it along the third dimension.

spin obeying the Fermi-Dirac statistics and integer spin particles obeying the Bose-Einstein statistics. Statistics can be interpreted as an interaction involving the exchange of two particles along a specific trajectory in space-time[10]. When the swap involves the same kind of particles then the process defines self-statistics and mutual statistics are defined for different types of particles, when one of them makes a full revolution around the other as shown in fig. 2.3. Indeed, in 3 spatial dimensions, point-like elementary excitations can be either bosons or fermions, as a double exchange has to be an identity transformation. Therefore, the only remaining possibility is the system acquiring a phase $e^{i\phi} = \pm 1$ after the single swap, $+1$ for bosons and -1 for fermions. On the other hand, when considering only 2 spatial dimensions the physics becomes much richer allowing for point-like particles, for which the exchange phase ϕ could be arbitrary, hence the name anyons – 'any-ons'. The situation is different in 2D because unlike in 3D the process of winding one particle around the other is topologically non-trivial as illustrated in the fig. 2.3(C). As long as the path made by a particle winding around another particle is not homotopic to the trivial path, the system after such an adiabatic transformation acquires a non-trivial Berry phase $|\Psi\rangle \to e^{i\phi}|\Psi\rangle$ in case of Abelian anyons. In case of non-Abelian anyons such a transformation may even lead to the mixing between different degenerate states: $|\Psi_a\rangle = \sum_b U_{ab}|\Psi_b\rangle$ [15]. The information about the mutual and self statistics of anyons can be encoded in modular S and T matrices respectively. Together they generate a representation of the modular group $\mathrm{SL}(2,\mathbb{Z})$, with the following properties [16]:

- S is symmetric $S = S^T$, unitary $S \cdot S^\dagger = 1$ and $S_{11} > 0$, where $a = 1$ represents a trivial anyon type.
- Two anyons can fuse to give a third anyon type

$$a \times b = \oplus_c \, N_{ab}^c \, c \tag{2.4}$$

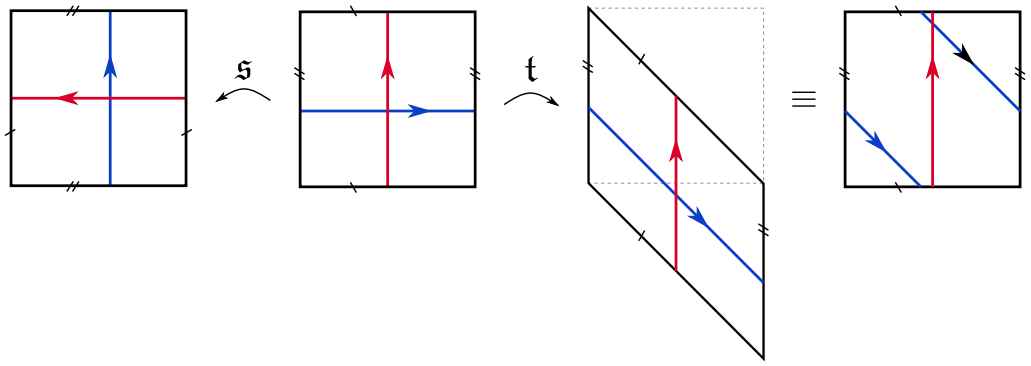

FIGURE 2.4: Modular transformations of the torus: $\mathfrak{s}$ transformation corresponds to a 90° rotation, while $\mathfrak{t}$ transformation is a Dehn twist, which effectively makes a blue flux to wind around the torus once.

according to the fusion rules encoded in the 3-index fusion tensor N_{ab}^{c}. Fusion rules can be obtained from the topological S matrix through the Verlinde formula [17]:

$$N_{ab}^{c} = \sum_{d} \frac{S_{da} S_{db} (S_{dc})^{*}}{S_{d1}} \in \mathbb{N} \tag{2.5}$$

- The first column/row of the topological S matrix encodes quantum dimensions of the anyons:

$$d_a = \frac{S_{1a}}{S_{11}} = \frac{S_{a1}}{S_{11}}, \qquad D = \sqrt{\sum_{a} d_a^2}, \tag{2.6}$$

where D is the total quantum dimension. It is also the largest magnitude eigenvalue of the matrix N_a with $(N_a)_b^c$ elements, and it describes the asymptotic growth of the fusion space of the anyon type a. For Abelian anyons $d_a = 1$, as there is always just one fusion outcome $a \times a = b$ (for self-inverse anyons $b = 1$), whereas for non-Abelian anyons $d_a > 1$, as the number of possible fusion outcomes grows with the number of fused particles, where for a single fusion $a \times a = \oplus_c N_{aa}^{c} c$ the fusion rules allow for more than one possible outcome, i.e. amount of labels c for which $N_{aa}^{c} \neq 0$ is two or more.

- T matrix is unitary and diagonal in this canonical basis, which we refer later to as the basis of Minimally Entangled States (MES) or well-defined anyon fluxes:

$$T_{ab} = \delta_{ab}\, \mathrm{e}^{-2i\pi\frac{c}{24}+2i\pi s_a}, \tag{2.7}$$

where s_a is a topological spin of an anyon and c is the chiral central charge.

- Together, S and T satisfy the conditions for the generators of modular transformations:

$$(ST)^3 = S^2 = C, \quad C^2 = 1, \quad C_{ab} = N_{ab}^{1}. \tag{2.8}$$

This last property relates them to the modular transformations of the torus generated by a $\frac{\pi}{2}$ rotation $\mathfrak{s}$ and a Dehn twist $\mathfrak{t}$:

$$\mathfrak{s} = \begin{pmatrix} 0 & 1 \\ -1 & 0 \end{pmatrix}, \qquad \mathfrak{t} = \begin{pmatrix} 1 & 1 \\ 0 & 1 \end{pmatrix}. \tag{2.9}$$

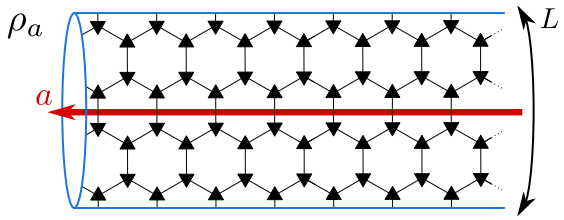

FIGURE 2.5: Reduced density matrix ρ_a on a half infinite cylinder of circumference L of a state with well-defined anyon flux a along the cylinder (denoted by red arrow). Such a state has minimal entanglement entropy on the entanglement cut shown on the left end of the cylinder.

Thus S and T transformations generate a unitary representation of the mapping class group $\mathrm{SL}(2,\mathbb{Z})$ for the torus – group of automorphisms of the torus shown in the Fig. 2.4 Together with chiral central charge c this set of data, (S,T,c) was conjectured to uniquely determine the topological order [18, 19, 20] and hence it was used in many numerical studies of topologically ordered systems including Ref. [1, 2] for models for which it indeed provides a unique classification. However, it was found that there exist distinct topological orders with the same modular data (S,T,c) [21], therefore the modular data (S,T,c) alone cannot always be used as a label distinguishing different topologically ordered phases of matter. In the next section 2.3 we introduce a different mathematical tool to characterize topological order based on category theory.

Despite its shortcomings, the modular data (S,T,c) is still capable of providing lots of information about the topological order, in many cases even a unique characterization of it. Moreover, although S and T matrices encode statistics of elementary excitations, they can be extracted already from the ground states as shown in [22]. A crucial step to achieve that is the identification of states with well-defined anyon fluxes along the torus in the subspace of degenerate ground states. The states with well-defined anyon flux are also called Minimally Entangled States (MES), which comes from the study of entanglement entropy of a reduced density matrix ρ obtained by a non-trivial cut of the torus. It was found by Kitaev and Preskill [23] that topologically ordered states exhibit non-vanishing universal correction to the entanglement entropy:

$$S(\rho) = \alpha \cdot L - \gamma, \qquad \gamma = \log(D) = \log\left(\sqrt{\sum_a d_a^2}\right), \tag{2.10}$$

where the first term contains a non-universal constant α and scales with the system size while D is the total quantum dimension and depends only on the universality class of the system. The universal correction γ is called topological entanglement entropy (TEE) and it is non-zero only for topologically ordered states. For a topologically ordered state with well-defined anyon flux a along the infinite cylinder with circumference L the entanglement entropy of a reduced density matrix ρ_a of a half-infinite cylinder (see Fig. 2.5) is minimal, given by:

$$S(\rho_a) = \alpha \cdot L - \log\left(\frac{D}{d_a}\right). \tag{2.11}$$

Any superposition of states with well-defined anyon flux will increase the entanglement entropy by decreasing the TEE, hence the name Minimally Entangled States (MES). Now the S matrix can be interpreted as a change of basis between MES in different directions

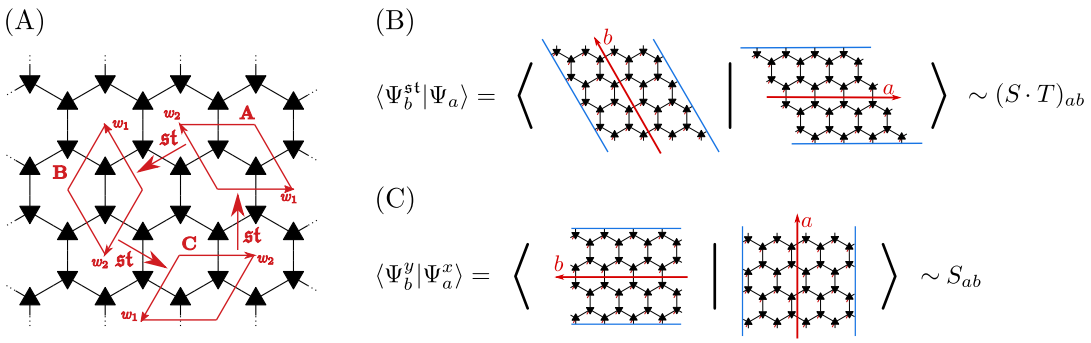

FIGURE 2.6: In (A) on a hexagonal lattice with 120° rotation symmetry a unit cell can be defined by unit vectors (w_1, w_2), which repeated many times in both directions designate a torus. There are three distinguished tori A, B, C all related by a $\mathfrak{st}$ transformation, which corresponds to 120° rotation with properly chosen unit vectors (w_1, w_2). In (B) and (C) the overlap between MES in different directions on tori related by some $f(\mathfrak{s}, \mathfrak{t})$ transformation gives matrix elements of the corresponding combination of topological matrices $f(S, T)$. In (B) $f(\mathfrak{s}, \mathfrak{t}) = \mathfrak{st}$ results in matrix elements of the topological $S\cdot T$ matrix, while in (C) $f(\mathfrak{s}, \mathfrak{t}) = \mathfrak{s}$ correspond to matrix elements of the product of S.

x and y related by a 90° degree rotation:

$$|\Psi_a^y\rangle = \sum_b S_{ab}|\Psi_b^x\rangle. \tag{2.12}$$

Minimally Entangled States in y direction is a superposition of MES in x direction, therefore its entanglement entropy at the non-trivial cut along x will be maximal. From (2.12) one realizes that the matrix elements of the S matrix can be obtained by calculating proper overlaps between MES in different directions:

$$\langle\Psi_c^x|\Psi_a^y\rangle = \langle\Psi_c^x|\left(\sum_b S_{ab}|\Psi_b^x\rangle\right) = \sum_b \delta_{bc}S_{ab} = S_{ac}, \tag{2.13}$$

where in the second equality we use the orthonormality of MES. In a similar way we can obtain the matrix elements of any combination of S and T matrices by taking overlaps between states on tori related by the corresponding combinations of $\mathfrak{s}$ and $\mathfrak{t}$ transformations. For example, the matrix elements of $S\cdot T$ can be obtained by calculation of overlaps between states on tori related via $\mathfrak{st}$ transformation:

$$(S\cdot T)_{ab} = \langle\Psi_b^{\mathfrak{st}}|\Psi_a\rangle. \tag{2.14}$$

With a proper choice of a unit cell on a hexagonal lattice designating the torus, given by a pair of unit vectors (w_1, w_2) in Fig.2.6, a $\mathfrak{st}$ transformation becomes a rotation by 120°, which rotates torus A to torus B and torus B to torus C as shown in Fig. 2.6. Independent calculation of MES on these three tori together with the calculation of the overlaps between them allows us to extract the matrix elements of the topological S and T matrices. And this is precisely the idea behind [1], where it was used for the first time to determine Abelian topological order using infinite Projected Entangled Pair States (see Chapter 3), as well as [2], where the formalism was extended to models with non-Abelian anyonic statistics.

2.3 String-nets and fusion category

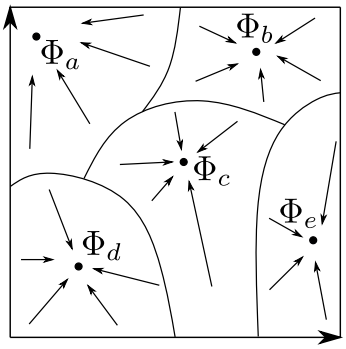

FIGURE 2.7: Schematic diagram of a renormalization group flow towards fixed point wave functions $\Phi_{a,b,c,d,e}$ with zero correlation length for different long range entangled phases divided by lines of phase transitions.

Topologically ordered phases of matter, as it was shown in section 2.1 can be divided into distinct universality classes. The universal properties of certain TO are best seen in the RG fixed point wave functions with zero correlation length and long range entanglement. All TO states within the same phase are related to its RG fixed points by generalized local unitary transformations, Fig. 2.7 Those RG fixed point wave functions are characterized by a set of local rules relating different amplitudes. Different topological orders can be found by solving those local rules. Before providing a general description of string-net models in terms of fusion categories, we start with a simple example below.

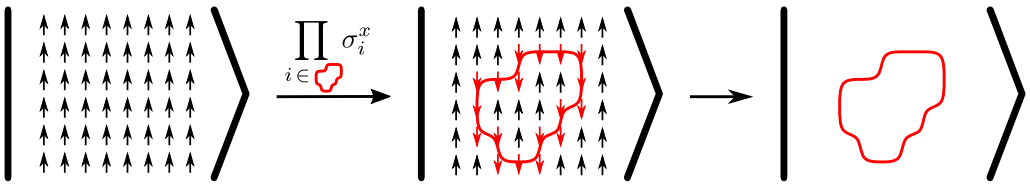

FIGURE 2.8: The action of a closed string of operators $\prod_{i\in loop} \sigma_i^x$ results in a formation of loops and the string-net models are defined through such closed string on the background of some physical degrees of freedom like spins-$\frac{1}{2}$ on a lattice.

In order to introduce a class of models called string-nets let us start with a simple product state of spins-$\frac{1}{2}$ on a lattice all pointing up – we can think of them as eigenstates of σ^z Pauli matrix to eigenvalue $+1$ (first ket in Fig.2.8). We may flip any number of spins, for example by an action of a string $\prod_{i\in loop} \sigma_i^x$ of Pauli-x matrices, in a way that they form a closed loop pattern and from now on we will only think in terms of such closed strings instead of spins as shown in Fig.2.8. The action of a local σ^x operator on one of the flipped spins forming the loop will open that loop, creating two endpoints of a string as shown in Fig.2.9. The action of a string of $\prod_{i\in\mathcal{C}} \sigma_i^x$ corresponds to moving one of the endpoints on the lattice along a path $\mathcal{C}$. Those endpoints are particle-like excitations in a sense that their existence results in higher energy-density distribution in some finite region on the lattice. Moreover, they are topological particle-like excitations, as a single endpoint cannot be created/annihilated by any local operator. In this setup they can be created and annihilated only in pairs and the action of moving one away from the system corresponds to an action of a string operator which size grows linearly with the system size. Those topological particle-like excitations are anyons. In the ground state configuration, there may be not one but many different closed strings crossing each other. However, this is still

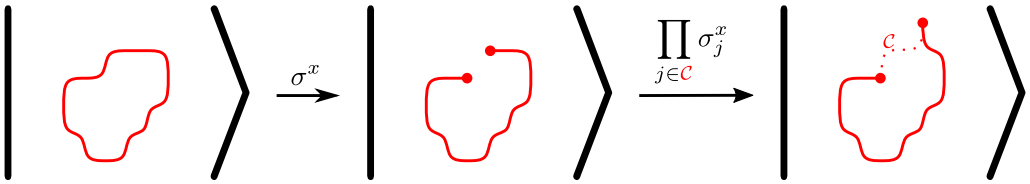

FIGURE 2.9: The action of a local operator on the closed string opens the string, therefore creating two endpoints – topological defects, which can be moved around the lattice by the action of a string $\prod_{i\in\mathcal{C}} \sigma_i^x$.

a product state and not an eigenstate of a topologically ordered Hamiltonian. In order to construct the simplest possible topologically ordered state, we take an equal-weight superposition over all possible closed strings:

$$|\Phi_{Z_2}\rangle = \sum_{all\ \ closed\ \ strings} \quad \text{  } \tag{2.15}$$

Such a string-net state describes an RG fixed point wave function of a toric code – the simplest topologically ordered state, first introduced by Alexei Kitaev in the context of fault-tolerant quantum computation in Ref.[24]. If the amplitudes are slightly modified, so that their sign depends on the total number of loops of a given configuration, then such state is a double semion string-net model – a completely different universality class than the toric code:

$$|\Phi_{ds}\rangle = \sum_{all\ \ closed\ \ strings} (-1)^{N_{loops}} \quad \text{  } \tag{2.16}$$

The two wave-functions introduced above describe exact renormalization group fixed points, with zero correlation length, of the toric code and double semion strings nets respectively. However, there is no basis in which those expressions would simplify to a product state, because they are long range entangled. Moreover, it becomes clear when going back to spin representation that these states have no order, they represent different kinds of spin liquid states and in general it is very hard to distinguish one from the other when dealing directly with the amplitudes of different closed string configurations (especially in the thermodynamic limit, when the number of possible configurations, hence terms in these superpositions, become infinite). Fortunately, there exist a local description relating different string configurations in terms of *F-symbols*, the associators of the underlying unitary fusion category $\mathcal{UFC}$.

$$\Phi\left(\begin{smallmatrix} \mathrm{i} & & \mathrm{l} \\ & \mathrm{m} & \\ \mathrm{j} & & \mathrm{k} \end{smallmatrix}\right) = \sum_n F^{ijk}_{lmn} \ \Phi\left(\begin{smallmatrix} \mathrm{i} & & \mathrm{l} \\ \mathrm{j} & \mathrm{n} & \mathrm{k} \end{smallmatrix}\right) \tag{2.17}$$

In the examples above, such a possible reconnecting move may happen in the area denoted by a red circle in Fig.2.10 when connecting the two string types i with a trivial string $\mathbf{1}$.

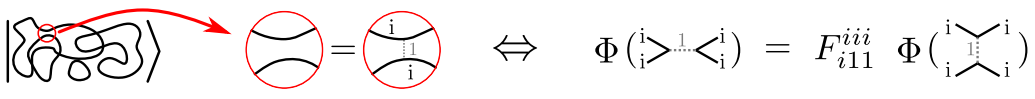

FIGURE 2.10: The global string pattern may be described with local moves given by F-symbols.

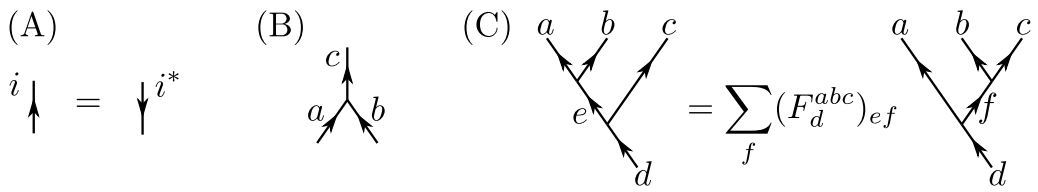

FIGURE 2.11: In (A) reversing the string orientation results in a dual (conjugate) string type. In (B) the fusion vertex N_{ab}^{c} describing the allowed fusions $a \times b \to c$. In (C) the F-symbols, defined with taking into account the string orientations.

In this case, we can distinguish the toric code and double semion string nets locally via its F symbols relating the amplitudes of the two string configurations with different number of loops N_{loops}:

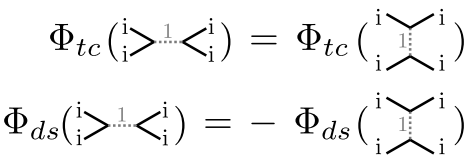

(2.18)

Given the examples we proceed with general definition of string-net models, which require the following data [25]:

- *string types*, $i = 1, 2, ...n$, with $i = 1$ being the trivial string type and n the total number of string types, which is $n = 2$ in the examples of toric code and double semion. Nevertheless, N can be bigger than 2, for example $n = 3$ for the double Ising string-net model, where the possible string types are $i = 1, \sigma, \psi$ (see Ref. [2, 3]) or $n = 6$ for the Rep(S_3) string-net (see Ref. [3]). Different anyon types are simple objects in the input category $\mathcal{C}$

- *branching rules*, describing all the allowed fusion rules at the vertices in terms of the aforementioned fusion tensors N_{ab}^{c}, shown in Fig. 2.11(B)

- *string orientation*, in general the dual string to a string type i is i^* with opposite orientation, Fig. 2.11(A), so that $N_{ii^*}^{1} = N_{i^*i}^{1} = 1$. In the examples of toric code and double semion $i = i^*$ and the string are unoriented and $N_{ii}^{1} = 1$. Therefore, the F-symbols take a simple form. However, for the oriented string types it is important to properly define the F tensors, taking into account possible orientations [26] as shown in Fig. 2.11(C). The only physical F-symbols are those allowed by fusion rules at each vertex:

$$F_{def}^{abc} \propto N_{ab}^{e} N_{ec}^{d} N_{bc}^{f} N_{af}^{d}. \tag{2.19}$$

  F-symbols are the associators in the fusion category $\mathcal{C}$, as they describe the associativity of the fusions of three simple objects:

$$(a \times b) \times c \;\sim\; a \times (b \times c) \tag{2.20}$$

For anyon models the F-symbols are unitary when treated as matrices in the e, f indices: [26] (hence the name *unitary fusion category*):

$$[(F_{d}^{abc})^{\dagger}]_{ef} = (F_{d}^{abc})_{fe}^{*} = [(F_{d}^{abc})^{-1}]_{ef}. \tag{2.21}$$

Moreover when any of the labels $a, b, c = 1$ and the remaining vertices satisfy the fusion rules then we require $F_{def}^{abc} = 1$, as fusion with identity is an identity and commutes with

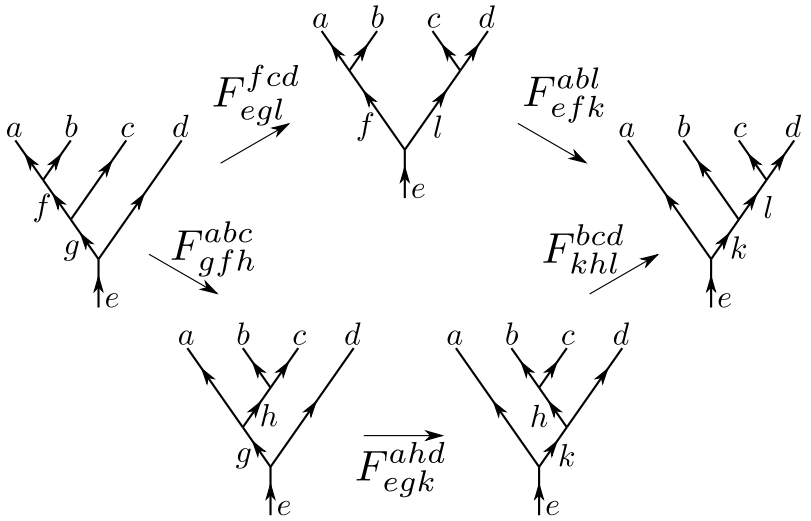

FIGURE 2.12: Associativity condition gives rise to a consistency equation for F-symbols and is called Pentagon equation due to the pentagon structure of the diagram, which shows two equivalent paths in which the F-moves can be performed in order to transform the leftmost fusion tree to the rightmost fusion tree.

other fusions. When more anyons are fused (or split) to the same anyon the associativity condition gives rise to a consistency equation between different F-symbols called Pentagon equation, shown in Fig. 2.12

$$F^{fcd}_{egl} F^{abl}_{efk} = \sum_{h} F^{abc}_{gfh} F^{ahd}_{egk} F^{bcd}_{khl}. \tag{2.22}$$

Pentagon equation has only discrete solutions, which means that one solution cannot be transformed into another by non-trivial small deformations, which comes under the name of Ocneanu rigidity (Ocneanu actually never published his proof). Thanks to this property F-symbols indeed are capable of labelling different topological orders unequivocally. However, there is still some redundancy in this description, coming from two issues:

- *gauge freedom*, the change of F-symbols by non-zero complex numbers $\lambda^c_{ab} \in \mathbb{C}$:

$$F^{abc}_{def} \;\to\; \frac{\lambda^e_{ab}\lambda^d_{ec}}{\lambda^f_{bc}\lambda^d_{af}} \cdot F^{abc}_{def}, \tag{2.23}$$

  does not affect the Pentagon equation. This redundancy can be eliminated by requiring the F^{abc}_{e} matrices to be unitary and fixing $F^{abc}_{def} = 1$ if any of a, b, c is trivial, as mentioned above.

- *Morita equivalence*, any two UFC $\mathcal{C}_1$ and $\mathcal{C}_2$ describe the same topological order if their Drinfeld centers are equal $Z(\mathcal{C}_1) = Z(\mathcal{C}_2)$, which can be seen by direct calculation of the Drinfeld center [25].

Having addressed both issues, we conclude that the monoidal center $Z(\mathcal{C})$ of the unitary fusion category $\mathcal{C}$ provides a unique description of the topological order and in that sense can be thought of as the mathematical description which uniquely determines the topologically ordered quantum phases, analogous to symmetry groups for Landau's symmetry breaking phases. The numerical method to calculate the F-symbols of UFC $\mathcal{C}$ together with the calculation of the Drinfeld center $Z(\mathcal{C})$ and topological S and T matrices of 2D

topologically ordered state (also states with non-zero correlation length – away from RG fixed points) is a task accomplished in Ref. [3]. The method relies heavily on the concept of virtual *matrix product operator* symmetries of *infinite projected entangled pair states*, which is a property that can be accessed only with tensor networks formalism, as the MPO symmetries are defined purely on the 'virtual' degrees of freedom of iPEPS (see Chapter 3) and therefore do not suffer from broadening caused by growing correlation length (unlike approaches based on the optimization of ribbon operator symmetries [27] at the physical level).

Chapter 3

Tensor networks

Tensor networks are numerical methods which already proved to be extremely useful tools in the studies of strongly correlated quantum systems, starting with the success of DMRG (*density matrix renormalization group*) [28, 29] initiated by Steve White in 1992. DMRG together with an independently developed MPS ansatz (*matrix product states*) [30, 31] became the most powerful methods to study one dimensional gapped, local quantum many body systems on a lattice [32, 33, 34]. The connection between DMRG and MPS was realized only later [35] as the DMRG is a variational algorithm which leads to an MPS representation of a state when converged. Subsequent developments lead to the extension of tensor network to higher dimensional systems with PEPS (*projected entangled pair states*) [36], as well as critical systems with MERA (*multiscale entanglement renormalization ansatz*) [37].

Tensor networks are variational methods, which makes them immune to the sign problem in case of fermions [38, 39, 40, 41], which is the notorious limitation of methods based on functional integrals [42] like Quantum Monte Carlo (QMC). Therefore, it makes them the methods of choice to study not only fermionic systems but also systems with geometric frustration. One of the remarkable successes of TN, specifically fermionic PEPS, is that it provided the best variational ground state energies of the Hubbard model [43], as well as simpler $t-J$ model [40, 44, 45], which are believed to exhibit high-temperature superconductivity. Moreover, unlike the exact diagonalization (ED) [46], tensor networks are not restricted by the system size and enable calculations in the thermodynamic limit at the same time capturing faithfully the correlations and entanglement structure of the system unlike mean-field based approaches. All this makes them the best available methods in the study and search of topological order, especially in realistic materials, where there are only few exactly solvable models [10, 24, 25]. Huge progress in the study of topological order with tensor networks has taken place over the last two decades and is concisely summarized in Section 3.5 after the introduction of certain crucial aspects of TN in Sections 3.1-3.4.

3.1 Variational ansatz

A tensor network is a variational ansatz for a ground state $|\Psi(p)\rangle$, or low-energy excited states, of local gapped Hamiltonians $\hat{H}$ of many-body systems, where the parameters to optimize p are the elements of the tensors. For example, in order to find a ground state of a Hamiltonian $\hat{H}$ one would minimize the energy $E(p)$ in order to obtain the optimal parameters $p^\star$ of the tensor network:

$$E(p) = \frac{\langle\Psi(p)|\hat{H}|\Psi(p)\rangle}{\langle\Psi(p)|\Psi(p)\rangle} \quad \rightarrow \quad 0 = \frac{\partial}{\partial p}\frac{\langle\Psi(p)|\hat{H}|\Psi(p)\rangle}{\langle\Psi(p)|\Psi(p)\rangle} \Rightarrow |\Psi_{gs}(p^\star)\rangle. \tag{3.1}$$

The parameters to optimize – the tensors are the main building blocks of the tensor network, usually represented as some shapes with links, the number of which denotes the rank

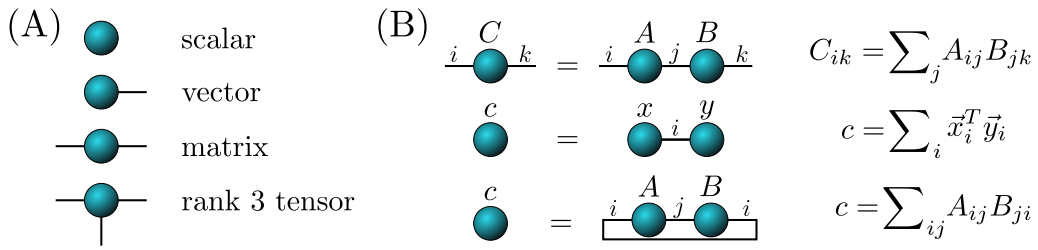

FIGURE 3.1: The basic building blocks of the tensor networks. In (A) different rank tensors may constitute the tensor network formalism. In (B) mathematical formulas behind the diagrammatic tensor network representation, namely in the row order: matrix multiplication, scalar product of two vectors and a trace of a product of two matrices.

of the tensor. Rank-0 tensor is just a scalar (a number), rank-1 tensor is a vector, rank-2 tensors is a matrix as shown in Fig. 3.1(A). Connecting tensors via a link represents a summation over certain indices of one or multiple tensors, as shown on several examples in Fig. 3.1(B). The idea of drawing shapes and links is analogous to Feynman's diagrams, which is to substitute long, complicated formulas (here summations) with some shortened diagrammatic representation.

The main purpose of tensor networks is an efficient representation of a certain class of many-body states. Instead of working directly with probability amplitudes $C_{i_1,i_2,\ldots,i_N}$ of different configurations of N local degrees of freedom (particles, spins), which can be interpreted as a rank N tensor, we decompose it into a network of tensors of much smaller rank:

$$|\Psi(p)\rangle = \sum_{i_1,i_2,\ldots i_N} C_{i_1,i_2,\ldots,i_N} |i_1 i_2 \ldots i_N\rangle = \sum_{i_1,i_2,\ldots,i_N} \sum_{\{\alpha\beta\ldots\omega\}} A^{i_1}_{\alpha} A^{i_2}_{\alpha\beta} \ldots A^{i_{N-1}}_{\chi\omega} A^{i_N}_{\omega} |i_1 i_2 \ldots i_N\rangle. \tag{3.2}$$

Here actually the decomposition represents a finite one dimensional tensor network – *matrix product states* – MPS and in the TN diagrammatic notation can be represented as:

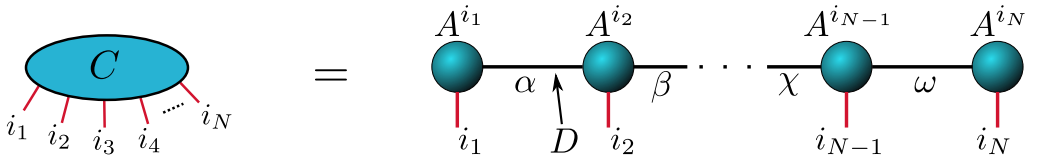

(3.3)

The open red indices correspond to some local degrees of freedom $i_k = 1, 2, \ldots d$, with d being the dimension of the local Hilbert space throughout this thesis. The connected black indices are called bond indices, $\alpha = 1, 2, \ldots D$ with D being the bond dimension (number of values the bond index may take), which when summed over reproduce the big tensor C. At this point we can compare the number of parameters needed to fully describe both representations of this many-body system consisting of N lattice sites, and we notice that in case of single tensor C the number of parameters is $n_C = d^N$, while in case of network of tensors A, the number of parameters is at most $n_A = ND^2d$. In the first case the number of parameters scales exponentially with the system size $n_C \propto \exp(N)$, while in the second case in general the scaling is at most polynomial $n_A \propto \text{poly}(N)$. Clearly, the tensor network ansatz outperforms methods dealing directly with probability amplitudes and enables numerical calculations in the thermodynamic limit for translationally invariant systems. The question remains: does TN methods provide accurate results, or what class

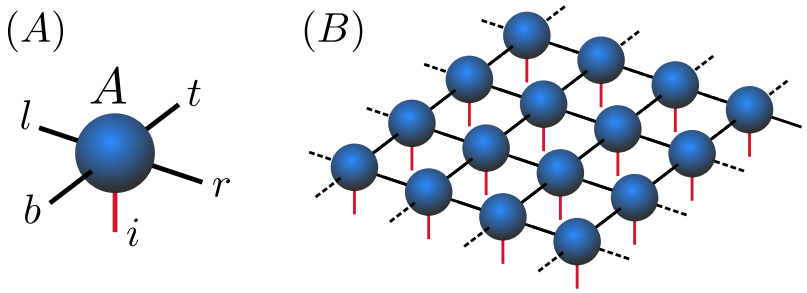

FIGURE 3.2: The iPEPS on a square lattice (B) is built from repeated tensors A^i_{trbl} (A). Here a single tensor A is rank 5 with one physical index i numbering states in a given lattice site and 4 black bond indices t, r, b, l encoding correlations and entanglement between different lattice sites. When the network from (B) is summed over all the black indices, it reproduces the probability amplitudes, but this procedure is never done in practice during numerical simulations, because it is extremely inefficient.

of states can be faithfully represented with tensor networks? The answers for these are provided in Section 3.3.

Apart from the well-known and commonly used MPS there exist other TN ansatz, including the two-dimensional *projected entangled pair states* – PEPS, shown in Fig. 3.2, which together with MPS are of central importance in this thesis. In 1D the tensors forming the state are rank 3, with one physical index i_k and two bond indices of dimension D (sometimes also denoted by χ), while in 2D the tensors are rank 4 or more, with one physical index and at least 3 virtual (bond) indices. This allows for efficient simulations of 2D systems on a lattice. Fig. 3.2 shows an exemplary infinite PEPS (iPEPS) on a square lattice built of tensors A^i_{trbl} with one physical index i and 4 bond indices t, r, b, l.

Tensor networks enable studies of systems on different lattice geometries and sizes, both finite and infinite (iMPS, iPEPS), as well as different boundary conditions: open (OBC) or periodic (PBC) as shown respectively in Fig. 3.3(C).

Analogously to states, operators can also be represented by tensor networks. Naturally in 1D they are called *matrix product operators* – MPO, shown in Fig. 3.3(A), whereas in 2D there are *projected entangled pair operators* – PEPO, shown in Fig. 3.3(B), where now each tensor has 2 physical indices.

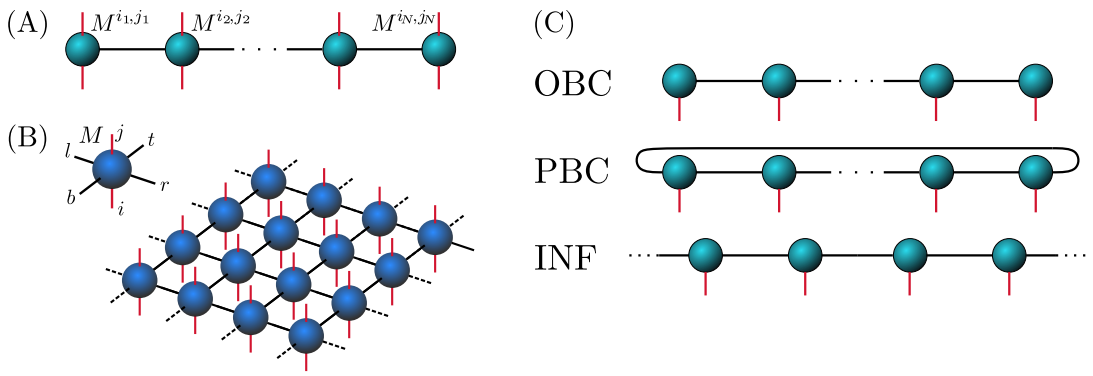

FIGURE 3.3: Similarly to states, TN are capable of encoding operators: (A) *matrix product operators* in one dimension, built from tensors M^{ij}, where i, j are the physical indices and (B) *projected entangled pair operators* in two dimensions. In (C) different boundary conditions for MPS are shown, from top to bottom: open, periodic and infinite MPS structure. Analogous diagrams can be drawn for 2D PEPS.

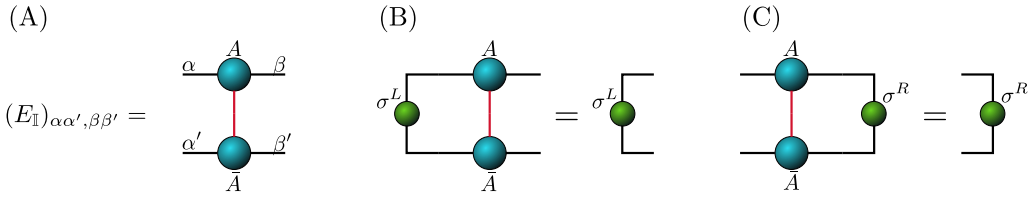

FIGURE 3.4: Definition of the MPS transfer matrix (A), and its leading left (B) and right (C) eigenvectors. Transfer matrix is a matrix between the grouped indices (α, α') to the left and (β, β') to the right. MPS tensors A^i can be normalized, so that the largest eigenvalue of the transfer matrix is 1, and so can be the eigenvectors $\langle \sigma^L | \sigma^R \rangle = 1$. The eigenvectors $\sigma^{L,R}$ are actually boundary density matrices, when we treat the indices coming from the bra and ket layer of the transfer matrix separately.

From now on, the attention is focused on translationally invariant tensor networks in the thermodynamic limit, if not specified otherwise. This means that the whole state $\Psi(A)$ is determined by a single tensor A and the number of parameters to describe the whole state is $D^c d$, where c is the connectivity of the network, $c = 2$ for 1D systems and $c > 2$ for higher dimensional systems (e.g. $c = 3$ for honeycomb lattices and $c = 4$ for square lattices in 2D). In general, translationally invariant TN network may have a larger unit cell, consisting of more than one tensor, however theoretically they can always be grouped into a single tensor for simplicity of the description (numerically it is rather not efficient to contract smaller tensors to bigger ones).

One of the main objects appearing in the calculations using TN are transfer matrices (TM). For an MPS, the transfer matrix is defined as follows (Fig. 3.4 (A)):

$$E_{\mathbb{I}} = \sum_i A^i \bar{A}^i, \quad \text{or in terms of matrix elements:} \quad (E_{\mathbb{I}})_{\alpha\alpha',\beta\beta'} = \sum_i A^i_{\alpha\beta} \bar{A}^i_{\alpha'\beta'}, \tag{3.4}$$

where the bar $\bar{A}$ denotes complex conjugation and the summation is performed over a physical index i. Actually the transfer matrix $E_{\mathbb{I}}$ is a rank-4 tensor of dimensions $D \times D \times D \times D$, however, we treat it as a matrix of dimensions $D^2 \times D^2$ between the grouped indices (α, α') and (β, β'). The name transfer matrix comes from similarity to 1D classical statistical mechanical models.

An MPS, which is a result of an optimization, will typically be *injective* (for exact definitions see Section 3.3), meaning that the largest magnitude eigenvalue λ_0 is unique and the corresponding left and right eigenvectors $|\sigma^{L,R}\rangle$ are positive definite. The latter follows from realization that the transfer matrix acting on the eigenvectors is a completely positive (CP) map, defined as [47, 48]:

$$\mathcal{E}_A(\sigma^L) = \sum_{i=1}^{d} A^i \sigma^L \bar{A}^i \quad \text{and its dual} \quad \mathcal{E}^*_A(\sigma^R) = \sum_{i=1}^{d} \bar{A}^i \sigma^R A^i, \tag{3.5}$$

shown in Fig. 3.4(B) and (C) respectively. Then the spectral decomposition of a transfer matrix $E_{\mathbb{I}}$ can be written as:

$$E_{\mathbb{I}} = \lambda_0 \ \left|\sigma^R\right) \left(\sigma^L\right| + \sum_{i=1}^{D^2-1} \lambda_i \ \left|v_i^R\right) \left(v_i^L\right|, \tag{3.6}$$

where instead of typical braket notation $|x\rangle\langle y|$ round brackets $|x)\,(y|$ are used to denote the inner product $(x|y) = x^T y$. For large system sizes N, especially for $N \to \infty$ the norm

of the periodic MPS is given by $\mathrm{tr}(E_{\mathbb{I}}^N) \simeq \lambda_0^N$, therefore the tensors A can always be rescaled $A \to \frac{1}{\sqrt{\lambda_0}} A$, such that the state is normalized to 1 and the corresponding CP map has a *spectral radius* $\lambda_0 = 1$. In Eq. 3.5 we used the fact, that it is convenient to write the eigenvectors as operators $\sigma^{L,R}$ with matrix elements $\sigma^{L,R}_{\alpha,\alpha'} = \langle \alpha, \alpha' | \sigma^{L,R} \rangle$. They can be normalized, so that:

$$\left(\sigma^L | \sigma^R\right) = \mathrm{tr}\left((\sigma^L)^T \sigma^R\right) = \quad = 1 \tag{3.7}$$

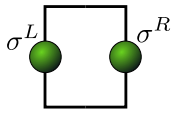

Then $\sigma^{L,R}$ are actually boundary density matrices related to the reduced density matrix of the state as explained in Section 3.3.

From the numerical perspective the injectivity means that in case of degenerate ground states, an MPS with finite bond dimension will typically choose one of the symmetry broken ground states or one of the minimally entangled states, as this requires lower bond dimension D than the superposition. This is indeed the case when simulating ground states of topologically ordered models using quasi 2D DMRG on infinite cylinders (see Section 3.5).

A more general MPS construction allows for an MPS, whose transfer matrix has several degenerate leading eigenvalues – non-injective MPS. This happens, for example in case of non-Abelian anyons, when an MPO symmetry Z_a (see Section 3.4) is acting on the injective-MPS eigenvectors $|v_i\rangle$ of the PEPS transfer matrix (introduced below) yielding a non-injective MPS as a result

$$Z_a |v_i\rangle = \oplus_k N_{ia}^k |v_k\rangle. \tag{3.8}$$

As an example, the action of the symmetry in the double Fibonacci string-net model is:

$$Z_\tau |v_\tau\rangle = |v_{1+\tau}\rangle = |v_1\rangle \oplus |v_\tau\rangle. \tag{3.9}$$

In general a tensor A^i generating a non-injective MPS can be brought to canonical form [47, 48], which is block diagonal:

$$A^i = \oplus_j \mu_j A_j^i, \qquad A^i = \begin{pmatrix} \mu_1 A_1^i & 0 & .. \\ 0 & \mu_2 A_2^i & .. \\ ... & & \end{pmatrix} \tag{3.10}$$

such that the CP maps $\mathcal{E}_{A_j}(\sigma) = \sum_i A_j^i \sigma \bar{A}_j^i$ related to each tensor A_j^i are irreducible[1]. The tensor A_j^i is then called *normal* tensors and the MPS they generate is also called *normal*. The coefficients μ_j are chosen such that CP map related to each tensor A_j^i has spectral radius $\lambda_j = 1$. Using the example of the double Fibonacci string-net model, we can represent the resulting tensor as:

$$A^i = A_{\mathbf{1}}^i \oplus A_\tau^i \tag{3.11}$$

The transformation bringing a non-injective MPS into block diagonal canonical form is a type of gauge transformation (see Section 3.4) and it is a basic step in the algorithm presented in Ref. [3].

Still, non-injective MPS appears extremely rarely in the studies using tensor networks, here only after an MPO symmetry acts on the MPS eigenvector, which is a result of

[1] The CP maps $\mathcal{E}_{A_j}(\sigma) = \sum_i A_j^i \sigma \bar{A}_j^i$ are irreducible if there is no non-trivial projector P, such that for any j and $D \times D$ matrix σ: $\mathcal{E}_{A_j}(P\sigma P) \in P\sigma P$ [48]

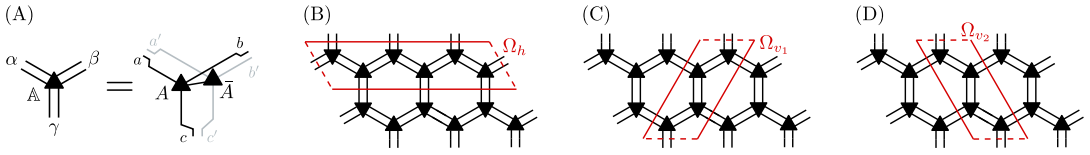

FIGURE 3.5: Definitions of PEPS transfer matrices on hexagonal lattice. In (A) the PEPS tensor is contracted through its physical index to obtain a double PEPS tensor $\mathbb{A}_{\alpha,\beta,\gamma} = \sum_i A^i_{a,b,c}\bar{A}_{a',b',b'}$. Figs. (B)-(D) represent three simplest possible choices of PEPS transfer matrix on a hexagonal lattice - all related by a 120° rotation.

algebraic, not numerical procedure. Therefore, the topic is continued with respect to injective MPS.

The expectation values can be easily calculated using the transfer matrix and its leading eigenvectors. Thanks to the translational invariance, the expectation value of some operator $\hat{O}$ in the thermodynamic limit is equal to:

$$\langle\Psi(A)|\hat{O}|\Psi(A)\rangle = \mathrm{tr}\left(E_{\mathbb{I}}^{N-1}E_{\hat{O}}\right) \xrightarrow{N\to\infty} \left(\sigma^L|E_{\hat{O}}|\sigma^R\right) = \quad (3.12)$$

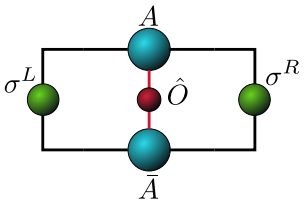

The second-largest eigenvalue of the transfer matrix is related to the correlation length:

$$\xi = -\frac{1}{\log(|\lambda_1/\lambda_0|)} = -\frac{1}{\log(|\lambda_1|)}, \quad (3.13)$$

where the second equality follows from the normalization condition. In order to compare two normalized states in the iMPS form $|\Psi(A)\rangle, |\Psi(B)\rangle$ it is enough to compute the leading eigenvalue of the mixed transfer matrix $E_{mix} = \sum_i A^i\bar{B}^i$ and due to orthogonality catastrophe the overlap is either 0 or 1:

$$\langle\Psi(B)|\Psi(A)\rangle = \mathrm{tr}(E_{mix}^N) = \mathrm{tr}(\lambda_0^N) \xrightarrow{N\to\infty} \begin{cases} 1, & \text{if } \lambda_0 = 1 \\ 0, & \text{if } \lambda_0 < 1. \end{cases} \quad (3.14)$$

In case of equality, the tensors A^i, B^i generating the states $|\Psi(A)\rangle$, $|\Psi(B)\rangle$ are related by a gauge transformation, which is explained in Section 3.4.

The transfer matrix of a 2D PEPS is a more complicated object, as it is actually an MPO and the related boundary eigenvector is an MPS. For simplicity of the discussion, we assume that PEPS is describing a state on a square lattice of $L_x \times L_y$ physical sites, where $L_x, L_y \to \infty$, but the generalization to other lattices is straightforward as shown in Fig. 3.5. Then there are two simplest choices for the transfer matrix, horizontal Ω_h of dimensions $(D^2)^{L_x} \times (D^2)^{L_x}$ and vertical Ω_v of dimensions $(D^2)^{L_y} \times (D^2)^{L_y}$:

$$\Omega_{h,v} = \sum_I \mathbf{A}_I^{h,v}(\mathbf{A}_I^{h,v})^*, \quad \text{where} \quad \mathbf{A}_I^h = \prod_{k=1}^{L_x} A^{i_k}, \quad \mathbf{A}_I^v = \prod_{k=1}^{L_y} A^{i_k}. \quad (3.15)$$

Here the bold tensor $\mathbf{A}_I$ corresponds to the whole 1D chain of tensors with all physical indices grouped into one big index I to resemble the definition of the 1D TM. The eigenvectors of the PEPS TM are given by MPS defined on the virtual space of PEPS or,

equivalently, when the bra and ket indices are treated separately – MPO, similarly as in the 1D case:

$$|\sigma^{L,R}) = \prod_{k=1}^{L} M^{\alpha_k,\alpha'_k} \, |\alpha_k, \alpha'_k) \, , \quad L \to \infty. \tag{3.16}$$

In the diagrammatic language the vertical transfer matrix Ω_v made of PEPS tensors A and its conjugate $\bar{A}$ together with its related right eigenvector in the form of MPS $|\sigma^R)$ is:

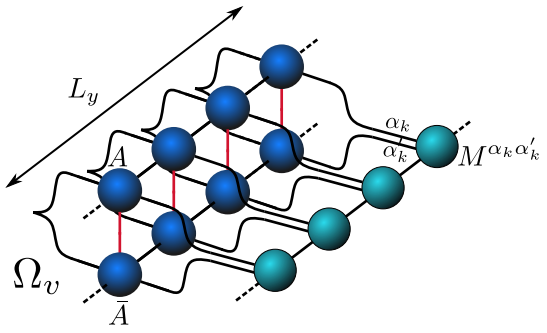

(3.17)

Unlike for MPS, PEPS transfer matrix can be degenerate, as long as the optimization of PEPS does not distinguish any direction, which would favour the choice of minimally entangled state in that direction. Also, it is possible to construct a critical PEPS [49]. Due to the fact that exact diagonalization of such big matrices, especially infinite matrices, is impossible, the possible degeneracy of the PEPS transfer matrix is restored through the number of orthogonal eigenvectors to the leading eigenvalue, where the orthogonality is checked according to Eq. 3.14. The eigenvectors can be found using one of the algorithms described in Section 3.2.

While MPS can be contracted exactly, PEPS has to be contracted approximately, either through the eigenvectors or through corner transfer matrices (see Section 3.2) in order to obtain the expectation values of local operators. Similarly, as with an MPS, one never contracts the amplitudes of the state $|\Psi(A)\rangle$, but the norm $\langle\Psi(A)|\Psi(A)\rangle$. Hence, all the reference to the contraction of PEPS (or iPEPS) should be implicitly understood as the contraction of double PEPS, where the double PEPS tensor is defined as:

$$\mathbb{A}_{\tau\rho\beta\lambda} = \sum_i A^i_{trbl} \bar{A}^i_{t'r'b'l'}, \tag{3.18}$$

where the tensor A^i_{trbl} (shown in the Fig. 3.2) generates the state $|\Psi(A)\rangle$, which is referred to as ket layer, and its conjugate $\bar{A}^i_{t'r'b'l'}$ generates $\langle\Psi(A)|$, which is referred to as the bra layer. Analogously, to make contact with Refs. [1, 2, 3], on a hexagonal lattice the double PEPS tensor is:

$$\mathbb{A}_{\alpha\beta\gamma} = \sum_i A^i_{abc} \bar{A}^i_{a'b'c'}, \tag{3.19}$$

which is shown in Fig. 3.6(A). The stripe of the double PEPS tensors connected via its bond indices is a transfer matrix, as shown in Eq. 3.17 and in Fig. 3.5.

In Ref. [1, 2] we use the contraction of iPEPS with its eigenvectors, as this way allows for clear definition of periodic boundary conditions and calculations performed on infinite torus. The spectral decomposition of the iPEPS transfer matrix reduces to:

$$\Omega = \sum_{i=1}^{n} \lambda \, |\sigma^R_i) \, (\sigma^L_i| \, , \tag{3.20}$$

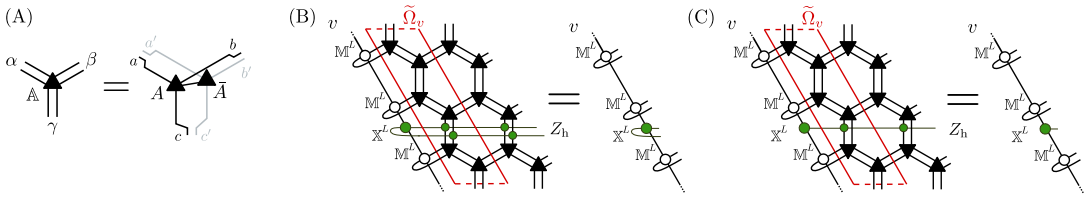

FIGURE 3.6: Examples of impurity transfer matrices. The tensor network on a honeycomb lattice is made of double PEPS tensors, i.e. tensors contracted via its physical indices as shown in (A). Then the impurity may be inserted in either bra, ket (C) or both layers (B).

where n denotes the degeneracy and $\sigma_i^{L,R}$ denote orthogonal left and right MPS boundary eigenvectors (fixed points). Then taking periodic boundary conditions is straightforward:

$$\mathrm{tr}(\Omega^N) \xrightarrow{N\to\infty} \sum_i \lambda^N = n \cdot \lambda^N, \tag{3.21}$$

and the normalization of iPEPS is chosen to be $\langle\Psi(A)|\Psi(A)\rangle = n$ by setting $\lambda = 1$.

In Ref. [1, 2] the notion of transfer matrices is extended to impurity transfer matrices (ITM), where apart from a repeatable PEPS tensors A^{i_k} there is a single line of iMPO generated by tensors Z, called an impurity:

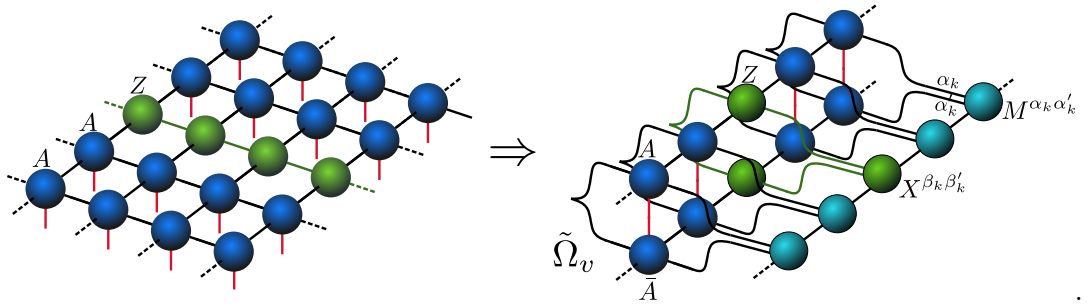

(3.22)

Here, the iMPO generated by Z tensors, denoted with a green colour, is defined solely on the virtual bond indices of iPEPS, i.e. its physical indices are connected with the bond indices of iPEPS. Then, the related eigenvector of such an ITM is an MPS generated by tensors M^{α_k,α'_k} with a single additional tensor $X^{\beta_k\beta'_k}$. Such an impurity may be inserted in both bra and ket layers of the iPEPS, as shown above and in Fig. 3.6(B), but it may be also inserted in just one of those layers, as shown in Fig. 3.6(C). Such an object is needed in order to contract iPEPS with inserted iMPO symmetries (see Section 3.4), which are necessary for calculating overlaps between different MES, which yield the matrix elements of topological S and T matrices according to Eq. 2.14

3.2 Algorithms

The name Tensor Networks stands for the structures, as well as efficient algorithms for their contraction and optimization. To name a few of the most common algorithms: [50]:

- *DMRG - density matrix renormalization group* [28, 29], the most known and used TN optimization algorithm based on renormalization procedure of the ground state wave functions of a 1D quantum systems on a lattice, yielding the optimal MPS representation [51]. With χ being the bond dimension of an MPS, the cost of the algorithm is only $\mathcal{O}(\chi^3)$ for iDMRG and systems with open boundary conditions and

$\mathcal{O}(\chi^5)$ when periodic boundary conditions are imposed. The usage of DMRG was extended also to 2D systems [52], where the MPS is wrapped around a cylinder in a snake-like pattern:

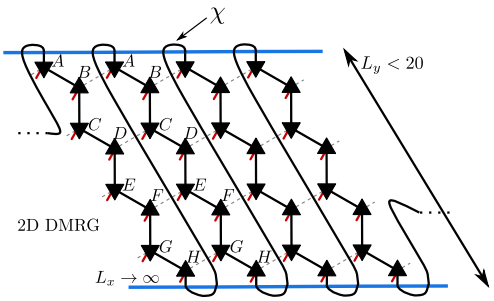

(3.23)

The real properties of the 2D system should then be recovered by finite-size scalings with the width of the cylinder L_y. This method is restricted only to models with short correlation length $\xi \simeq 1 \sim 2$ (less than 20 lattice sites), as the computational cost grows exponentially with the cylinder's circumference and the MPS with finite bond dimension χ cannot capture the entanglement properties of a realistic 2D system.

- *CTM - corner transfer matrix* [53, 54, 55] is a method of approximate truncation of double PEPS. In order to calculate the partition function or any local observable of a large or infinite 2D tensor network, it has to be contracted approximately, as there is no way to do it exactly unlike for 1D systems. Therefore, the CTM approach focuses on approximating the environment of a single tensor (or a small group of tensors) by substituting it with corner (C) and transfer (T) matrices, which are optimized new tensors with finite bond dimension χ:

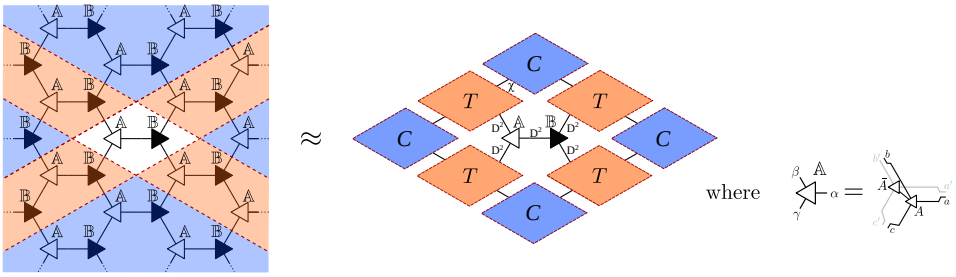

(3.24)

In the end, the partition function of a state encoded with iPEPS can be obtained by calculating the trace of the product of all four corner matrices:

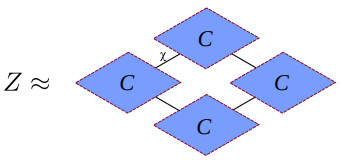

(3.25)

while calculation of a local observable requires additionally transfer matrices T:

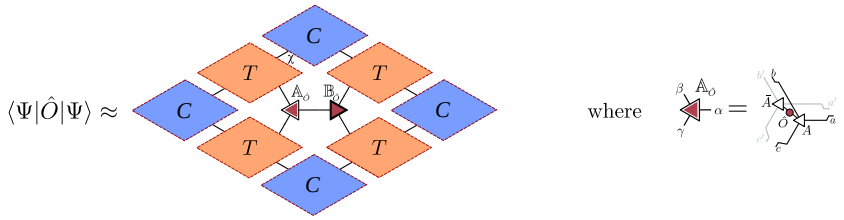

(3.26)

The cost of the contraction of iPEPS is $\mathcal{O}(D^6\chi^3)$, with D being the bond dimension of iPEPS tensor [56].

- *Boundary MPS* is another method of contracting 2D double PEPS, using the transfer matrix, which is an MPO, defined in Eq.3.15. For finite systems one can start with an actual MPS boundary $|\psi_A^{(0)}\rangle$ generated by tensor A and contract it with an MPO transfer matrix formed by a stripe of double PEPS Ω, as in Fig. 3.5 or Eq. 3.17, however due to proliferation of indices, after each multiplication a new MPS, generated by tensor B, have to be found to approximate that product [57]:

$$\Omega\ |\psi_A^{(i-1)}\rangle = |\psi_A^{(i)}\rangle \quad \rightarrow \quad \min_B || \ |\psi_A^{(i)}\rangle - |\psi_B^{(i)}\rangle||^2. \tag{3.27}$$

  In case of infinite systems the iMPS boundary is obtained as a fixed point $|\Phi\rangle$ of the iPEPS transfer matrix Ω, by subsequent application of the TM Ω to a random initial vector in the form of iMPS $|\Phi^0\rangle$ until convergence, yielding an eigenvector $|\Phi\rangle$ to the largest eigenvalue λ of Ω [58]:

$$\Omega^N|\Phi^0\rangle \xrightarrow{N\rightarrow\infty} \lambda^N|\Phi\rangle \tag{3.28}$$

  The cost of contracting the boundary MPS with a PEPS transfer matrix is $\mathcal{O}(\chi^3D^6 + \chi^2D^8d)$, where χ is the bond dimension of the boundary MPS, D is the iPEPS bond dimension and d being the dimension of the physical local Hilbert space. This cost can be lowered if the iPEPS is contracted in a diagonal way [58]. If the transfer matrix is degenerate, then the method yields several orthogonal MPS eigenvectors, the number of which corresponds to the degeneracy in the system, n in the Eq. 3.20. This is a crucial difference of the boundary MPS method with respect to the CTM method, where corner and transfer matrices may encode degenerate iPEPS in a much less obvious way. Boundary MPS method is the main ingredient of the algorithm for distinguishing topological order presented in Refs. [1, 2, 3]. In Ref. [1] the boundary MPS is obtained using the power method of Eq. 3.28, while in Refs. [2] and [3] a qualitatively better method is used, resulting in faster convergence, based on the tangent space to the MPS manifold.

- *Tangent Space Methods* [59], state-of-the-art methods for handling variety of problems, starting from time evolution of matrix product states (*TDVP - time dependent variational principle* [60]), study of excitations and spectral functions, but also variational optimization of the expectation value of a Hamiltonian as in Eq. 3.1 – the VUMPS algorithm [61] and approximation of fixed-points of 1D transfer matrices, which can be used as a boundary MPS method of contraction of PEPS. These group of methods is based on the idea that a set of uniform MPSs $|\Psi(A)\rangle$ generated by tensors A of dimensions $D \times d \times D$ form a manifold in the full Hilbert space of the system under investigation. This manifold is not a linear subspace (as the addition of two MPSs with the same bond dimension does not belong to this manifold), therefore a tangent space is associated to every point of $|\Psi(A)\rangle$ by differentiating with respect to the parameters A. Then the tangent vector is defined as:

$$|\Phi(B,A)\rangle = \sum_i B^i \frac{\partial}{\partial A^i}|\Psi(A)\rangle \equiv \sum_i B^i|\partial_i\Psi(A)\rangle, \tag{3.29}$$

where the partial derivative effectively removes the tensor A and the summation over i denotes all

$$\frac{\partial}{\partial A^i}|\Psi(A)\rangle =$$

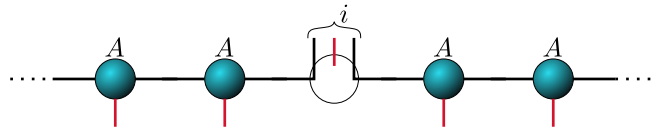

(3.30)

The overlap between two tangent vectors is:

$$\langle\Phi(B',A)|\Phi(B,A)\rangle = \sum_{ij} \bar{B'}^i \left(\langle\partial_i\Psi(A)|\partial_j\Psi(A)\rangle\right) B^j = \sum_{ij} \bar{B'}^i G_{ij} B^j, \tag{3.31}$$

where G_{ij} can be considered as a metric matrix and in the diagrammatic form it is:

$$G_{ij} =$$

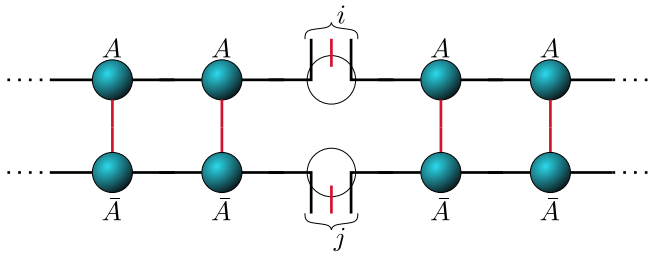

(3.32)

Many problems under consideration can be projected onto and minimized in the tangent space, which is analogous to calculating and minimizing the gradient of a cost function of interest. The power of these methods lies in the usage of mixed orthonormal gauge of MPS (see Section 3.4), which allows writing the metric matrix as the identity, which is otherwise very often singular:

$$G_{ij} =$$

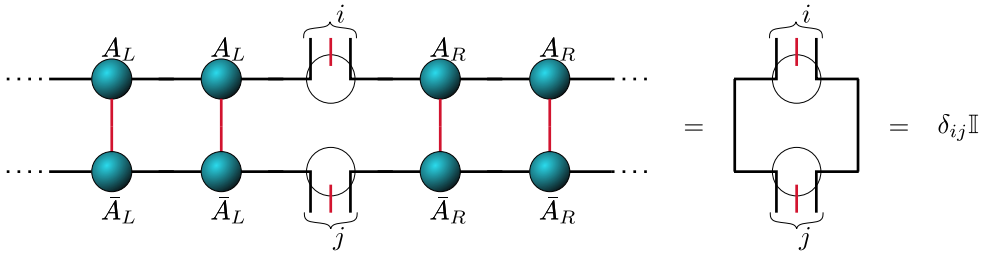

(3.33)

A broad review of all the algorithms based on tangent space methods can be found in Ref. [62].

- *PEPS optimization* methods – apart from efficient contraction of PEPS, there are also several methods to obtain optimal PEPS tensors describing the state. They fall into two categories: *variational* PEPS, both for finite [57, 63] and infinite systems [64, 65], based on minimizing the energy according to Eq. 3.1 and *imaginary time evolution*, which may be performed using different schemes:
  - simple update [66] is a local update, which makes it computationally cheap but not very optimal,
  - more optimal full update [58], which is more expensive, because it takes into account full wave function,
  - and fast-full update [67], which like full update takes into account the full PEPS environment, but instead of calculating the new environment after every iteration from scratch, it recycles the environment from the previous iteration.

– an intermediate neighbourhood tensor update [68], which takes into account only the nearest neighbour environment of updated tensors, which can be contracted exactly.

However, out of all those methods, only the variationally optimized iPEPS was able to recover topologically ordered state as was found in Ref. [1].

The tensor network structures and algorithms listed above are only a small subset of all, but they are most commonly used and crucial to this thesis, therefore we do not delve into other structures and algorithms.

3.3 Entanglement

The entropy in classical thermodynamics is usually used to quantify the lack of information about the microstate of the system under consideration. The higher the entropy is, the less information we possess about it. However, in quantum mechanics of many-body systems the positive entropy may appear even when the state of the system is known, as the origins of non-vanishing entropy are related to quantum entanglement[69]. The perfect example is given by a quantum many-body system at zero temperature, which is expected to be in its ground state $|\psi\rangle$, which is non-degenerate and pure $\rho = |\psi\rangle\langle\psi|$, therefore its von-Neumann entropy is zero:

$$S(\rho) = -\mathrm{tr}\,(\rho\,\log\rho) = 0. \tag{3.34}$$

However, if we divide this many body state into two connected but non-overlapping regions A and $B \equiv A^c$ (B is the complement of A), then the entropy of the subsystem A, which is now described by a reduced density matrix $\rho_A = \mathrm{tr}_B\rho$, is in general positive $S(\rho_A) \geq 0$. The equality $S(\rho_A) = 0$ happens in a special case when the state $|\psi\rangle = |\varphi_A\rangle \otimes |\varphi_B\rangle$ factorizes and there is no entanglement between subsystems A and B, with the simplest example being a product state, in which case the division into any two subsystems results in vanishing von-Neumann entropy of a reduced state. Therefore, the entropy of a subregion quantifies the amount of entanglement in the system and is called the *entanglement entropy*. The entanglement entropy, or rather its scaling, is important for studies of critical phenomena, as well as the ability to represent quantum many-body states, both trivial ones and topologically ordered ones, where we observe a universal correction to the scaling law – the *topological entanglement entropy*.

From the perspective of quantum many body systems, we are mostly interested if tensor networks are capable of representing them faithfully, or rather, what class of states can be represented faithfully. For a generic quantum many body state the entanglement entropy is typically an extensive quantity, i.e. it grows with the volume of the system, hence it obeys *volume law*. However, there is a tiny subset of all states in the full Hilbert space – ground states of local, gapped Hamiltonians (see Fig 3.7), which are most relevant from the perspective of realistic quantum systems, and they obey the so-called *area law*. Area law means that the entanglement entropy scales with the boundary area of the subsystem under consideration.

It was strictly proven by Hastings [33] that area law holds for 1D gapped systems with finite range of interactions, so with Hamiltonians of the form:

$$H = \sum_j h_{j,j+1}, \tag{3.35}$$

which is a Hamiltonian with only nearest neighbour (NN) interactions, but any finite number of sites can be grouped together to result in an NN Hamiltonian. The boundary

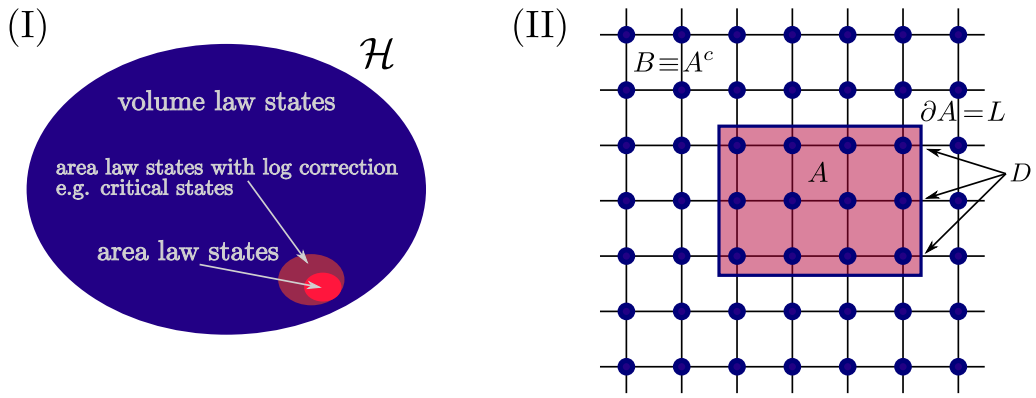

FIGURE 3.7: For a generic quantum state from the full Hilbert $\mathcal{H}$ space of a many body system the entanglement entropy is an extensive quantity, however there is a tiny relevant subspace of ground states and low excited states of local gapped Hamiltonians that obey the so-called *area law* for the entanglement entropy. This means that the entanglement entropy scales with the size of the boundary ∂A of some region, A as shown in (I). Tensor networks in (II) satisfy area law by construction, as the entanglement entropy is bounded by $S(\rho_A) \leq L\log(D)$, where D is the bond dimension and L is the amount of bond indices, which are cut by the division of the system into subsystem A and its complement A^c.

of a region A of 1D chain is actually just a point (one or two sites, depending on the choice of boundary conditions), therefore, the entanglement should be bounded by a number $S(\rho_A) \leq S_{max}$. Indeed, such a number can be found [33], but it grows exponentially with the correlation length ξ:

$$S(\rho_A) \leq S_{max} = c_0 \xi \, \ln(6\xi) \, \ln(d) \, 2^{6\xi \ln(d)}, \tag{3.36}$$

with d being the dimension of local Hilbert space at each site and a numerical constant $c_0 \propto \mathcal{O}(1)$. When the correlation length diverges, the system becomes scale invariant, in other words critical. If the critical system can be described in terms of conformal field theory, then the whole entanglement spectrum can be calculated, and the entanglement entropy diverges only logarithmically from the area law [70] (see Fig. 3.7).

The situation becomes a bit more complicated in two and higher dimensions, as it is hard to prove the area law in a mathematically rigorous way. Generally, it is believed that gapped systems with local interactions always satisfy area law. In some specific cases it can be proven, like for the free bosonic [71] or fermionic systems [72, 73], as well as interacting quantum systems at finite temperature and systems with sufficiently fast decay of correlations [74]. However, there is no general proof for interacting quantum systems in dimensions higher than one. Still, what is important from the point of view of this thesis is that topologically ordered states obey an area law with an additive correction: $\alpha L - \gamma$, where γ is always positive which means that TO states are less entangled than the trivial ones, which is due to the symmetries reducing the support of the local reduced density matrices [75].

At the same time, Tensor Network States, both MPS and PEPS satisfy area law by construction. Namely, for an MPS the entanglement entropy is bounded just by a number, which depends on the bond dimension D and for PEPS it scales with the size L of the boundary ∂A of a region A and also depends on the bond dimension D:

$$S_{MPS}(\rho_A) \simeq \log(D), \qquad S_{PEPS}(\rho_A) \simeq L \, \log(D). \tag{3.37}$$

To see this, we proceed with the construction of projected entangled pair states. A state:

$$|\psi_D\rangle = \frac{1}{\sqrt{D}} \sum_{\alpha=1}^{D} |\alpha\rangle_1 |\alpha\rangle_2 \tag{3.38}$$

is a maximally entangled state of a pair of particles with D degrees of freedom. The entanglement entropy of a reduced density matrix of 1 particle in such a state is:

$$\begin{aligned} \rho_1 = \mathrm{tr}_2(\rho_D) = \mathrm{tr}_2(|\psi_D\rangle\langle\psi_D|) = \frac{1}{D}\sum_{\beta=1}^{D} |\beta\rangle_1\langle\beta|_1 \\ S(\rho_1) = -\mathrm{tr}(\rho_1 \log(\rho_1)) = -\sum_{\beta} \frac{1}{D} \log\left(\frac{1}{D}\right) = \log(D). \end{aligned} \tag{3.39}$$

We create a product state of such maximally entangled pairs $|\psi_D\rangle^{\otimes n}$ and we group the particles in such a way that every physical lattice site is maximally entangled to its neighbours:

for MPS: 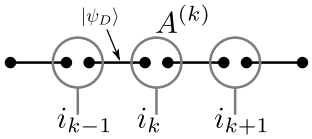

for PEPS: 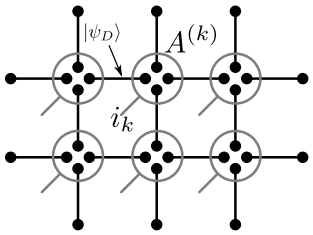

(3.40)

Now, both MPS and PEPS tensors can be written in terms of a projector of a Hilbert space of 2 or 4 virtual particles, which are maximally entangled to their neighbours [76, 77]. The projectors on site k are:

$$\begin{aligned} A[k] : \mathbb{C}^D \otimes \mathbb{C}^D \to \mathbb{C}^d, \quad A^[k] = \sum_{i_k=1}^{d} \sum_{\alpha,\beta=1}^{D} A^{i_k}_{\alpha,\beta} |i_k\rangle\langle\alpha,\beta|, \quad \text{for an MPS} \\ A[k] : \left(\mathbb{C}^D\right)^{\otimes 4} \to \mathbb{C}^d, \quad A[k] = \sum_{i_k=1}^{d} \sum_{\alpha,\beta,\gamma,\delta=1}^{D} A^{i_k}_{\alpha,\beta,\gamma,\delta} |i_k\rangle\langle\alpha,\beta,\gamma,\delta|, \quad \text{for PEPS.} \end{aligned} \tag{3.41}$$

Then a physical state in terms of TN is given by $|\Psi\rangle = \otimes_k A[k] |\psi_D\rangle^{\otimes n}$. If the projector $A[k]$ is an injective map from virtual space to physical space, i.e. there exist an inverse: $A[k]^{-1} : \mathbb{C}^d \to \mathbb{C}^{D \otimes c}$, with c the connectivity of the network, such that $A[k]^{-1} A[k]$, then the TN is called *injective*, or sometimes in case of an MPS *pure*.

The upper bound for the entanglement entropy from Eq. 3.37 follows directly from this construction. Another way to see it is through a Schmidt decomposition of a pure state $|\Psi\rangle$ partitioned into two subsystems A and B.

$$|\Psi\rangle = \sum_{\alpha} \lambda_\alpha |\phi_\alpha\rangle_A |\phi_\alpha\rangle_B, \tag{3.42}$$

where $|\phi_\alpha\rangle_A$, $|\phi_\alpha\rangle_B$ form orthonormal bases for Hilbert spaces, $\mathcal{H}_A$, $\mathcal{H}_B$ respectively. Schmidt decomposition always exists, which can be proven with SVD, which in terms of

matrix components is:

$$\Psi_{ij} = \sum_{\alpha,\beta=1}^{D} U_{i\alpha}\Lambda_{\alpha\beta}(V^\dagger)_{\beta j} = \sum_{\alpha=1}^{D} U_{i\alpha}\lambda_\alpha(V^\dagger)_{\alpha j}, \tag{3.43}$$

with isometries U, V satisfying $U^\dagger U = \mathbb{I}_D$ and $V^\dagger V = \mathbb{I}_D$, where the Schmidt rank $D \leq \min(d_a, d_b)$ being at most the dimension of the smaller of the two Hilbert spaces $\mathcal{H}_A$, $\mathcal{H}_B$. Assuming translational invariance TN have finite bond dimension D at each cut and assuming maximal entanglement between the two subsystems along the boundary of L sites as in the construction above, we obtain:

$$S(\rho_A) = -\mathrm{tr}(\rho_A \log(\rho_A)) = -\sum_{\alpha=1}^{D^L} \frac{1}{D^L} \log\left(D^{-L}\right) = L\,\log(D). \tag{3.44}$$

In 1D $L = 1$ if A is half-infinite chain or $L = 2$ if the chain is periodic and the boundary consists of 2 lattice sites, whereas in 2D L is the number of virtual degrees of freedom, which are cut as shown in Fig.3.7. This proves an area law for MPS and PEPS.

To conclude, if a state satisfies an area law for any bipartition A, B, $S(\rho_A) \leq \mathcal{O}(\partial A)$ then it has a faithful TN representation [78, 34, 49].

Area law suggests that all the relevant information about the entanglement in the bulk should be contained in its boundary. Indeed, it was shown in Ref. [79] that the entanglement spectrum ξ_i, defined as the logarithm of the square of Schmidt values:

$$|\psi\rangle = \sum_i \mathrm{e}^{-\frac{1}{2}\xi_i} |\psi_A^i\rangle |\psi_B^i\rangle \tag{3.45}$$

in certain cases reveals more information than just a single number – the entanglement entropy: $S = \sum_i \xi_i \exp(-\xi_i)$ and can determine the topological order in the bulk. Specifically, the low-lying entanglement spectrum for quantum Hall states is isomorphic with the spectrum of the corresponding Hamiltonian of the CFT at the boundary. Interestingly, PEPS provides a very natural description of this *bulk-boundary correspondence* via boundary density operators [80]. A reduced density matrix of half of an infinite cylinder ρ_c can be written in terms of the left and right boundary density operators σ_L, σ_R respectively, which on the other hand can be expressed by the leading eigenvectors of the PEPS transfer matrix on the infinite cylinder:

$$\rho_c = U\sqrt{\sigma_L^T}\sigma_R\sqrt{\sigma_L^T}U^\dagger, \tag{3.46}$$

where the isometry U maps the virtual space of bond indices onto the physical Hilbert space. This isomorphism can be used to calculate second Rényi entropies[81]:

$$S_\alpha(\rho) = \frac{1}{1-\alpha}\log\left(\mathrm{tr}(\rho^\alpha)\right) \xrightarrow{\alpha=2} -\log\left(\mathrm{tr}(\sigma_{\mathrm{L}}^{\mathrm{T}}\sigma_{\mathrm{R}}\sigma_{\mathrm{L}}^{\mathrm{T}}\sigma_{\mathrm{R}})\right) \tag{3.47}$$

for topologically ordered states, for which it was shown, on the other hand, that all Rényi entropies are the same (for all α) and no additional information can be recovered by studying the entanglement spectrum. Then, in order to extract the topological entanglement entropy γ all methods used to extrapolate the results from the large cylinder's width L to zero, leading to some finite size effects, while the method introduced in Refs. [1, 2] allows obtaining results already in the thermodynamic limit. There the additive constant γ follows directly from the structure of the projectors onto MES and does not require any extrapolations, which is also the reason why it does not vanish despite numerical errors, in

contrast to methods based on extrapolations, where even the slightest perturbation breaking the symmetry of the tensors causes the topological order to 'break down' with the TEE $\gamma \to 0$ [82, 83].

An alternative derivation of the formula for the second Rényi entropy can be done using tensor networks. The reduced density operator of a half-infinite cylinder is then defined as:

$\rho_c = \mathrm{tr}_L(|\Psi\rangle\langle\Psi|) =$

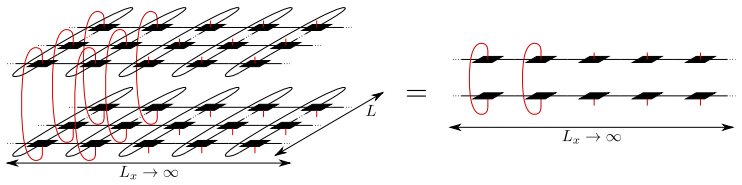

(3.48)

where the partial trace is taken on the left side of the infinite cylinder. In the second equality, the tensor network is contracted in the y direction for better visibility. Then:

$\mathrm{tr}\left(\rho_c^2\right) = \mathrm{tr}$

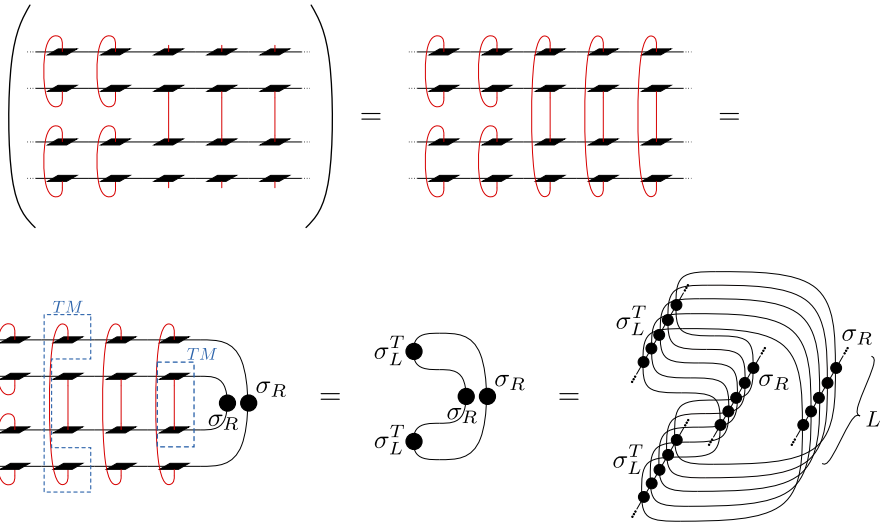

(3.49)

Here, in the second line, transfer matrix structure appears with its leading eigenvectors $\sigma_{L,R}$. In TN the numbering of indices is a matter of convention, therefore keeping this in mind, together with the original definition of the eigenvectors of the TM in Section 3.1, we arrive at the same result as in Eq. 3.47.

3.4 Gauge transformations and symmetries

Tensor network representation of a state is not unique, namely different tensors A^i and B^i (i being the physical index) may generate the same state $|\Psi(A)\rangle = |\Psi(B)\rangle$. This happens, for example, when the tensors A^i and B^i are related by a gauge transformation. Actually, in 1D it was proven that if $|\Psi(A)\rangle = |\Psi(B)\rangle$ then the tensors generating states must be related by a gauge transformation, which goes under the name of Fundamental Theorem of MPS [47, 48]. For a fixed physical index i the rank 3 tensors A^i, B^i become matrices and according to the fundamental theorem of MPS there must exist a non-singular matrix G, such that:

$$A^i = G \cdot B^i \cdot G^{-1}. \tag{3.50}$$

When the tensors are contracted via their bond indices, the matrices $G^{-1}G = GG^{-1} = 1$ cancel out as shown in the Fig. 3.8(A), hence the transformation leaves the state invariant. The same situation may happen in 2D (or higher dimensions as well) for PEPS as shown

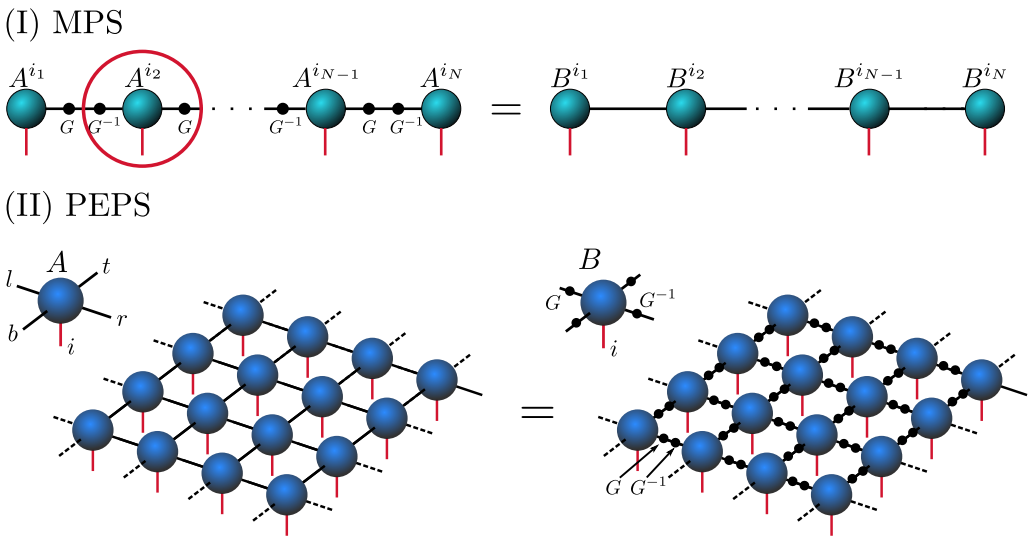

FIGURE 3.8: Gauge transformations in MPS (panel A) and PEPS (panel B) in general change the tensor generating the state $A \neq B$ but leave the state invariant $|\Psi(A)\rangle = |\Psi(B)\rangle$.

in Fig. 3.8(B), with a slight difference that there may exist two nonsingular matrices G, H such that for fixed i:

$$A^i_{trbl} = \sum_{t'r'b'l'} H_{tt'} G_{rr'} B^i_{t'r'b'l'} H^{-1}_{b'b} G^{-1}_{l'l}. \tag{3.51}$$

This may hold for certain class of PEPS [84], however according to Ref. [85] it is impossible to prove general Fundamental Theorem of PEPS, as already for 2D translationally invariant PEPS there is no algorithm capable of showing if the generated states $|\Psi(A)\rangle_N, |\Psi(B)\rangle_N$ on $N \times N$ lattice are the same for any N.

A special type of gauge transformation in 1D is the one, which brings an iMPS into an orthonormal form:

$$A_L = L \cdot A L^{-1}, \quad \text{where} \quad L^\dagger L = \sigma^L. \tag{3.52}$$

The MPS generated by tensors A_L is then called *left-orthonormal*, because the leading left eigenvector of its related transfer matrix is an identity:

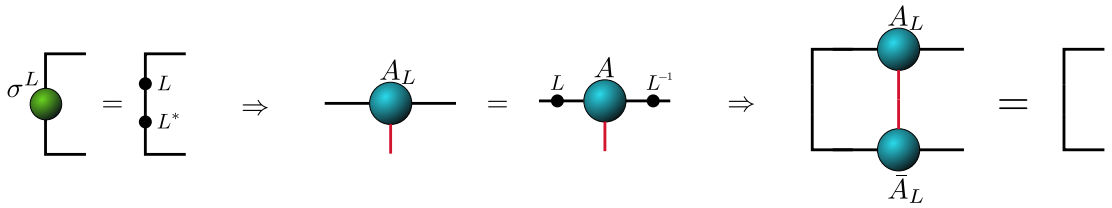

(3.53)

Similarly, the *right-orthonormal* gauge is defined:

$$A_R = RAR^{-1}, \quad \text{where} \quad R^\dagger R = \sigma^R \quad \text{and}$$

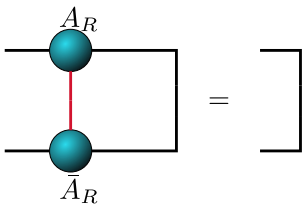

(3.54)

And finally, the mixed-canonical gauge is the one, where we choose a central site A_C, from where all tensors to the left are left-canonical and all tensors to the right are right-canonical,

and the tensor A_C fulfils the relations:

$$A_C = LAR = LAL^{-1}LR = A_L C = C A_R,$$

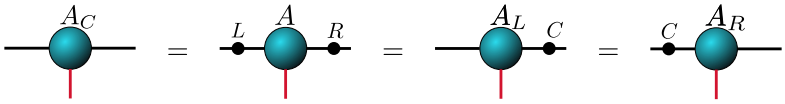

(3.55)

These transformations are sometimes referred to as gauge-fixing, however it still leaves the possibility of unitary gauge transformation, which does not affect the boundary eigenvectors, but it affects the central tensor C, for example the tensor C can be brought to the diagonal form.

Advantages of working with a canonical gauge, especially mixed-orthonormal form, follow directly from the fact that its related transfer matrix eigenvectors are identities, therefore there is no need to calculate them anymore.

Numerically, MPS can be brought to orthonormal form by calculating the eigenvectors of the MPS TM and then decomposing it, either by diagonalization or Cholesky decomposition:

$$\sigma^L = (U_L^\dagger \sqrt{g_l})\ (\sqrt{g_l}\ U_L) = L^\dagger L. \tag{3.56}$$

Then, however the final (left) orthonormal tensor A_L is obtained according to Eq. 3.52, where L^{-1} can be ill-conditioned and taking its pseudo-inverse is required. Moreover, taking the square root of the eigenvalues g_l effectively means that the error of the resulting gauge-transformation can be several orders of magnitude larger than that of the boundary density matrix $\epsilon_\sigma \to \sqrt{\epsilon_\sigma}$, which makes this method very inefficient, however sometimes necessary (see Ref. [3]). Therefore, whenever possible (especially in case of non-injective MPS, with degenerate spectrum of the TM), it is better to use repeated QR decomposition [62] until convergence, i.e. the procedure of decomposing:

$$L^{(k)} A = A_L^{(k+1)} L^{(k+1)} \tag{3.57}$$

has to be repeated until $L^{(k)} = L^{(k+1)} = L$, with a matrix $A_L^{(k)}$ of dimensions $Dd \times D$, such that $A_L^{(k)\dagger} A_L^{(k)} = 1$ and L^k an upper triangular matrix of dimensions $D \times D$. Then the converged tensor A_L is left-canonical by construction, the method does not suffer from error magnification, and it is inverse-free. Unless the aim is to know the exact form of the gauge transformation from Eq. 3.50, $\{G, G^{-1}\}$. Both of these methods of finding the gauge transformation are needed in Ref.[3] to find the exact gauge transformation, between the product of MPO symmetries $Z_a Z_b$ and a single MPO symmetry Z_c, according to the equation:

$$Z_a \cdot Z_b = \sum_c N_{ab}^c Z_c, \tag{3.58}$$

which obeys the same fusion rules as in Eq. 2.4. This gauge transformation is called a zipper X_{ab}^c, because it zips the product of iMPOs $Z_a \cdot Z_b$ into a single iMPO Z_c:

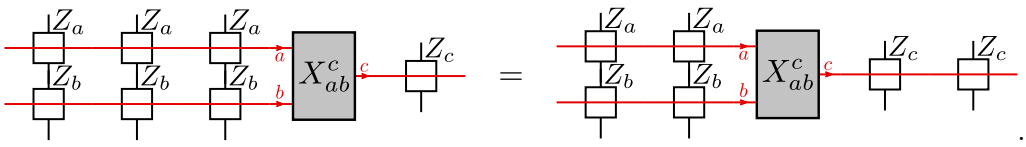

. (3.59)

It is important to stress that the labels a, b, c are the labels of iMPO symmetries $Z_{a,b,c}$ and not the labels of the indices.

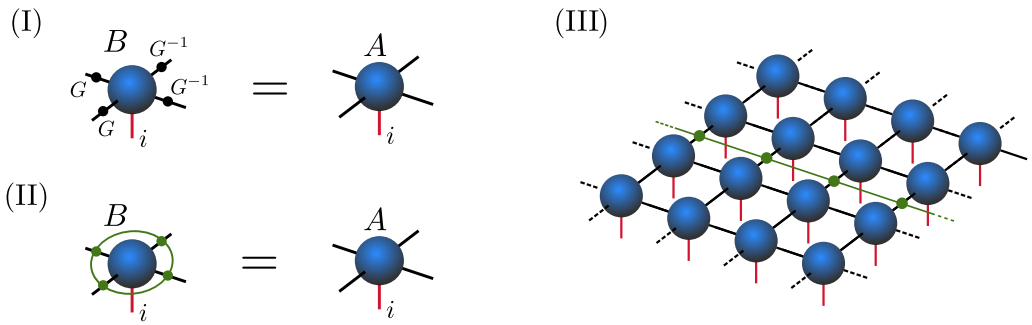

FIGURE 3.9: Symmetries in tensor networks: G-symmetry denoted by black dots representing a G matrix in (I) is a special case of MPO symmetry of PEPS in (II) with green internal bond dimension equal to 1. In (III) green iMPO symmetry of iPEPS when inserted along a single cut of the iPEPS leaves the state invariant, preserving also the translational invariance, as it can be inserted in any parallel cut. The iMPO symmetry in (III) may exist despite the tensors not being symmetric by itself like in (II).

Staying with the topic of symmetries, another special type of gauge transformation is a symmetry, when the transformation leaves the tensor itself invariant:

$$A^i = G \cdot B^i \cdot G^{-1} = B^i. \tag{3.60}$$

These virtual symmetries in tensor networks play a crucial role in the classification of phases, e.g. SPT phases in 1D and topological order in 2D. In 2D PEPS a symmetry can be just a local group element - a matrix acting on the bond indices as shown in Fig. 3.9(I). However, this is a special case of an MPO with internal bond dimension 1 and in general the MPO-symmetry of PEPS, depicted in Fig.3.9(II) can have any bond dimension (denoted by the green indices). The MPO symmetries of iPEPS Z_a are crucial objects in the study of topologically ordered systems in two dimensions with tensor networks. In Ref. [1, 2] we show how to find them numerically from generic iPEPS. Their existence is a necessary condition for the iPEPS to be topologically ordered. It is also a basic step in the construction of exact correlation length zero fixed-point wave functions of string net models with MPO-injective PEPS as shown in Ref. [86, 87, 88]. However, the exact symmetry between tensors as shown in Fig. 3.9(II) is too restrictive from the numerical point of view, and we relax it slightly to consider only infinite MPO symmetries along a single cut of the iPEPS as shown in Fig. 3.9(III), which does not require keeping the tensors symmetric in any way during the iPEPS ground state optimization. Later the symmetries are used to check the fusion ring according to Eq. 3.58, which allows for the construction of either projectors onto MES as in Ref. [1, 2], or zipper tensors X^c_{ab} as in Ref. [3], which are used to find the F-symbols of the underlying unitary fusion category C:

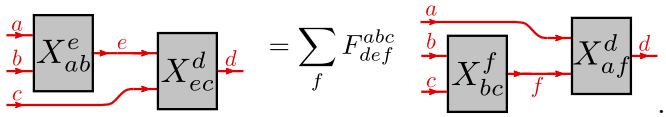

. (3.61)

3.5 Topological order with tensor networks

Initial studies of spin liquids (SL) in frustrated models, especially in the spin-$\frac{1}{2}$ Heisenberg antiferromagnet:

$$H = J \sum_{<i,j>} \mathbf{S}_i \cdot \mathbf{S}_j \tag{3.62}$$

on kagome lattice (see Fig.3.10) were performed using quasi 2D DMRG on finite tori[89], thus leading to large truncation erros [29, 90]. Since Ref. [90] 2D DMRG on long cylinders instead became the common practice in the study of ground states of such highly frustrated models in the possible spin liquid phase. In Ref.[90] the maximal circumference of $c = 12$ lattice sites allowed for correlation length $\xi = 1.5$ lattice spacings and concluded that the ground state is a gapped spin liquid which could be represented by a *resonating valence bond* – RVB state, first proposed by Anderson [91]. Later study [92] on cylinder with circumference up to $c = 17$ lattice sites and short correlation length $\xi \simeq 1$ revealed a gapped nonchiral $\mathbb{Z}_2$ spin liquid via calculation of energy gap, exponential decay of 2-point correlation functions as well as topological entanglement entropy (TEE) yielding $\gamma = \log(2)$ at the non-trivial cut across the cylinder. However, apart from few physical arguments, it does not fully exclude the possibility of double-semion spin liquid. It was pointed out that for unique characterization of the nature of the ground state of spin-$\frac{1}{2}$ Heisenberg antiferromagnet on kagome lattice one would need to calculate the overlaps between minimally entangled states (MES) in different directions in order to obtain the topological S and T matrices [22]. The big advantage of 2D DMRG on long cylinders is that a single energy optimization naturally chooses one of the MES along the cylinder [93] (see Fig. 3.11). On the other hand, the optimization may be biased towards only one of the ground states, falsely suggesting no topological ground state degeneracy but at the same time exhibiting non-trivial TEE.

The discovery of gapped $\mathbb{Z}_2$ SL in the kagome Heisenberg antiferromagnet, although later challenged by the studies using iPEPS [94], started the interest in the realistic frustrated Heisenberg materials on different lattices and with different coupling ranges, yielding chiral spin liquid in kagome Heisenberg model with second and third-nearest neighbour (NN) interactions [95, 96], with a phase transition towards the known gapped $\mathbb{Z}_2$ SL in the limit of disappearing second and third NN interactions (see Fig.3.10). The existence of gapped $\mathbb{Z}_2$ SL was also confirmed in spin-$\frac{1}{2}$ $J_1 - J_2$ Heisenberg model on triangular lattice in the intermediate range of the J_2/J_1 ratio. On the other hand, 2D DRMG studies on long cylinders excluded the existence of spin liquid in the spin-$\frac{1}{2}$ honeycomb $J_1 - J_2$ Heisenberg model [97], as well as in frustrated XY models on the honeycomb lattice [98].

In the meantime a robust numerical method of characterizing topological order starting from general lattice Hamiltonian using infinite 2D DMRG, based on the calculation of topological S and T matrices, as well as gapless edge theory (in case of CSL) was proposed in Ref. [99]. Together with a systematic method of accessing all topological sectors with the iDMRG [100] it remained the method of choice to study different frustrated models, like spin-$\frac{1}{2}$ XXZ kagome antiferromagnets, where first, second and third NN anisotropic Heisenberg-like interactions on kagome lattice allow phase transition to the chiral semion model [101] or bosonic fractional quantum Hall system with emerging Ising anyons in the non-Abelian Moore-Read state [102].

Despite vast theoretical research on quantum spin liquids, their experimental realization is generally very elusive, even up to now, due to non-existence of a single experimental feature distinguishing QSL [103]. Materials, which are more likely to exhibit QSL at low temperatures are those characterized by e.g. large frustration parameter or continuum excitation spectra inferred from elastic and inelastic scattering measurements. Such features

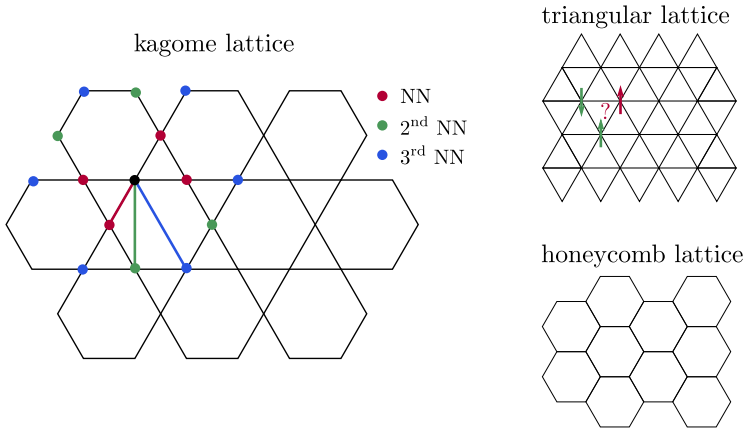

FIGURE 3.10: Kagome, triangular and honeycomb lattices. On the kagome lattice, red dots denote nearest neighbours to the black dot, green dots – second NN and third NN are shown with blue dots. On kagome and triangular lattices, geometric frustration (demonstrated by the arrows on the triangular lattice: two green arrows are the lowest energy spin configurations in case of antiferromagnetic interaction, but then the third red arrow will always increase the energy, whichever direction it is placed) plays a crucial role in the creation of so-called spin liquids.

were first observed in α-$RuCl_3$ using polarized Raman scattering [104] and inelastic neutron scattering experiments [105, 106, 107]. Motivated by the experimental results, Ref. [108] performed iDMRG simulations on infinite cylinders with circumference $L_{circ} = 6$ lattice sites of the effective $K-\Gamma$ model:

$$\begin{aligned} H \;=\; \sum_{\langle ij\rangle\in x} K_x S_i^x S_j^x + \Gamma_x(S_i^y S_j^z + S_i^z S_j^y) + \sum_{\langle ij\rangle\in y} K_y S_i^y S_j^y + \Gamma_y(S_i^x S_j^z + S_i^z S_j^x) + \\ \sum_{\langle ij\rangle\in y} K_z S_i^z S_j^z + \Gamma_z(S_i^x S_j^y + S_i^y S_j^x), \end{aligned} \tag{3.63}$$

with K being the Kitaev interaction and Γ symmetric-anisotropic interactions, which were considered most likely dominant interactions in α-$RuCl_3$. The numerical results revealed high entanglement entropy and no sign of magnetic order for arbitrary ratio Γ/K with ferro-like Kitaev interaction, which together with the existence of coherent two-dimensional multi-particle excitations inferred from the transfer matrix spectrum, provided evidence for QSL. Final experimental confirmation of the Kitaev spin liquid in α-$RuCl_3$ compound came with the observation of quantization of thermal Hall conductance after the parallel magnetic field is applied [8], which opens the gap in the energy spectrum and leads to a non-Abelian phase with chiral thermal edge current [10]. Another DMRG studies [109, 110] focused on the phase diagram of pure Kitaev model on honeycomb lattice coupled to the magnetic field:

$$H \;=\; \sum_{\langle i,j\rangle} K_\gamma S_i^\gamma S_j^\gamma - \sum_i \mathbf{H}\cdot\mathbf{S}_i, \tag{3.64}$$

revealing gapped non-Abelian topological phase for very weak magnetic fields in the case of ferromagnetic Kitaev interactions, $H^{FM} < 0.02$, and a much more stable topologically ordered phase for antiferromagnetic Kitaev interactions, $H^{AFM} < 0.2$. Ref. [110] performed their analysis on cylinders with circumference $L_{circ} = 6$ and $L_{circ} = 10$ lattice sites and confirmed the existence of the non-Abelian topological phase by measurement of topological entanglement entropy, yielding 2 Abelian anyons with quantum dimensions

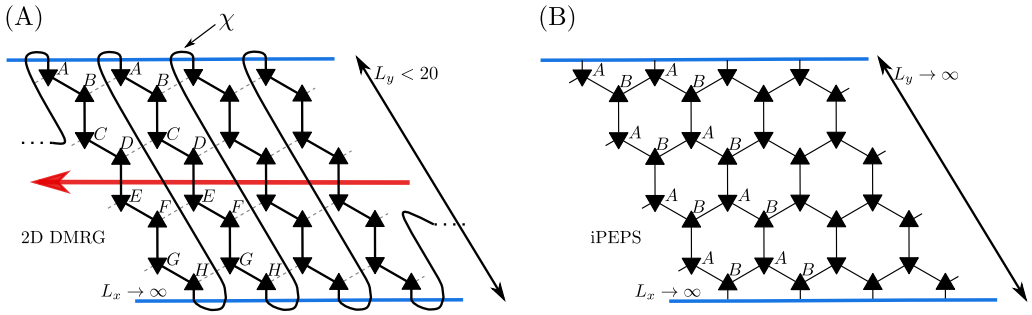

FIGURE 3.11: In (A) 2D DMRG on an infinite cylinder of circumference of 8 lattice sites, where an MPS has to be wrapped around the cylinder in a snake-like pattern. Single energy minimization on long or infinite cylinders minimizes the entanglement entropy along the cylinder, therefore it yields a minimally entangled state. The bond dimension χ grows exponentially with the circumference, as it has to accommodate the interactions between the nearest neighbour sites, denoted by grey dashed lines. On the other hand, the bonds in iPEPS in (B) connect the neighbouring sites by construction, therefore allowing for the simulation of systems in the thermodynamic limit.

$d_A = 1$ and one non-Abelian with quantum dimension $d_{nA} = \sqrt{2}$, which corresponds to Ising anyons. Thanks to the discretized time-evolution using matrix product operator, the dynamical spin-structure factor can be calculated, thus providing information about the excitation spectrum and gap opening when the magnetic field is applied, which can be directly compared with the data from inelastic neutron scattering experiments.

Despite its remarkable success, the 2D DMRG on infinite cylinders allows for the efficient analysis of topologically ordered states with correlation lengths up to $\xi \simeq 1-2$ lattice sites, but with direct access to all minimally entangled states, as well as edge entanglement spectra, Fig. 3.11(A). In case of competing low energy eigenstates, which are completely different in nature, 2D DMRG may be biased towards those, which are lower in energy on a finite system but not necessarily in the thermodynamic limit. This is probably the case with the aforementioned Heisenberg antiferromagnet on Kagome lattice, in which case, the recent study with a variant of 2D TNS favours gapless SL with $U(1)$ symmetry in the thermodynamic limit [94]. There, it is also argued that enforcing symmetries of tensors in the ground state optimization may in fact lead to the excited states.

Therefore, a natural extension of an unbiased method of determining topological order to 2D systems with arbitrary long correlation length was desirable and could be achieved with a tensor network, which is 2D by construction – infinite PEPS, Fig. 3.11(B). However, unlike in 2D DMRG case, single energy optimization of iPEPS leads to a superposition of different MES along different directions, hence the first step towards the characterization of topological order with iPEPS has to be the extraction of different degenerate anyonic sectors before the calculation of modular data (topological S and T matrices). This task was accomplished for Abelian anyon models in Ref.[1] as well as non-Abelian ones in Ref. [2] by algebraic manipulations of variationally optimized iMPO symmetries of iPEPS (see section 3.4, Fig. 3.9(III)), where the correct modular data can be obtained for models with correlation lengths an order of magnitude larger than with 2D DMRG, $\xi \simeq 10-15$.

In the meantime, a similar study of $\mathbb{Z}_2$ topological order via unbiased iPEPS simulations appeared [111]. There is also no a priori imposed symmetry of the tensors, like in Refs. [112, 113, 114], but instead after the iPEPS optimization the PEPS tensors are brought to a gauge in which they exhibit an approximate virtual $\mathbb{Z}_2$ symmetry and later are additionally symmetrized to obtain a stable topological order with non-trivial TEE also for very large cylinder sizes.

Although modular data does not uniquely determine all possible topological orders [21], it is sufficient in case of most common models analysed in Ref.[1, 2]. Indeed, the unequivocal description of topological order starting from iPEPS can be obtained by application of fundamental theorem of MPS [47] to variationally optimized iMPO symmetries Z_a and extraction of F-symbols of the underlying unitary fusion category (see section 2.3), from the associativity of multiplication of iMPO symmetries – the task accomplished in Ref.[3].

The analysis of topological order with iPEPS was tested on many non-chiral examples, and it is not yet known whether there exist an iPEPS description of a gapped chiral topologically ordered state. On the contrary, there exist a no-go theorem [115] prohibiting existence of a gapped fermionic Gaussian PEPS, however it does not imply criticality in the interacting case. While Refs. [116] and [117] made an approach towards the description of the chiral non-Abelian topologically ordered ground state of Kitaev Spin Liquid, our analysis in Ref. [2] shows that the ansatz for the chiral topological order from Ref. [116] rather describes an Abelian toric code phase. A more promising ansatz is given in Ref. [117], where the Kitaev model on a honeycomb-triangular lattice is studied and the numerically obtained edge entanglement spectrum is consistent with the theoretical expectations for the non-Abelian Ising anyons. However, according to Ref. [118] the gap opens in the second order perturbation expansion, yielding the non-Abelian anyons while Ref. [117] takes into account terms in the first order in their ansatz. However, Ref. [119], claims to have used successfully the ansatz from Ref. [116] in order to simulate $K-\Gamma-\Gamma'$ model. As the Kitaev model itself is not enough to capture all possible interactions in α-$RuCl_3$, which displays zig-zag (ZZ) magnetic order at low temperatures, the minimal models considered in the theoretical studies are $K-\Gamma-\Gamma'$ and $K-\Gamma-J_3$, where K stands for Kitaev interactions, Γ is the anisotropic-symmetric interaction as in Eq. 3.63, and interactions responsible for the ZZ ordering: anisotropic Γ' or Heisenberg interaction J_3.

$$H=\sum_{<ij>_\gamma} H_{ij}^{\gamma}, \quad H_{ij}^{\gamma}=-\frac{\mathbf{h}}{3}\cdot(\mathbf{S}_i+\mathbf{S}_j)+KS_i^{\gamma}S_j^{\gamma}+\Gamma(S_i^{\mu}S_j^{\nu}+S_i^{\nu}S_j^{\mu})+ \\ \Gamma'(S_i^{\mu}S_j^{\gamma}+S_i^{\gamma}S_j^{\mu}+S_i^{\nu}S_j^{\gamma}+S_i^{\gamma}S_j^{\nu}), \tag{3.65}$$

where $<ij>$ denotes nearest neighbour on the bonds $\gamma=x,y,z$, with (γ,μ,ν) forming cyclic permutations of (x,y,z). In Ref.[119] Γ' is small, the Kitaev interaction is ferromagnetic $K<0$ while the $\Gamma>0$ is antiferromagnetic, which are relevant interactions for α-$RuCl_3$ compound. The optimization, using imaginary time evolution, and measurements of energy, magnetization and plaquette operator of the Kitaev model [10] reveals 5 distinct phases, among which a small region of phase diagram correspond to the chiral KSL phase (KSL regime seems to be smaller than the one revealed by previous studies with ED and DRMG, suggesting that finite sizes of the cylinders strongly influence the results). The focus of Ref. [119] is however on the exact phase diagram of the $K-\Gamma-\Gamma'$ model and the only indicator of the chiral KSL seems to be the plaquette operator:

$$W_p=\sigma_1^x\sigma_2^y\sigma_3^z\sigma_4^x\sigma_5^y\sigma_6^z\approx 1, \tag{3.66}$$

and no magnetization $m<\frac{1}{2}$, which again just puts this phase into the general spin-liquid box.

It still remains unclear whether iMPO symmetries can be applied to chiral topological order, and it is to be seen whether the method introduced in [1, 2], based on the calculation of topological S and T matrices, is capable of determining chiral topological order or not.

Chapter 4

Articles

To summarize all the scattered information about the following articles [1, 2, 3] throughout the previous chapters, let me conclude with the main results.

In the following, we provide a robust numerical method of determining topological order, starting from a lattice Hamiltonian, without a priori assuming any symmetries, which could potentially influence the result and in the thermodynamic limit to avoid finite-size effects. We use iPEPS TN methods to find the ground state $|\Psi_g\rangle$ of a Hamiltonian of interest and use the iMPS techniques to contract and analyse the resulting state. The choice of iPEPS in contrast to 2D DMRG allows working with states which have a correlation length order of magnitude larger $\xi_{PEPS} \approx 10\ \xi_{MPS}$. Moreover, TN representation of the topologically ordered ground state provides enough information to fully characterize the phase of the system, together with its excitations, due to the direct access to the entanglement properties, so that all the states exhibiting no long-range order do not have to be put into the same spin liquid box.

In the first two articles [1, 2] we determine the topological order via modular data (S, T, c) introduced in Section 2.2, while in the third article we show how to calculate the F symbols of the underlying unitary fusion category introduced in Section 2.3. The first steps in both cases are the same. We proceed by numerically finding the iMPO symmetries Z_a of the iPEPS ground state $|\Psi_g\rangle$, which are operators acting between different boundary fixed points $|v_i^{L,R}\rangle$ of the iPEPS transfer matrix Ω:

$$\Omega = \sum_{i=1}^{n} |v_i^R)(v_i^L| \qquad \Rightarrow \qquad \forall a \quad Z_a|v_1^L) = |v_a^L), \quad (Z_a)^T|v_1^R) = |v_{\bar{a}}^R) \tag{4.1}$$

where n is the degeneracy of Ω and we admit the situation that the action of Z_a on the left eigenvector $|v_1^L)$ in general is not the same as the action of the transpose $(Z_a)^T$ on the right eigenvector $|v_1^R)$, hence the label $\bar{a}$. The multiplication of iMPO symmetries forms the fusion ring:

$$Z_a Z_b = \sum_c N_{ab}^c Z_c, \tag{4.2}$$

where the coefficients N_{ab}^c correspond to the fusion rules of anyons of the input category. This data is not yet enough to distinguish different topological orders, e.g. toric code and double semion models. From this point, the two methods diverge. In the case of modular data, the fusion ring in Eq. 4.2 allows constructing projectors P_a onto minimally entangled states in one of the directions on the torus. Due to the fact that initial degeneracy n of iPEPS TM Ω is not yet the full degeneracy of $|\Psi_g\rangle$, we need to project onto one of the MES in one direction to gain access to the full spectrum in the other direction. Therefore, we introduce the impurity transfer matrix $\tilde{\Omega}$, where the impurities are the iMPO projectors P_a inserted into iPEPS bond indices and repeat the previous steps of finding the impurity eigenvectors $|\tilde{v}_i\rangle$, and impurity iMPO symmetries and finally all the projectors $\tilde{P}_a$ onto all

MES $\{|\tilde{\Psi}\rangle\}$:

$$|\Psi_g\rangle \xrightarrow{\Omega,\ |v_i\rangle,\ Z_a} \{|\Psi_a\rangle\}_{a=1}^{n} \xrightarrow{\tilde{\Omega},\ |\tilde{v}_i\rangle,\ \tilde{Z}_a} \{|\tilde{\Psi}_a\rangle\}. \tag{4.3}$$

We perform the procedure on different tori, related by a modular $\mathfrak{st}$ transformation in order to calculate overlaps between all the MES on those tori, which yields the topological S and T matrices:

$$(S \cdot T)_{ab} = \langle \tilde{\Psi}_b^{\mathfrak{st}} | \tilde{\Psi}_a \rangle. \tag{4.4}$$

In the second method, after finding the iMPO symmetries Z_a and their fusion rules, we find the gauge transformation, so-called zipper tensors X_{ab}^c, which fuse a product of two iMPO symmetries $Z_a Z_b$ into a single iMPO Z_c:

$$(X_{ab}^c)^{-1}\ (Z_a Z_b)\ X_{ab}^c = Z_c \tag{4.5}$$

Then, using the associativity condition we calculate the F-symbols of the UFC $\mathcal{C}$:

$$(Z_a Z_b) Z_c = Z_a (Z_b Z_c) \quad \Rightarrow \quad (X_{ab}^e \otimes \mathbf{1}_c) X_{ec}^d = \sum_f F_{def}^{abc} (\mathbf{1}_a \otimes X_{bc}^f) X_{af}^d. \tag{4.6}$$

Later, purely algebraic manipulations allow us to obtain the center of the UFC $Z(\mathcal{C})$ and again topological S and T matrices.

We successfully applied the first methods to both Abelian: toric code and double semion fixed point string-net models, toric code string net model with perturbation as well as the Kitaev model on honeycomb lattice in the gapped regime, and non-Abelian models: fixed point and perturbed double Fibonacci and double Ising models, yielding correct modular data with a good accuracy. As a direct consequence of having the explicit formulas of the projectors onto MES we were able to obtain precise results of topological entanglement entropy γ without the need of extrapolations. The second method seems even simpler, because it consists of fewer steps and apart from the first step of calculating the eigenvectors of the iPEPS TM, it uses only methods of 1D tensor networks. Similarly, as the first method, it was successfully applied to the aforementioned models, as well as the twisted quantum double of Z_3 string-net model and two different representation of quantum double of S_3 string-nets.

Rapid Communications

Determining topological order from infinite projected entangled pair states

Anna Francuz,[1] Jacek Dziarmaga,[1] Guifre Vidal,[2,3] and Lukasz Cincio[4,*]
[1]*Institute of Physics, Jagiellonian University, Łojasiewicza 11, PL-30348 Kraków, Poland*
[2]*Perimeter Institute for Theoretical Physics, Waterloo, Ontario, Canada N2L 2Y5*
[3]*X, The Moonshot Factory, Mountain View, California 94043, USA*
[4]*Theory Division, Los Alamos National Laboratory, Los Alamos, New Mexico 87545, USA*

(Received 1 November 2019; revised manuscript received 24 December 2019; published 21 January 2020)

We present a method of extracting information about the topological order from the ground state of a strongly correlated two-dimensional system computed with the infinite projected entangled pair state (iPEPS). For topologically ordered systems, the iPEPS wrapped on a torus becomes a superposition of degenerate, locally indistinguishable ground states. Projectors in the form of infinite matrix product operators onto states with well-defined anyon flux are used to compute topological S and T matrices (encoding mutual and self-statistics of emergent anyons). The algorithm is shown to be robust against a perturbation driving string-net toric code across a phase transition to a ferromagnetic phase. Our approach provides accurate results near quantum phase transition, where the correlation length is prohibitively large for other numerical methods. Moreover, we used numerically optimized iPEPS describing the ground state of the Kitaev honeycomb model in the toric code phase and obtained topological data in excellent agreement with theoretical prediction.

DOI: 10.1103/PhysRevB.101.041108

Introduction. Topologically ordered phases [1] have in recent years attracted significant attention, mostly due to the fact that they support anyonic excitations—exotic quasiparticles that obey fractional statistics. They are of interest not only from a fundamental perspective but also because of the possibility of realizing fault-tolerant quantum computation [2] based on the braiding of non-Abelian anyons. An important challenge is to identify microscopic lattice Hamiltonians that can realize such exotic phases of matter. Apart from a number of exactly solvable models [2–4], verifying whether a given microscopic Hamiltonian realizes a topologically ordered phase and accessing its properties has traditionally been regarded as an extremely hard task.

A leading computational approach is to use density matrix renormalization group (DMRG) [5,6] on a long cylinder [7–20]. In the limit of infinitely long cylinders, DMRG naturally produces ground states with well-defined anyonic flux, from which one can obtain full characterization of a topological order, via so-called topological S and T matrices [21]. Since the proposal of Ref. [21], the study of topological order by computing the ground states of an infinite cylinder with DMRG has become a common practice [22–39].

The cost of a DMRG simulation grows exponentially with the width of cylinder, effectively restricting this approach to thin cylinders. Instead, (infinite) projected entangled pair states (iPEPS) allow for much larger systems [40–42]. However, (variationally optimized) iPEPS naturally describe ground states with a superposition of anyonic fluxes. Here we show, starting with one such PEPS, how to produce a PEPS-like tensor network for each ground state with well-defined flux. Such tensor networks are suitable for extracting topological S and T matrices by computing overlaps between ground states.

Our approach does not assume a clean realization of certain symmetries on the bond indices, in contrast to [43–46]. It also has much lower cost than methods based on the tensor renormalization group [47].

In this Rapid Communication we employ a variational method to minimize the energy of the iPEPS [48]. The optimized state is then wrapped on a torus and the boundary conditions (with respect to the symmetry acting on the bond indices of PEPS) are suitably modified to recover all anyonic sectors. Figure 1 presents an overview of our approach. Computations are performed in the limit of an infinitely large torus allowing for accurate description of a topologically ordered phase even for models displaying a large correlation length. For clarity, we specialize the construction to PEPS describing the toric code realized by a string-net model on a honeycomb lattice [4]. The method can be applied to other Abelian anyon models, as discussed below, and extended to non-Abelian ones [49].

In the toric code, the entanglement spectrum along the topologically nontrivial cut of a torus is supported on a vector space, which is a direct sum of four sectors, corresponding to the identity $\mathbb{I}$, bosonic e and m, and fermionic ϵ fluxes:

$$\mathbb{V}^{\mathrm{TC}} = \mathbb{V}^{\mathbb{I}} \oplus \mathbb{V}^{e} \oplus \mathbb{V}^{m} \oplus \mathbb{V}^{\epsilon}. \tag{1}$$

We proceed by constructing projectors on ground states with definite anyon flux. The projectors are optimized and represented by matrix product operators (MPOs). When inserted into PEPS and wrapped on the torus, the optimal MPO projects onto the desired ground state. Topological S and T matrices are extracted [50,51] by calculating overlaps between states with well-defined flux on tori related by modular transformations.

*Corresponding author: lcincio@lanl.gov

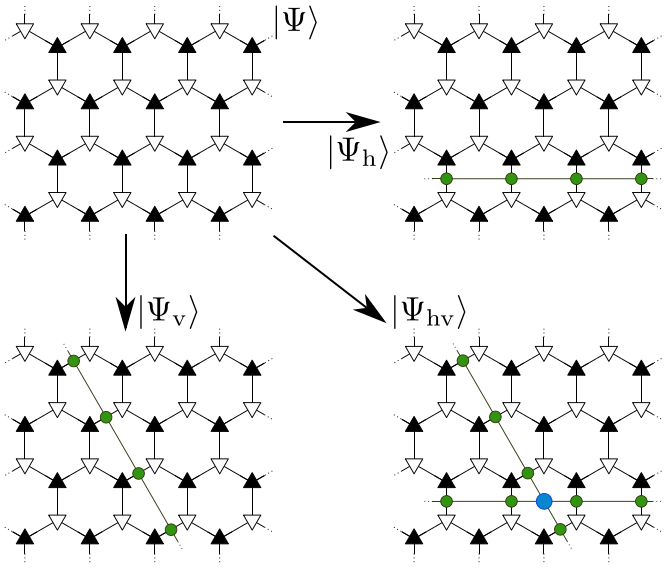

FIG. 1. A set of states $|\Psi_{\rm v}\rangle$, $|\Psi_{\rm h}\rangle$, $|\Psi_{\rm hv}\rangle$ is constructed from a single PEPS $|\Psi\rangle$ by inserting various MPOs in its bond indices. For a topologically ordered phase (toric code on a honeycomb lattice in this example), a proper combination of four states $|\Psi\rangle$, $|\Psi_{\rm v}\rangle$, $|\Psi_{\rm h}\rangle$, and $|\Psi_{\rm hv}\rangle$ is used to construct a basis of states with well-defined anyonic flux in a given direction. Physical indices are not drawn for simplicity. See text for details.

Transfer matrices and their eigenvectors. PEPS for a toric code on a honeycomb lattice may be characterized by two tensors A and B with elements A^i_{abc} and B^i_{abc}, respectively. Here, i is a physical index and a, b, c are bond indices. Let $\mathbb{A}$ and $\mathbb{B}$ denote double tensors $\mathbb{A} = \sum_i A^i \otimes (A^i)^*$ and $\mathbb{B} = \sum_i B^i \otimes (B^i)^*$ with double bond indices $\alpha = (a, a')$, etc. [see Fig. 2(a)]. PEPS transfer matrix (TM) Ω is defined by a line of tensors $\mathbb{A}$ and $\mathbb{B}$ contracted via some of their indices, as shown in Fig. 2(b).

For a toric code PEPS we observe that Ω contains a direct sum of $n = 2$ topological sectors. Thus, the reduced density matrix on the virtual indices (which is directly related to the physical reduced density matrix [52]) at a topologically nontrivial cut is a direct sum of two contributions

$$\mathbb{V}_{\rm cut} = \mathbb{V}^{\mathbb{I}} \oplus \mathbb{V}^{e} \;\Rightarrow\; \rho_{\rm cut} = \rho^{\mathbb{I}} \oplus \rho^{e} \tag{2}$$

(recall that the ground state degeneracy of a toric code on a torus is $n^2 = 4$). The use of a pure MPS [53] as an ansatz for

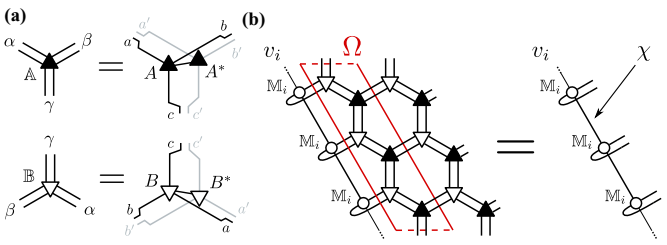

FIG. 2. (a) Graphical representation of double tensors $\mathbb{A}$ and $\mathbb{B}$. (b) Left eigenvector v_i of vertical TM Ω takes an MPO form. Vector v_i is constructed with a single tensor $\mathbb{M}_i$ with bond dimension χ, for $i = 1, 2$ and is obtained using a boundary MPS method described in detail in Appendix A of the Supplemental Material [55].

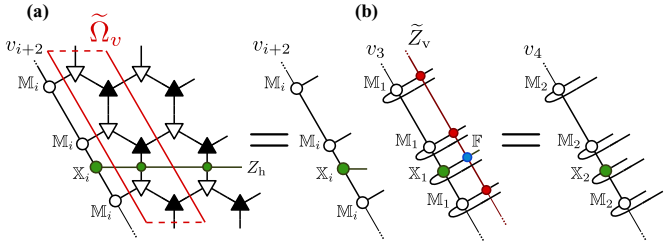

FIG. 3. (a) Two eigenvectors v_3 and v_4 are obtained as pure MPOs from v_1 and v_2 by introducing additional tensors $\mathbb{X}_1$ and $\mathbb{X}_2$, which are obtained variationally. Tensors $\mathbb{X}_i$ are chosen such that v_3 and v_4 are leading eigenvectors of "impurity" TM $\widetilde{\Omega}_{\rm v}$. Double lines are dropped to improve clarity. (b) Graphical illustration of one of the conditions for $\widetilde{Z}_{\rm v}$ in Eq. (8).

the dominant eigenvectors v_1, v_2 of Ω selects a specific linear combination of sectors. We note that only the method based on boundary MPS (presented here) is capable of breaking the degeneracy of the dominant eigenvectors into minimally entangled states. Methods based on corner transfer matrix treat vertical and horizontal directions on the same footing and therefore will not select a minimally entangled state in a given direction. Numerically, eigenvectors v_i may be obtained using a power method or by more advanced approaches such as the VUMPS algorithm [54] (see Appendix A of the Supplemental Material [55] for details). In the diagonal basis, they take the following form:

$$v_1 = \rho^{\mathbb{I}} \oplus \rho^{e}, \quad v_2 = \rho^{\mathbb{I}} \oplus -\rho^{e}, \tag{3}$$

where we regard vector v_i as an operator represented by an MPO constructed with a single tensor $\mathbb{M}_i$ as shown in Fig. 2(b). Here, $\rho^{\mathbb{I}}$ and ρ^{e} are boundary density matrices in identity and bosonic sectors, respectively. For clarity, we omitted the fact that vectors v_i may contain a zero component, that is, $v_1 = \rho^{\mathbb{I}} \oplus \rho^{e} \oplus 0$ and similarly for v_2. This leads to numerical instabilities and other complications that we discuss in detail in Appendix A of the Supplemental Material [55].

Matrix product description of v_1 and v_2 allows us to find an operator $Z_{\rm v}$ in the form of an MPO that maps v_1 into v_2 and back by demanding that

$$v_1 Z_{\rm v} = v_2, \quad Z_{\rm v} v_2 = v_1. \tag{4}$$

In the diagonal basis of Eq. (3), $Z_{\rm v} = \mathbb{I} \oplus -\mathbb{I}$. We stress that we are able to obtain the generator of the global $\mathbb{Z}_2$ "spin-flip" symmetry that acts on the bond indices of PEPS, even though the symmetry is not realized on site. In other words, PEPS tensors A and B do not have to be symmetric, as required in [43–46], for our construction to work.

Similarly, we define horizontal TM $\Omega_{\rm h}$ and obtain its $n = 2$ degenerate leading eigenvectors h_1 and h_2. Again, we are able to find an operator $Z_{\rm h}$ such that

$$h_1 Z_{\rm h} = h_2, \quad Z_{\rm h} h_2 = h_1. \tag{5}$$

Finally, we build vertical "impurity" TM $\widetilde{\Omega}_{\rm v}$ by inserting the $Z_{\rm h}$ operator on a horizontal cut of PEPS, as shown in Fig. 3(a). $Z_{\rm h}$ implements antiperiodic boundary conditions with respect to $\mathbb{Z}_2$ "spin-flip" symmetry acting in the PEPS bond indices. Note that, even if the $\mathbb{Z}_2$ symmetry is not

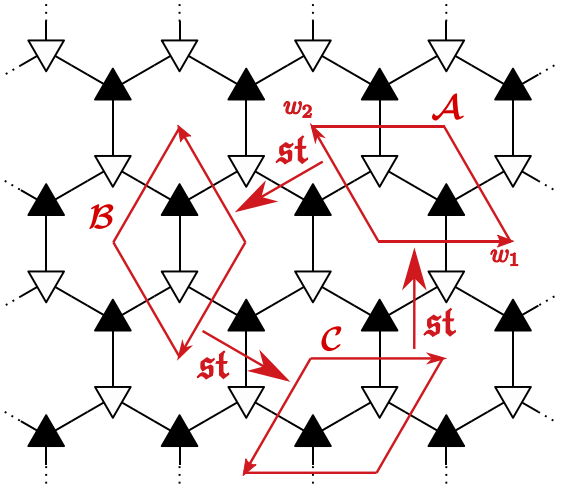

FIG. 4. Three tori $\mathcal{A}$, $\mathcal{B}$, and $\mathcal{C}$ on a honeycomb lattice considered in our method. Torus $\mathcal{A}$ is defined by a pair of vectors (w_1, w_2). Each torus is obtained by $\mathfrak{st}$ modular transformation from another torus. Transformation $\mathfrak{st}$ corresponds to 120° rotation, $(\mathfrak{st})^3 = \mathbb{I}$. The described approach requires 120° rotation symmetry of the lattice. Generalization to other symmetries is straightforward. Physical indices are not drawn for simplicity.

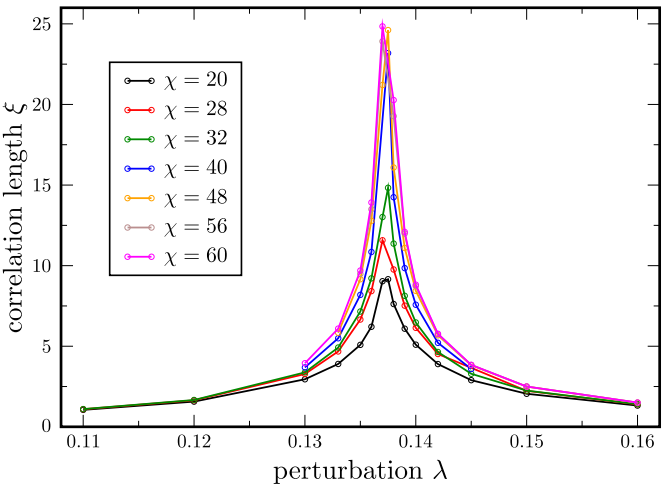

FIG. 5. Correlation length ξ as a function of perturbation strength λ and a bond dimension χ of the TM eigenvectors v_i. Increasing χ reveals a quantum phase transition at $\lambda = 0.137\ldots0.138$. It separates toric code and ferromagnetic phases.

realized on site, we still know that Z_h changes the boundary conditions from periodic to antiperiodic. Thus, inserting Z_h allows us to access two remaining sectors

$$\widetilde{\mathbb{V}}_{\text{cut}} = \mathbb{V}^m \oplus \mathbb{V}^\epsilon \;\Rightarrow\; \widetilde{\rho}_{\text{cut}} = \rho^m \oplus \rho^\epsilon. \tag{6}$$

As expected, we find $n = 2$ leading eigenvectors of $\widetilde{\Omega}_v$ that in some basis take the form

$$v_3 = \rho^m \oplus \rho^\epsilon, \quad v_4 = \rho^m \oplus -\rho^\epsilon. \tag{7}$$

Eigenvectors v_3 and v_4 are obtained as pure MPOs [53] from v_1 and v_2 by allowing for additional tensors $\mathbb{X}_i$, as depicted in Fig. 3(a). Note that tensors $\mathbb{X}_i$ are obtained variationally. In the limit of vanishing correlation length ξ in the toric code PEPS studied here, the above ansatz for v_3 and v_4 becomes exact. In other models, bond dimension χ of all v_i is increased to account for potentially large ξ. Our ansatz is validated by the results presented below. There, the correlation length $\xi \approx 25$ does not significantly impact the quality of the final result (see Fig. 5 and the discussion below it).

$\mathbb{Z}_2$ symmetry acting on the antiperiodic sectors is realized by an operator $\widetilde{Z}_v$ satisfying

$$v_3\widetilde{Z}_v = v_4, \quad \widetilde{Z}_v v_4 = v_3. \tag{8}$$

The construction of $\widetilde{Z}_v$ mirrors that of v_3 and v_4. $\widetilde{Z}_v$ is obtained from Z_v by allowing for additional variational tensor $\mathbb{F}$. Figure 3(b) shows one condition from Eq. (8) that is used to compute $\mathbb{F}$. $\mathbb{F}$ is one of the generators of C^* algebra, from which central idempotents can be found [44].

Appendix A of the Supplemental Material [55] details some numerical issues associated with finding vectors v_i, $i = 1, \ldots, 4$ as well as solving Eqs. (4) and (8).

Projectors onto definite anyon fluxes. Symmetry group generators Z_v and $\widetilde{Z}_v$ can be used to construct ground states with well-defined flux in the horizontal direction. Recall that Z_v realizes $\mathbb{Z}_2$ symmetry in the periodic sector $\mathbb{V}^{\mathbb{I}} \oplus \mathbb{V}^e$. Operators $P^\pm = (\mathbb{I} \pm Z_v)/2$ are thus projectors on definite anyonic sectors and states

$$|\Psi^{\mathbb{I}}\rangle \sim |\Psi\rangle + |\Psi_v\rangle\,, \quad |\Psi^e\rangle \sim |\Psi\rangle - |\Psi_v\rangle \tag{9}$$

have well-defined identity and electric flux in the horizontal direction, respectively. Note that projectors $P^\pm$ do not act on the physical Hilbert space. Instead, they are defined on the bond indices of PEPS. The above construction is summarized in Fig. 1. Here, $|\Psi\rangle$ denotes the initial PEPS state and $|\Psi_v\rangle$ is the state obtained by inserting Z_v into bond indices of PEPS that defines $|\Psi\rangle$. We remark that projectors $P^\pm$ play the same role as projector MPO's in the construction of MPO-injective PEPS [44].

Similarly, $\widetilde{Z}_v$ generates the $\mathbb{Z}_2$ symmetry group in the antiperiodic sector $\mathbb{V}^m \oplus \mathbb{V}^\epsilon$. It defines projectors $\widetilde{P}^\pm = (\mathbb{I} \pm \widetilde{Z}_v)/2$. States with well-defined magnetic $|\Psi^m\rangle$ and fermionic $|\Psi^\epsilon\rangle$ flux are obtained by first changing the boundary conditions on the bond indices with Z_h and then projecting onto the proper subspace. That is,

$$|\Psi^m\rangle \sim |\Psi_h\rangle + |\Psi_{hv}\rangle, \quad |\Psi^\epsilon\rangle \sim |\Psi_h\rangle - |\Psi_{hv}\rangle, \tag{10}$$

where $|\Psi_h\rangle$ stands for $|\Psi\rangle$ with Z_h inserted and $|\Psi_{hv}\rangle$ denotes $|\Psi_h\rangle$ that has $\widetilde{Z}_v$ embedded in together with the tensor $\mathbb{F}$. Figure 1 summarizes the construction of $|\Psi_h\rangle$ and $|\Psi_{hv}\rangle$.

Topological S and T matrices. States $|\Psi^i\rangle$ with well-defined flux $i = \mathbb{I}, e, m, \epsilon$ are used to calculate topological S and T matrices. The T matrix is diagonal and stands for self-statistics, while the S matrix encodes mutual statistics. Together they form a representation of a modular group $SL(2, \mathbb{Z})$, by which they are related to the modular transformations of a torus generated by $\mathfrak{s}$ and $\mathfrak{t}$ transformations [56]. It follows that overlaps between $|\Psi^i\rangle$ transformed by a combination of modular transformations $\mathfrak{s}$ and $\mathfrak{t}$ constitute entries of a corresponding combination of topological S and T matrices.

Throughout this Rapid Communication, for concreteness, we work with the transformations on a lattice with 120°

rotational symmetry. The construction is, however, general and applicable to lattices with other symmetries as well. We start by defining torus $\mathcal{A}$ in Fig. 4 with unit vectors w_1, w_2 and corresponding transfer matrices: vertical $(w_1, N_v w_2)$ and horizontal $(N_h w_1, w_2)$ [see Fig. 2(b) for comparison]. Similarly, we consider tori $\mathcal{B}$ and $\mathcal{C}$ together with their corresponding transfer matrices as shown in Fig. 4.

Our method requires finding three complete sets of ground states

$$\{|\Psi^i_{\mathcal{A}}\rangle\}, \quad \{|\Psi^i_{\mathcal{B}}\rangle\}, \quad \{|\Psi^i_{\mathcal{C}}\rangle\}, \quad i = \mathbb{I}, e, m, \epsilon \tag{11}$$

with well-defined anyon fluxes corresponding to three different tori: $\mathcal{A}$, $\mathcal{B}$, $\mathcal{C}$. Each torus is related to the previous one by a modular transformation $\mathfrak{st}$, which generates 120° counterclockwise rotation (see Fig. 4). Topological S and T matrices are extracted from all possible overlaps between states in (11). This computation is presented in [51] and described in Appendix B of the Supplemental Material [55]. We stress that the presented method does not require any rotational invariance of the iPEPS tensors.

Toric code versus double semion and quantum double of $\mathbb{Z}_3$. PEPS tensors that represent ground states of string-net models on a honeycomb lattice with zero correlation length can be found analytically [4,57]. As a proof of principle, we numerically obtain topological S and T matrices for the toric code and the double semion model. Moreover, the described method gave exact S and T matrices for the quantum double of $\mathbb{Z}_3$ model defined on a square lattice [58]. In this Rapid Communication we restrict the description to the toric code phase realized in the (i) perturbed string-net model and (ii) Kitaev honeycomb model for which we analyze the iPEPS ground state obtained by numerical energy optimization.

Perturbed string-net model. In order to drive the iPEPS away from the fixed point with zero correlation length, we apply a perturbation $e^{-\lambda V}$ towards a ferromagnetic phase similarly as in [59–61] but with a two-site interaction $V = -\sum_{\langle i,j\rangle} \sigma^x_i \sigma^x_j$ (see Appendix C of the Supplemental Material [55]).

Our method allows us to obtain accurate results even close to the critical point, in the regime of very long correlation lengths ξ (see Fig. 5). Indeed, for $\lambda = 0.136$, where $\xi \approx 25$, we obtain $S = S_{\text{tc}} + \epsilon_S$, $T = T_{\text{tc}} + \epsilon_T$, where

$$S_{\text{tc}} = \frac{1}{2}\begin{pmatrix} 1 & 1 & 1 & 1 \\ 1 & 1 & -1 & -1 \\ 1 & -1 & 1 & -1 \\ 1 & -1 & -1 & 1 \end{pmatrix},$$

$$T_{\text{tc}} = \begin{pmatrix} 1 & 0 & 0 & 0 \\ 0 & 1 & 0 & 0 \\ 0 & 0 & 1 & 0 \\ 0 & 0 & 0 & -1 \end{pmatrix}. \tag{12}$$

The maximal element of $|\epsilon_S|$ and $|\epsilon_T|$ is of the order of 10^{-3} and 10^{-8}, respectively.

In the ferromagnetic phase we find two eigenvectors of TM Ω, $v_1 = \rho_1 \oplus 0$ and $v_2 = 0 \oplus \rho_2$. However, in contrast to the topologically ordered phase described by Eq. (4), there is no operator that maps v_1 to v_2. Numerically, this situation is detected by monitoring the distance (per lattice site) between $v_1 Z_v$ and v_2. In the topologically trivial phase the distance converges to a finite value with growing bond dimension of v_i.

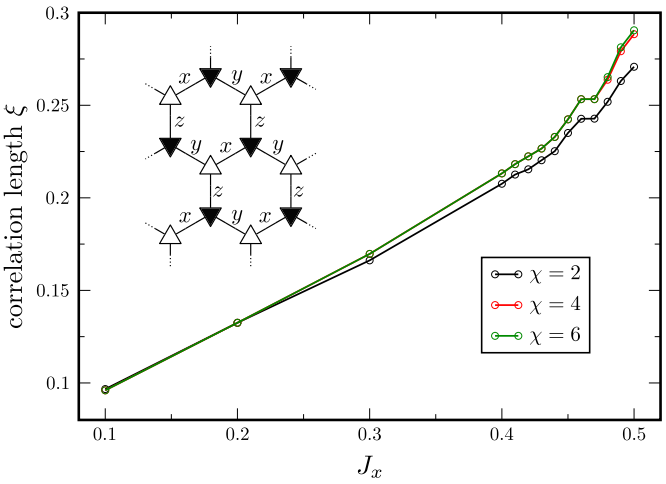

FIG. 6. Correlation length ξ as a function of $J_x = J_y$ in the Kitaev honeycomb model. Results for several values of bond dimension χ of TM eigenvectors v_i are shown. Inset: graphical illustration of the Hamiltonian defined in Eq. (13) displaying three different types of coupling: x, y, and z.

Kitaev honeycomb model. The model is defined by the following Hamiltonian:

$$\mathcal{H} = -\sum_{\alpha=x,y,z} J_\alpha \sum_{\alpha \text{ links}} \sigma^\alpha_i \sigma^\alpha_j \tag{13}$$

on a honeycomb lattice. Here, σ^α_i, $\alpha = x, y, z$ are Pauli matrices acting on site i. We set $J_z = 1$ and study the model along the line $J_x = J_y \in (0, 0.5)$ (see Fig. 6). The iPEPS ground state is obtained using variational optimization. We find that the bond dimension $\chi = 4$ of boundary MPO's v_i suffices to faithfully capture the entanglement properties of the phase.

We obtain correct topological S and T matrices within very small error. We are able to uniquely determine the anyon model for a range of parameters $J_x = J_y \in [0.2, 0.48]$. Most notably for $J_x = J_y = 0.44$, which is close to the critical point at $J_x = J_y = 0.5$, we compute topological matrices $S = S_{\text{tc}} + \epsilon_S$, $T = T_{\text{tc}} + \epsilon_T$, where the maximal element of $|\epsilon_S|$ ($|\epsilon_T|$) is 1.3×10^{-3} (2.2×10^{-3}). The errors $|\epsilon_S|$, $|\epsilon_T|$ grow with increasing J, however stay below 4% in the interval $J_x = J_y \in [0.2, 0.48]$. This accuracy is sufficient to unambiguously determine the type of topological order.

Conclusions. We presented a method of identifying topological order from a microscopic lattice Hamiltonian that does not have explicit limitations on the size of the system. The method is based on extracting topological S and T matrices from a single iPEPS. Our techniques allow us to analyze systems with much bigger correlation length than the state-of-the-art two-dimensional DMRG. Finally, we analyzed numerically optimized iPEPS describing the ground state of the Kitaev honeycomb model in the toric code phase. This computation shows that our approach does not require an artificially implemented realization of topological symmetries. Instead, it is applicable to generic, variationally obtained iPEPS.

Acknowledgments. A.F. would like to thank Jutho Haegeman, Frank Verstraete, Robijn Vanhove, and Laurens Lootens for explaining their work [44]. Numerical calculations [62–65] were performed in MATLAB with the help of the ncon function for tensor contractions. This research was supported by the Polish Ministry of Science and Education under Grant No. DI2015 021345 (A.F.) and by Narodowe Centrum Nauki (NCN) under Grant No. 2016/23/B/ST3/00830 (A.F., J.D.). L.C. was supported initially by the U.S. DOE through the J. Robert Oppenheimer fellowship and subsequently by the DOE, Office of Science, Basic Energy Sciences, Materials Sciences and Engineering Division, Condensed Matter Theory Program. G.V. is a CIFAR fellow in the Quantum Information Science Program. This research was supported in part by Perimeter Institute for Theoretical Physics. Research at Perimeter Institute is supported by the Government of Canada through the Department of Innovation, Science and Economic Development Canada and by the Province of Ontario through the Ministry of Research, Innovation and Science. X is formerly known as Google[x] and is part of the Alphabet family of companies, which includes Google, Verily, Waymo, and others.

[1] X. G. Wen, Topological orders in rigid states, Int. J. Mod. Phys. B **4**, 239 (1990).
[2] A. Kitaev, Fault-tolerant quantum computation by anyons, Ann. Phys. (NY) **303**, 2 (2003).
[3] A. Kitaev, Anyons in an exactly solved model and beyond, Ann. Phys. (NY) **321**, 2 (2006).
[4] M. A. Levin and X.-G. Wen, String-net condensation: A physical mechanism for topological phases, Phys. Rev. B **71**, 045110 (2005).
[5] S. R. White, Density Matrix Formulation for Quantum Renormalization Groups, Phys. Rev. Lett. **69**, 2863 (1992).
[6] S. R. White, Density-matrix algorithms for quantum renormalization groups, Phys. Rev. B **48**, 10345 (1993).
[7] S. Yan, D. A. Huse, and S. R. White, Spin-liquid ground state of the $S = 1/2$ kagome Heisenberg antiferromagnet, Science **332**, 1173 (2011).
[8] H.-C. Jiang, Z. Wang, and L. Balents, Identifying topological order by entanglement entropy, Nat. Phys. **8**, 902 (2012).
[9] S.-S. Gong, D. N. Sheng, O. I. Motrunich, and M. P. A. Fisher, Phase diagram of the spin-1/2 J_1-J_2 Heisenberg model on a honeycomb lattice, Phys. Rev. B **88**, 165138 (2013).
[10] Z. Zhu, D. A. Huse, and S. R. White, Weak Plaquette Valence Bond Order in the $S = 1/2$ Honeycomb J_1-J_2 Heisenberg Model, Phys. Rev. Lett. **110**, 127205 (2013).
[11] S.-S. Gong, W. Zhu, and D. N. Sheng, Emergent chiral spin liquid: Fractional quantum Hall effect in a kagome Heisenberg model, Sci. Rep. **4**, 6317 (2014).
[12] Z. Zhu and S. R. White, Quantum phases of the frustrated XY models on the honeycomb lattice, Mod. Phys. Lett. B **28**, 1430016 (2014).
[13] S.-S. Gong, W. Zhu, L. Balents, and D. N. Sheng, Global phase diagram of competing ordered and quantum spin-liquid phases on the kagome lattice, Phys. Rev. B **91**, 075112 (2015).
[14] W.-J. Hu, S.-S. Gong, W. Zhu, and D. N. Sheng, Competing spin-liquid states in the spin-1/2 Heisenberg model on the triangular lattice, Phys. Rev. B **92**, 140403(R) (2015).
[15] W. Zhu, S. S. Gong, D. N. Sheng, and L. Sheng, Possible non-Abelian Moore-Read state in double-layer bosonic fractional quantum Hall system, Phys. Rev. B **91**, 245126 (2015).
[16] Z. Zhu and S. R. White, Spin liquid phase of the $S = 1/2 J_1$-J_2 Heisenberg model on the triangular lattice, Phys. Rev. B **92**, 041105(R) (2015).
[17] M. P. Zaletel, Z. Zhu, Y.-M. Lu, A. Vishwanath, and S. R. White, Space Group Symmetry Fractionalization in a Chiral Kagome Heisenberg Antiferromagnet, Phys. Rev. Lett. **116**, 197203 (2016).
[18] T.-S. Zeng, W. Zhu, J.-X. Zhu, and D. N. Sheng, Nature of continuous phase transitions in interacting topological insulators, Phys. Rev. B **96**, 195118 (2017).
[19] M.-S. Vaezi and A. Vaezi, Numerical observation of parafermion zero modes and their stability in 2D topological states, arXiv:1706.01192.
[20] Z. Zhu, I. Kimchi, D. N. Sheng, and L. Fu, Robust non-Abelian spin liquid and a possible intermediate phase in the antiferromagnetic Kitaev model with magnetic field, Phys. Rev. B **97**, 241110(R) (2018).
[21] L. Cincio and G. Vidal, Characterizing Topological Order by Studying the Ground States on an Infinite Cylinder, Phys. Rev. Lett. **110**, 067208 (2013).
[22] Y.-C. He, D. N. Sheng, and Y. Chen, Chiral Spin Liquid in a Frustrated Anisotropic Kagome Heisenberg Model, Phys. Rev. Lett. **112**, 137202 (2014).
[23] W. Zhu, S. S. Gong, F. D. M. Haldane, and D. N. Sheng, Topological characterization of the non-Abelian Moore-Read state using density-matrix renormalization group, Phys. Rev. B **92**, 165106 (2015).
[24] W. Zhu, S. S. Gong, and D. N. Sheng, Chiral and critical spin liquids in a spin-1/2 kagome antiferromagnet, Phys. Rev. B **92**, 014424 (2015).
[25] B. Bauer, L. Cincio, B. P. Keller, M. Dolfi, G. Vidal, S. Trebst, and A. W. W. Ludwig, Chiral spin liquid and emergent anyons in a Kagome lattice Mott insulator, Nat. Commun. **5**, 5137 (2014).
[26] W. Zhu, S. S. Gong, F. D. M. Haldane, and D. N. Sheng, Fractional Quantum Hall States at $\nu = 13/5$ and $12/5$ and Their Non-Abelian Nature, Phys. Rev. Lett. **115**, 126805 (2015).
[27] A. G. Grushin, J. Motruk, M. P. Zaletel, and F. Pollmann, Characterization and stability of a fermionic $\nu = 1/3$ fractional Chern insulator, Phys. Rev. B **91**, 035136 (2015).
[28] Y.-C. He, S. Bhattacharjee, F. Pollmann, and R. Moessner, Kagome Chiral Spin Liquid as a Gauged $U(1)$ Symmetry Protected Topological Phase, Phys. Rev. Lett. **115**, 267209 (2015).
[29] Y.-C. He and Y. Chen, Distinct Spin Liquids and Their Transitions in Spin-1/2 XXZ Kagome Antiferromagnets, Phys. Rev. Lett. **114**, 037201 (2015).
[30] Y.-C. He, S. Bhattacharjee, R. Moessner, and F. Pollmann, Bosonic Integer Quantum Hall Effect in an Interacting Lattice Model, Phys. Rev. Lett. **115**, 116803 (2015).

[31] S. Geraedts, M. P. Zaletel, Z. Papić, and R. S. K. Mong, Competing Abelian and non-Abelian topological orders in $\nu = 1/3 + 1/3$ quantum Hall bilayers, Phys. Rev. B **91**, 205139 (2015).
[32] R. S. K. Mong, M. P. Zaletel, F. Pollmann, and Z. Papić, Fibonacci anyons and charge density order in the $12/5$ and $13/5$ quantum Hall plateaus, Phys. Rev. B **95**, 115136 (2017).
[33] Y.-C. He, F. Grusdt, A. Kaufman, M. Greiner, and A. Vishwanath, Realizing and adiabatically preparing bosonic integer and fractional quantum Hall states in optical lattices, Phys. Rev. B **96**, 201103(R) (2017).
[34] E. M. Stoudenmire, D. J. Clarke, R. S. K. Mong, and J. Alicea, Assembling Fibonacci anyons from a Z_3 parafermion lattice model, Phys. Rev. B **91**, 235112 (2015).
[35] Y.-C. He, M. P. Zaletel, M. Oshikawa, and F. Pollmann, Signatures of Dirac Cones in a DMRG Study of the Kagome Heisenberg Model, Phys. Rev. X **7**, 031020 (2017).
[36] S. N. Saadatmand and I. P. McCulloch, Symmetry fractionalization in the topological phase of the spin-$1/2$ J_1-J_2 triangular Heisenberg model, Phys. Rev. B **94**, 121111(R) (2016).
[37] C. Hickey, L. Cincio, Z. Papić, and A. Paramekanti, Haldane-Hubbard Mott Insulator: From Tetrahedral Spin Crystal to Chiral Spin Liquid, Phys. Rev. Lett. **116**, 137202 (2016).
[38] M. P. Zaletel, Y.-M. Lu, and A. Vishwanath, Measuring space-group symmetry fractionalization in Z_2 spin liquids, Phys. Rev. B **96**, 195164 (2017).
[39] T.-S. Zeng, W. Zhu, and D. Sheng, Tuning topological phase and quantum anomalous Hall effect by interaction in quadratic band touching systems, npj Quantum Mater. **3**, 49 (2018).
[40] F. Verstraete and J. I. Cirac, Renormalization algorithms for quantum many-body systems in two and higher dimensions, arXiv:cond-mat/0407066.
[41] V. Murg, F. Verstraete, and J. I. Cirac, Variational study of hard-core bosons in a two-dimensional optical lattice using projected entangled pair states, Phys. Rev. A **75**, 033605 (2007).
[42] F. Verstraete, V. Murg, and J. I. Cirac, Matrix product states, projected entangled pair states, and variational renormalization group methods for quantum spin systems, Adv. Phys. **57**, 143 (2008).
[43] M. B. Şahinoğlu, D. Williamson, N. Bultinck, M. Mariën, J. Haegeman, N. Schuch, and F. Verstraete, Characterizing topological order with matrix product operators, arXiv:1409.2150.
[44] N. Bultinck, M. Mariën, D. J. Williamson, M. B. Şahinoğlu, J. Haegeman, and F. Verstraete, Anyons and matrix product operator algebras, Ann. Phys. (NY) **378**, 183 (2017).
[45] M. Iqbal, K. Duivenvoorden, and N. Schuch, Study of anyon condensation and topological phase transitions from a Z_4 topological phase using the projected entangled pair states approach, Phys. Rev. B **97**, 195124 (2018).
[46] C. Fernández-González, R. S. K. Mong, O. Landon-Cardinal, D. Pérez-García, and N. Schuch, Constructing topological models by symmetrization: A projected entangled pair states study, Phys. Rev. B **94**, 155106 (2016).
[47] H. He, H. Moradi, and X.-G. Wen, Modular matrices as topological order parameter by a gauge-symmetry-preserved tensor renormalization approach, Phys. Rev. B **90**, 205114 (2014).
[48] P. Corboz, Variational optimization with infinite projected entangled-pair states, Phys. Rev. B **94**, 035133 (2016).
[49] A. Francuz (unpublished).
[50] Y. Zhang, T. Grover, A. Turner, M. Oshikawa, and A. Vishwanath, Quasiparticle statistics and braiding from ground-state entanglement, Phys. Rev. B **85**, 235151 (2012).
[51] Y. Zhang, T. Grover, and A. Vishwanath, General procedure for determining braiding and statistics of anyons using entanglement interferometry, Phys. Rev. B **91**, 035127 (2015).
[52] J. I. Cirac, D. Poilblanc, N. Schuch, and F. Verstraete, Entanglement spectrum and boundary theories with projected entangled-pair states, Phys. Rev. B **83**, 245134 (2011).
[53] The notions of pure MPSs and pure MPOs are introduced in Appendix A of the Supplemental Material [55].
[54] L. Vanderstraeten, J. Haegeman, and F. Verstraete, Tangent-space methods for uniform matrix product states, SciPost Phys. Lect. Notes **7** (2019).
[55] See Supplemental Material at http://link.aps.org/supplemental/10.1103/PhysRevB.101.041108 for details on numerical methods used in the main text that were omitted for clarity.
[56] X.-G. Wen, A theory of 2+1D bosonic topological orders, Natl. Sci. Rev. **3**, 68 (2015).
[57] O. Buerschaper, M. Aguado, and G. Vidal, Explicit tensor network representation for the ground states of string-net models, Phys. Rev. B **79**, 085119 (2009).
[58] M. D. Schulz, S. Dusuel, R. Orus, J. Vidal, and K. P. Schmidt, Breakdown of a perturbed topological phase, New J. Phys. **14**, 025005 (2012).
[59] J. Haegeman, K. Van Acoleyen, N. Schuch, J. I. Cirac, and F. Verstraete, Gauging Quantum States: From Global to Local Symmetries in Many-Body Systems, Phys. Rev. X **5**, 011024 (2015).
[60] J. Haegeman, V. Zauner, N. Schuch, and F. Verstraete, Shadows of anyons and the entanglement structure of topological phases, Nat. Commun. **6**, 8284 (2015).
[61] G.-Y. Zhu and G.-M. Zhang, Gapless Coulomb State Emerging from a Self-Dual Topological Tensor-Network State, Phys. Rev. Lett. **122**, 176401 (2019).
[62] R. N. C. Pfeifer, G. Evenbly, S. Singh, and G. Vidal, NCON: A tensor network contractor for MATLAB, arXiv:1402.0939.
[63] I. P. McCulloch, Infinite size density matrix renormalization group, revisited, arXiv:0804.2509.
[64] J. Jordan, R. Orús, G. Vidal, F. Verstraete, and J. I. Cirac, Classical Simulation of Infinite-Size Quantum Lattice Systems in Two Spatial Dimensions, Phys. Rev. Lett. **101**, 250602 (2008).
[65] H. N. Phien, J. A. Bengua, H. D. Tuan, P. Corboz, and R. Orús, Infinite projected entangled pair states algorithm improved: Fast full update and gauge fixing, Phys. Rev. B **92**, 035142 (2015).

Editors' Suggestion

Determining non-Abelian topological order from infinite projected entangled pair states

Anna Francuz* and Jacek Dziarmaga
Institute of Theoretical Physics, Jagiellonian University, ul. Łojasiewicza 11, PL-30-348 Kraków, Poland

(Received 24 August 2020; revised 16 November 2020; accepted 17 November 2020; published 4 December 2020)

We generalize the method introduced in Phys. Rev. B **101**, 041108 (2020) of extracting information about topological order from the ground state of a strongly correlated two-dimensional system represented by an infinite projected entangled pair state (iPEPS) to non-Abelian topological order. When wrapped on a torus the unique iPEPS becomes a superposition of degenerate and locally indistinguishable ground states. We find numerical symmetries of the iPEPS, represented by infinite matrix product operators (MPO) and their fusion rules. The rules tell us how to combine the symmetries into projectors onto states with well defined anyon flux. A linear structure of the MPO projectors allows for efficient determination for each state its second Renyi topological entanglement entropy on an infinitely long cylinder directly in the limit of infinite cylinder's width. The same projectors are used to compute topological S and T matrices encoding mutual and self-statistics of emergent anyons. The algorithm is illustrated by examples of Fibonacci and Ising non-Abelian string net models.

DOI: 10.1103/PhysRevB.102.235112

I. INTRODUCTION

Topologically ordered phases [1] support anyonic quasiparticles. They open the possibility of realizing fault-tolerant quantum computation [2] based on braiding of non-Abelian anyons. Apart from a number of exactly solvable models [2–4], verifying whether a given microscopic Hamiltonian realizes a topologically ordered phase has traditionally been regarded as an extremely hard task. Recently, observation of quantized Hall effect in Kitaev-like ruthenium chloride α-$RuCl_3$ in magnetic field [5] granted the problem with urgent experimental relevance.

A leading numerical method is to use density matrix renormalization group (DMRG) [6,7] on a long cylinder [8–23]. In the limit of infinitely long cylinders, DMRG naturally produces ground states with well-defined anyonic flux, from which one can obtain full characterization of a topological order, via so-called topological S and T matrices [24]. Since the proposal of Ref. [24], this approach has become a common practice [25–42].

Unfortunately, the cost of a DMRG simulation grows exponentially with the circumference of cylinder, limiting this approach to thin cylinders (up to a width of $\simeq$14 sites) and short correlation lengths (up to 1–2 sites). Instead, infinite projected entangled pair states (iPEPS) in principle allow for much longer correlation lengths [43–45]. A unique ground state on an infinite lattice can be represented by an iPEPS that is either a variational ansatz [46] or a result of numerical optimization [47,48]. When wrapped on a cylinder the iPEPS becomes a superposition of degenerate ground states with definite anyonic fluxes. Here we generalize the approach of Ref. [48] to non-Abelian topological order and show how to produce a PEPS-like tensor network for each ground state with well-defined flux. Such tensor networks are suitable for extracting topological S and T matrices by computing overlaps between ground states. Furthermore, we show that they allow for computation of topological second Renyi entropy directly in the limit of infinite cylinder's width. The approach of Ref. [48] does not assume clean realization of certain symmetries on the bond indices, in contrast to Refs. [49–52]. This has been demonstrated in Ref. [48] by examples of toric code and double semions perturbed away from a fixed point towards a ferromagnetic phase as well as for the numerical iPEPS representing the ground state of the Kitaev model in the gapped phase. The last example shows that the method does not require restoring the symmetries by suitable gauge transformations of a numerical iPEPS, a feat that was accomplished in Ref. [53] for the toric code with a perturbation. Finally, it also has much lower cost than methods based on the tensor renormalization group [54].

The ferromagnetic Kitaev model in a weak (1,1,1) magnetic field supports non-Abelian chiral topological order [3,23] and Ref. [5] is believed to provide the first experimental realization of this universality class. However, as the magnetic field is a tiny perturbation of a critical state, the correlation length should be long [46]. This drives the problem beyond accurate DMRG simulation on a thin cylinder and, therefore, the non-Abelian phase observed in the experiment [5] may require iPEPS for its accurate description.

In this work we consider mainly string-net models. The key elements of the method introduced in Ref. [48] are shown in Fig. 1. Virtual indices of iPEPS on a torus or cylinder can be inserted with horizontal/vertical matrix product operator (MPO) symmetries. Their action on iPEPS is the same as flux operators(Wilson loops) winding around the torus in the same horizontal/vertical direction. However, the MPO symmetries are much easier to find than the nonlocal operators that—in interacting systems—become complicated operator ribbons rather than simple strings. Just as projectors on definite anyon

*Corresponding author: anna.francuz@uj.edu.pl

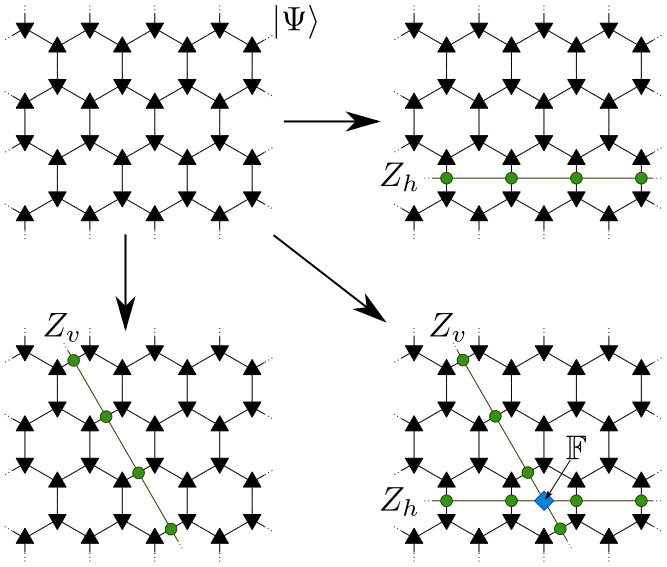

FIG. 1. General picture. From the unique ground state on an infinite lattice represented by an iPEPS $|\Psi\rangle$, we construct various states inserted with MPO symmetries. Their linear combinations, whose coefficients are determined by fusion rules of the MPO symmetries $Z_{h,v}$ (corresponding to anyonic fusion rules), become a basis of states with well defined anyonic flux. Here physical indices are not drawn for simplicity.

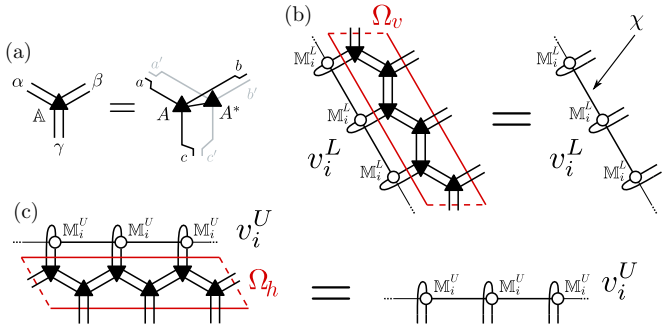

FIG. 2. Transfer matrix. In (a), graphical representation of a double tensor $\mathbb{A}$. In (b), leading left eigenvector $(v_i^L|$ of vertical transfer matrix Ω_v takes an MPO form v_i^L. The uniform v_i^L is made of tensors $\mathbb{M}_i^L$ with bond dimension χ that can be obtained with the VUMPS algorithm [55,56]. In (c), up eigenvector v_i^U of horizontal TM Ω_h.

fluxes could be in principle constructed as linear combinations of flux operators, virtual projectors can be made as combinations of the MPO symmetries.

The paper is organized in Secs. II–VIII where we gradually introduce subsequent elements of the algorithm. Most sections open with a general part introducing a new concept. Then a series of subsections follows illustrating the general concept with a series of examples: the Abelian toric code (to make contact with Ref. [48]), Fibonacci string net, and Ising string net. In the end the algorithm is summarized in Sec. IX. Additionally, in Appendix E we apply some of the same tools to a variational ansatz proposed for the Kitaev model in magnetic field [46]. A detailed plan is as follows.

In Sec. II we define fixed points of the iPEPS transfer matrix in the form of MPS and introduce MPO symmetries that map between different fixed points. We also identify fusion rules of the MPO symmetries that are isomorfic with anyonic fusion rules. In Sec. III we consider an iPEPS wrapped on an infinite cylinder—that we visualize as horizontal without loss of generality—and use the fusion rules to construct vertical projectors on states with definite anyon flux along the horizontal cylinder. In Sec. IV we consider again an iPEPS wrapped on an infinite cylinder but this time the iPEPS is inserted with a horizontal MPO symmetry that alters boundary conditions in the vertical direction. We construct its vertical MPO symmetries that we call impurity MPO (IMPO) symmetries. We also identify their fusion rules. In Sec. V the fusion rules are used to construct vertical projectors as linear combinations of the IMPO symmetries. The impurity projectors select states with definite horizontal anyon flux in the iPEPS inserted with the horizontal MPO symmetry. In Sec. VI we show how the structure of vertical projectors enables efficient evaluation of the topological second Renyi entanglement entropy directly in the limit of infinite cylinder's width. In Sec. VII the same is done with impurity projectors. Finally, in Sec. VIII we show how to obtain the topological S and T matrices from overlaps between states with definite anyon flux. In the case of string net models they provide full characterization of the topological order. The paper is closed with a brief summary in Sec. IX.

II. GENERATORS OF SYMMETRIES

Uniform iPEPS on a honeycomb lattice can be characterized by a tensor A with elements A^i_{abc}. Here, i is a physical index and a, b, c are bond indices. Let $\mathbb{A}$ denote a double tensor $\mathbb{A} = \sum_i A^i \otimes (A^i)^*$ with double bond indices $\alpha = (a, a')$, etc., see Fig. 2(a) and Appendix B. iPEPS transfer matrix (TM) Ω is defined by a line of double tensors $\mathbb{A}$ contracted via their bond indices along the line as shown in Figs. 2(b) and 2(c). These figures show vertical TM Ω^v and horizontal TM Ω^h, respectively. Their leading eigenvectors are TM fixed points. In the thermodynamic limit only the leading eigenvectors survive in TM's spectral decomposition:

$$\Omega^v \approx \omega \sum_{i=1}^{n} |v_i^R)(v_i^L|, \quad \Omega^h \approx \omega \sum_{i=1}^{n} |v_i^U)(v_i^D|. \tag{1}$$

The leading eigenvalue ω is the same for both vertical and horizontal TM. The leading eigenvectors are biorthonormal:

$$\delta_{ij} = (v_i^L|v_j^R) = \mathrm{Tr}\,(v_i^L)^T v_j^R, \tag{2}$$

$$\delta_{ij} = (v_i^U|v_j^D) = \mathrm{Tr}\,(v_i^U)^T v_j^D. \tag{3}$$

Here we use both the MPS $|v_i)$ and MPO v_i forms. MPS $|v_i)$ is MPO v_i between bra and ket indices of the double iPEPS TM. The ansatz for a fixed point boundary v_i^X is a pure MPO with spectral radius 1 [57] made out of tensors M_i^X.

Different fixed points are connected by symmetries whose existence is a distinctive feature of topologically ordered states encoded in iPEPS. In contrast, in the trivial ferromagnetic phase the two boundary fixed points, $v_\uparrow$ and $v_\downarrow$, corresponding to two different magnetizations have orthogonal support spaces and, therefore, the operator mapping

between them does not exist. The symmetries act on virtual indices of the tensor network. They are called MPO symmetries and, apart from a few exactly solvable models for which they can be found analytically [49], they have to be found numerically as described in Ref. [48]. The MPO symmetries Z_a are operators which form certain algebra under their multiplication:

$$Z_a Z_b = \sum_c N_{ab}^c Z_c, \tag{4}$$

where the possible values of N_{ab}^c are 0,1. Each MPO symmetry Z_a (including the trivial identity $Z_1 \equiv 1$) corresponds to a certain anyon type a in a sense that their algebra is the same as the fusion rules of the anyons, see Appendix A. Once all boundary fixed points v_i are found numerically, the MPO symmetries z_{ij} are obtained as MPO's mapping between the boundaries:

$$v_i \cdot z_{ij} = v_j. \tag{5}$$

The same set of symmetries exists for L/R and U/D boundary fixed points. We completed these numerical procedures in the following models.

A. Toric code

We begin with this basic example to make contact with Ref. [48] where the Abelian version of the present method was applied to this model and its realistic implementation with the Kitaev model [3]. Each TM has two boundary fixed points. To be more specific, for vertical transfer matrix Ω^v in addition to $Z_1^v = 1$ we find numerically one nontrivial MPO symmetry $z_{12}^v = z_{21}^v \equiv Z_2^v$ that satisfies

$$v_1^L \cdot Z_2^v = v_2^L, \quad v_2^L \cdot Z_2^v = v_1^L. \tag{6}$$

These equations imply $\mathcal{Z}_2$ algebra:

$$Z_2^v \cdot Z_2^v = 1. \tag{7}$$

It has to be strongly emphasized that in general the numerical solution Z_2^v of equation (6) has zero modes that make the algebra valid only in the sense that $v_i^L \cdot Z_2 \cdot Z_2 = v_i^L$ for any i. The same reservation applies to all fusion rules (4) to be identified numerically in the rest of this paper. This is also why all (numerically obtained) MPO symmetries throughout the paper are used only in iPEPS embedding: The zero modes do not matter when inserted between columns/rows of an iPEPS. Keeping this in mind, for all fixed point tensors considered in this paper the algebra (4) is satisfied with close to machine precision.

B. Fibonacci string net

Here we employed the iPEPS tensors for a fixed point Fibonacci string net model presented in Appendix B. For each TM we found numerically two boundary fixed points and one nontrivial MPO symmetry Z_2 satisfying, e.g.,

$$v_1^L \cdot Z_2^v = v_2^L. \tag{8}$$

The same MPO was found to satisfy also

$$v_2^L \cdot Z_2^v = v_1^L + v_2^L. \tag{9}$$

These two equations imply the Fibonacci fusion rule

$$Z_2^v \cdot Z_2^v = 1^v + Z_2^v. \tag{10}$$

Again, due to zero modes, the rule holds only when applied to iPEPS boundaries. Similar MPO symmetries were also found for the horizontal boundary fixed points.

C. Ising string net

Here we employed the iPEPS tensors for a fixed point Ising string net model presented in Appendix B. This time each TM has three boundary fixed points. We found two nontrivial MPO symmetries, labeled as Z_σ and Z_ψ, as numerical solutions to equations, e.g.,

$$v_1^L \cdot Z_\sigma^v = v_2^L, \quad v_1^L \cdot Z_\psi^v = v_3^L. \tag{11}$$

Furthermore, we found that the solutions satisfy

$$\begin{aligned} &v_2^L \cdot Z_\sigma^v = v_1^L + v_3^L,\ v_3^L \cdot Z_\psi^v = v_1^L, \\ &v_2^L \cdot Z_\psi^v = v_2^L,\ v_3^L \cdot Z_\sigma^v = v_2^L. \end{aligned} \tag{12}$$

These six equations imply nontrivial fusion rules:

$$\begin{aligned} &Z_\sigma^v \cdot Z_\sigma^v = 1^v + Z_\psi^v, \\ &Z_\sigma^v \cdot Z_\psi^v = Z_\sigma^v = Z_\psi^v \cdot Z_\sigma^v, \\ &Z_\psi^v \cdot Z_\psi^v = 1^v, \end{aligned} \tag{13}$$

which justify the labeling. For our numerical Z_ψ^v and Z_σ^v the rules hold only when applied to v_i^L. Similar MPO symmetries were also found for the horizontal boundary fixed points.

III. VERTICAL PROJECTORS

The MPO symmetries alone are enough to construct some of the projectors on states with definite anyon fluxes. Let us consider vertical MPO symmetries Z_a^v for definiteness. Their linear combinations

$$P = \sum_a c_a Z_a^v, \tag{14}$$

which satisfy $P \cdot P = P$, make vertical projectors. When these projectors are inserted into iPEPS wrapped on an infinite horizontal cylinder, they yield states with definite anyon fluxes along that cylinder. The remaining projectors that can be applied when the iPEPS is inserted with a line of Z^h are the subject of the following section.

A. Toric code

The $\mathcal{Z}_2$ algebra (7) allows for two projectors,

$$P_\pm = \tfrac{1}{2}\left(1 \pm Z_2^v\right), \tag{15}$$

that satisfy $P_\pm \cdot P_\pm = P_\pm$ and $P_+ \cdot P_- = 0 = P_- \cdot P_+$. Later on they will be identified as $P_+ \equiv P_{\text{vac}}$ and $P_- \equiv P_e$, i.e., projectors on the vacuum and the electric flux, respectively.

B. Fibonacci string net

The fusion rules (10) determine two projectors:

$$P_\pm = \frac{1}{\sqrt{5}}\left(\phi^{\pm 1} 1 \mp Z_2^v\right). \tag{16}$$

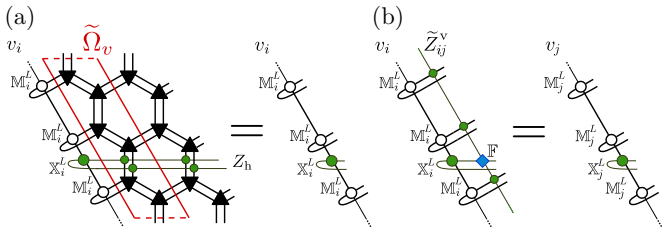

FIG. 3. Impurity transfer matrix. In (a), with Z^h inserted into both bra and ket layers of the iPEPS the transfer matrix Ω^v becomes impurity transfer matrix $\tilde{\Omega}^v$. Its leading left eigenvectors $(x^L|$ are obtained from MPOs from v^L by inserting additional tensors $\mathbb{X}^L$. Here double lines are dropped to improve clarity. In (b), graphical illustration of Eq. (22).

Here $\phi = (\sqrt{5}+1)/2$. They will be identified as $P_+ \equiv P_{\text{vac}}$ and $P_- \equiv P_{\tau\bar{\tau}}$, i.e., projectors on the vacuum and the sector with both Fibonacci anyons: τ and $\bar{\tau}$.

C. Ising string net

The fusion rules (13) allow for six projectors:

$$P_{1,2} = \frac{1}{2}\left(1^v \pm Z^v_\psi\right), \tag{17}$$

$$P_{3,4} = \frac{1}{4}\left(3\,1^v - Z^v_\psi\right) \pm \frac{1}{\sqrt{8}} Z^v_\sigma, \tag{18}$$

$$P_{5,6} = \frac{1}{4}\left(1^v + Z^v_\psi\right) \pm \frac{1}{\sqrt{8}} Z^v_\sigma. \tag{19}$$

Not all of them are the minimal projectors on definite anyon flux. It is easy to check that $P_3 \cdot P_4 = P_2$ and, therefore, out of the three it is enough to keep only P_2. Furthermore, we can see that $P_5 + P_6 = P_1$ hence we can skip P_1. After this selection we are left with three minimal projectors $P_{2,5,6}$ that satisfy $P_a \cdot P_b = P_a \delta_{ab}$. They will be identified as $P_5 \equiv P_{\text{vac}}$, $P_6 \equiv P_{\psi\bar{\psi}}$, and $P_2 \equiv P_{\sigma\bar{\sigma}}$.

IV. IMPURITY MPO SYMMETRIES

In order to construct the remaining projectors that are to be applied to an iPEPS inserted with a nontrivial horizontal MPO symmetry Z^h, we need to introduce an impurity transfer matrix (ITM), see Fig. 3(a). In general ITM has a number of leading left and right eigenvectors, respectively $(x^L_i|$ and $|x^R_j)$, that are biorthonormal: $(x^L_i|x^R_j) = \delta_{ij}$. The eigenvectors are constructed by inserting the eigenvectors of the vertical TM, respectively v^L and v^R, with additional tensors $\mathbb{X}^L_i$ and $\mathbb{X}^R_j$, see Fig. 3(a). The same figure shows equations that need to be satisfied by the additional tensors. They are efficiently obtained from a generalized eigenvalue problem:

$$\left(x^L_i\middle|\tilde{\Omega}_v\middle|x^R_j\right) = \lambda\left(x^L_i\middle|x^R_j\right). \tag{20}$$

Here $\lambda = 1$ is the maximal generalized eigenvalue. The problem is to be understood as

$$\left(\mathbb{X}^L_i\right)^T \cdot \mathcal{M} \cdot \mathbb{X}^R_j = \lambda \left(\mathbb{X}^L_i\right)^T \cdot \mathcal{N} \cdot \mathbb{X}^R_j, \tag{21}$$

where $\mathbb{X}^L_i$ and $\mathbb{X}^R_j$ are vectorized and matrices $\mathcal{M}$ and $\mathcal{N}$ are tensor environments of $\mathbb{X}^L_i$ and $\mathbb{X}^R_j$ in $(x^L_i|\tilde{\Omega}_v|x^R_j)$ and $(x^L_i|x^R_j)$, respectively.

Furthermore, as shown in Fig. 3(b), the left eigenvector $(x^L_i|$ can be acted on by any vertical MPO symmetry Z^v, including the trivial identity $Z^v_1 = 1^v$. In order to make the action possible, Z^v has to be inserted with additional tensor $\mathbb{F}$ that acts on Z^h. With the appropriate choice of $\mathbb{F}_{ij}$ their combination gives rise to impurity MPO-symmetry $\tilde{z}^v_{ij}$ such that

$$x^L_i \tilde{z}_{ij} = x^L_j. \tag{22}$$

A necessary condition for symmetry $\tilde{z}^v_{ij}$ to exist is that v^L in x^L_i, here denoted by $v^L(i)$, and v^L in x^L_j, here denoted by $v^L(j)$, are related by $v^L(i) \cdot Z^v = v^L(j)$.

A straightforward but essential observation is that, in analogy to MPO symmetries, the IMPO symmetries also satisfy their own fusion rules:

$$\tilde{Z}^v_a \cdot \tilde{Z}^v_b = \sum_c \tilde{N}^c_{ab} \tilde{Z}^v_c. \tag{23}$$

Here we keep only the minimal set of independent IMPO symmetries denoted by a capital $\tilde{Z}$ and labeled with a single index a, b, c. In general the coefficients $\tilde{N}^c_{ab}$ do not need to be integers as they depend on normalization of the eigenvectors $(x^L_i|$ and $|x^R_j)$.

V. IMPURITY PROJECTORS

In analogy to the vertical MPO symmetries and vertical projectors, as a product of two IMPO symmetries is a linear combination of IMPO symmetries, see Eq. (23), we can find projectors as linear combinations of IMPO symmetries,

$$\tilde{P} = \sum_a \tilde{c}_a \tilde{Z}^v_a. \tag{24}$$

The condition $\tilde{P} \cdot \tilde{P} = \tilde{P}$ is equivalent to a set of quadratic equations for coefficients $\tilde{c}_a$. Numerically it seems more efficient to find the coefficients by repeated Lanczos iterations:

$$\tilde{P}' \propto \tilde{P} \cdot \tilde{P}. \tag{25}$$

In each iteration the IMPO fusion rules (23) are used to express the product $\tilde{P} \cdot \tilde{P}$ as a new linear combination $\tilde{P}' = \sum_a \tilde{c}'_a \tilde{Z}^v_a$ and then new coefficients $\tilde{c}'_a$ are normalized so that the maximal magnitude of the eigenvalues of $\tilde{P}'$ is 1. Therefore, each iteration is a map $\{c_a\} \to \{c'_a\}$ which is repeated until the coefficients converge. These computations are performed in the biorthonormal eigenbasis of impurity eigenvectors, $(x^L_a|$ and $|x^R_a)$, where all involved MPO's become small matrices like, e.g., $(x^L_a|\tilde{Z}^v_c|x^R_b) \equiv [Z^v_c]_{ab}$. Repeating the Lanczos scheme with random initial coefficients we obtain all impurity projectors.

A. Toric code

There is one ITM with $Z^h = Z^h_2$. It has two eigenvectors $(x^L_a|$, one for each TM eigenvector v^L_a. In addition to an identity, $\tilde{1}^v$, there is one nontrivial IMPO symmetry $\tilde{z}^v_{12} = \tilde{z}^v_{21} \equiv \tilde{Z}^v_2$. A nontrivial fusion $\mathcal{Z}_2$ algebra, $\tilde{Z}^v \cdot \tilde{Z}^v = 1^v$, implies two projectors:

$$\tilde{P}_\pm = \tfrac{1}{2}\left(\tilde{1}^v \pm \tilde{Z}^v_2\right). \tag{26}$$

They will be identified as magnetic and fermionic projectors, $\widetilde{P}_+ \equiv \widetilde{P}_{\rm m}$ and $\widetilde{P}_- \equiv \widetilde{P}_\epsilon$, respectively.

B. Fibonacci string net

There is one ITM with $Z^h = Z_2^h$. It has one eigenvector $(x_1^L|$ embedded in v_1^L and two eigenvectors $(x_{2,3}^L|$ embedded in v_2^L. We choose the two to be Hermitian and orthonormal but this still leaves (gauge) freedom of their rotation. In addition to the trivial identity, $\tilde{1}^v$, there are two ITM symmetries: $\widetilde{z}_{12}^v$ and $\widetilde{z}_{13}^v$. Their fusion rules do depend on the gauge but independently of the gauge we find numerically three projectors $\widetilde{P}_{1,2,3}$. Only two of them project on states that are orthogonal to the states obtained with vertical projectors, as can be verified by calculating overlaps between their respective projected iPEPS on infinite torus. The new projectors will be identified as $\widetilde{P}_1 \equiv \widetilde{P}_\tau$ and $\widetilde{P}_2 \equiv \widetilde{P}_{\bar\tau}$.

Interestingly, the third one, $\widetilde{P}_3$, projects on the same horizontal anyon flux as vertical projector P_- and both will be identified as $\widetilde{P}_{\tau\bar\tau}$ and $P_{\tau\bar\tau}$, respectively. This way we have two equivalent ways to obtain $\tau\bar\tau$ flux: one with and one without Z_2^h MPO symmetry. In other words, with or without inserted Z_2^h symmetry the iPEPS wrapped on an infinite cylinder has a nonzero overlap with the ground state with $\tau\bar\tau$ flux.

C. Ising string net

There are two ITM with Z_σ^h and Z_ψ^h. For each of them independently we construct impurity projectors. In case of Z_σ^h we find four projectors to be identified later as $\widetilde{P}_\sigma$, $\widetilde{P}_{\bar\sigma}$, $\widetilde{P}_{\sigma\bar\psi}$, and $\widetilde{P}_{\psi\bar\sigma}$. In the case of Z_ψ^h we find three projectors to be identified as $\widetilde{P}_\psi$, $\widetilde{P}_{\bar\psi}$, and $\widetilde{P}_{\sigma\bar\sigma}$. The last one provides a new way to obtain $\sigma\bar\sigma$ flux in addition to vertical projector $P_2 \equiv P_{\sigma\bar\sigma}$. This is similar redundancy as in the Fibonacci model.

VI. TOPOLOGICAL ENTROPY: VERTICAL PROJECTORS

The topological entanglement entropy (TEE) [58] is not full characterization of topological order but it may provide quick and numerically stable diagnostic for an iPEPS obtained by numerical minimization. Studies of von Neumann TEE of PEPS wave functions have long tradition [59] but they require finding full entanglement spectrum of an infinite half-cylinder and extrapolation to the limit of its infinite width, a task that may be hard to accomplish for a long correlation length. In contrast, the projector formalism is naturally compatible with the second Renyi entropy allowing for its efficient evaluation directly in the thermodynamic limit. What is more, in the realm of string net models the Renyi and von Neumann TEE were shown to be the same [60].

Here we consider a vertical cut in an iPEPS wrapped on an infinite horizontal cylinder of width L_v. Its right/left boundary fixed point on the left/right half-cylinder is σ_L/σ_R. A reduced density matrix for a half cylinder is isomorfic to [59]

$$\rho \propto \sqrt{\sigma_L^T}\sigma_R\sqrt{\sigma_L^T} \tag{27}$$

and its second Renyi entropy is

$$S_2 = -\log \mathrm{Tr}\,\rho^2 = -\log \mathrm{Tr}\,\sigma_L^T\sigma_R\sigma_L^T\sigma_R. \tag{28}$$

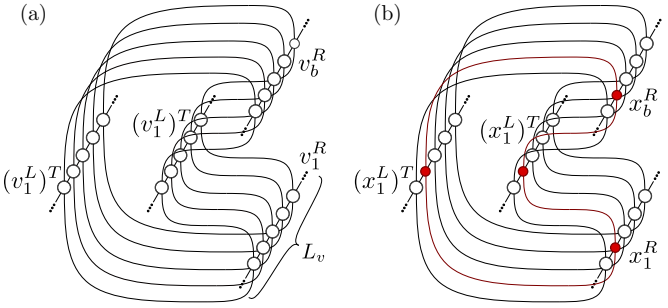

FIG. 4. Topological entropy. In (a), tensor network representing $(v_1^L)^T v_1^R (v_1^L)^T v_b^R$ on a vertical cut in an infinite horizontal cylinder of vertical width L_v. The network is L_vth power of a transfer matrix. In (b), tensor network representing $(x_1^L)^T x_1^R (x_1^L)^T x_b^R$. The network is L_vth power of the same transfer matrix inserted with a layer of impurities $\mathbb{X}_b^{L,R}$.

We want the entropy in a state with a definite anyon flux a along the cylinder.

Towards this end, we begin with $\sigma_{L,R} \propto v_1^{L,R}$ that is a combination of all anyon fluxes. After inserting projector P_a into the vertical cut we obtain

$$\rho_a = \mathcal{N}_a \sqrt{\left(v_1^L\right)^T}\left(v_1^R \cdot P_a^T\right)\sqrt{\left(v_1^L\right)^T}. \tag{29}$$

Here the projector was applied to $\sigma_R \propto v_1^R$ without loss of generality and normalization $\mathcal{N}_a$ is such that $\mathrm{Tr}\rho_a = 1$. The entropy becomes

$$\begin{aligned} S_2(a) &= -\log \mathrm{Tr}\,\rho_a^2 \\ &= -\log \mathcal{N}_a^2\,\mathrm{Tr}\left(v_1^L\right)^T\left(v_1^R \cdot P_a^T\right)\left(v_1^L\right)^T\left(v_1^R \cdot P_a^T\right) \\ &= -\log \mathcal{N}_a^2\,\mathrm{Tr}\left(v_1^L\right)^T v_1^R\left(v_1^L\right)^T P_a^* v_1^R \cdot P_a^T \\ &= -\log \mathcal{N}_a^2\,\mathrm{Tr}\left(v_1^L\right)^T v_1^R\left(v_1^L\right)^T v_1^R P_a^T P_a^T \\ &= -\log \mathcal{N}_a^2\,\mathrm{Tr}\left(v_1^L\right)^T v_1^R\left(v_1^L\right)^T\left(v_1^R \cdot P_a^T\right). \end{aligned} \tag{30}$$

Here we used $P_a^T (v_1^L)^T = (v_1^L)^T P_a^*$ and $P_a^* v_1^R = v_1^R P_a^T$ that follow from the fact that v's are edges of a double-layer iPEPS with bra and ket layers. In this way we are left with only one projector that yields a linear combination,

$$v_1^R \cdot P_a^T = \sum_b s_b^a v_b^R, \tag{31}$$

with coefficients s_b^a that follow from the properties of the MPO symmetries whose linear combination is P_a.

The normalization $\mathrm{Tr}\,\rho_a = 1$ and the biorthonormality, $\mathrm{Tr}(v_1^L)^T v_b^R = \delta_{1b}$, fix $\mathcal{N}_a = 1/s_1^a$. The entropy becomes

$$S_2(a) = -\log \sum_b \frac{s_b^a}{\left(s_1^a\right)^2}\mathrm{Tr}\left(v_1^L\right)^T v_1^R\left(v_1^L\right)^T v_b^R. \tag{32}$$

The trace is a tensor network in Fig. 4(a). It is equal to a trace of L_vth power of a transfer matrix. For large enough L_v the network becomes

$$\mathrm{Tr}\left(v_1^L\right)^T v_1^R\left(v_1^L\right)^T v_b^R = G_b\,\Lambda_b^{L_v}. \tag{33}$$

Here Λ_b is the leading eigenvalue of the transfer matrix and G_b its degeneracy. For large enough L_v the entropy is dominated

by terms with the maximal leading eigenvalue,

$$\Lambda = \mathrm{Max}_b\, \Lambda_b, \tag{34}$$

and becomes

$$S_2(a) = -\log \Lambda^{L_v} \widetilde{\sum_b} \frac{G_b s_b^a}{\left(s_1^a\right)^2} \equiv \alpha L_v - \gamma_a. \tag{35}$$

Here the sum is restricted to indices b with $\Lambda_b = \Lambda$. The area law has a coefficient

$$\alpha = -\log \Lambda \tag{36}$$

that does not depend on anyon flux a and the TEE is

$$\gamma_a = \log \widetilde{\sum_b} \frac{G_b s_b^a}{\left(s_1^a\right)^2}. \tag{37}$$

We evaluate this expression in several examples.

A. Toric code

The projector yields $v_1^R \cdot P_\pm^T = (v_1^R \pm v_2^R)/2$, hence $s_1^\pm = 1/2$ and $s_2^\pm = \pm 1/2$. Furthermore, we obtain $\mathrm{Tr}(v_1^L)^T v_1^R (v_1^L)^T v_b^R = \Lambda^{L_v}$ when $b = 1$ and zero otherwise. There is no degeneracy, $G_1 = 1$. Therefore,

$$\gamma_\pm = \log \widetilde{\sum_b} 4 s_b^\pm = \log 4 s_1^\pm = \log 2. \tag{38}$$

This number is consistent with the anticipated identification $P_+ \equiv P_{\mathrm{vac}}$ and $P_- \equiv P_e$.

B. Fibonacci string net

The projector yields $v_1^R \cdot P_\pm^T = (\phi^{\pm 1} v_1^R \mp v_2^R)/\sqrt{5}$, hence $s_1^\pm = \phi^{\pm 1}/\sqrt{5}$ and $s_2^\pm = \mp 1/\sqrt{5}$. We obtain with numerical precision:

$$\gamma_+ = \log \mathcal{D}, \quad \gamma_- = \log \frac{\mathcal{D}}{d_\tau d_{\bar\tau}}, \tag{39}$$

where $\mathcal{D} = 2 + \phi$ is the total quantum dimension and $d_\tau = d_{\bar\tau} = \phi$. These numbers are consistent with the identification $P_+ \equiv P_{\mathrm{vac}}$ and $P_- \equiv P_{\tau\bar\tau}$.

C. Ising string net

Following similar lines for the double Fibonacci string net we obtain

$$\gamma_5 = \log \mathcal{D}, \quad \gamma_6 = \log \frac{\mathcal{D}}{d_\psi d_{\bar\psi}}, \quad \gamma_2 = \log \frac{\mathcal{D}}{d_\sigma d_{\bar\sigma}} \tag{40}$$

with numerical precision. Here the total quantum dimension $\mathcal{D} = 4$, $d_\sigma = d_{\bar\sigma} = \sqrt{2}$, and $d_\psi = d_{\bar\psi} = 1$. They are consistent with the identifications: $P_5 \equiv P_{\mathrm{vac}}$, $P_6 \equiv P_{\psi\bar\psi}$, and $P_2 \equiv P_{\sigma\bar\sigma}$.

VII. TOPOLOGICAL ENTROPY: IMPURITY PROJECTORS

For impurity projectors that act on an iPEPS that is inserted with Z^h calculation of entropy goes along similar lines but with modifications accounting for Z^h. Accordingly, we begin with $\sigma^{L,R} = x_1^{L,R}$. Here x_i^L and x_j^R are MPO forms of impurity eigenstates $(x_i^L|$ and $|x_j^R)$, respectively. As usual, their left/right indices correspond to the bra/ket layer. The action of $\tilde P_a$ yields

$$x_1^R \cdot \tilde P_a^T = \sum_b \tilde s_b^a x_b^R. \tag{41}$$

Here coefficients $\tilde s_b^a$ are real because x_b^R are Hermitian. Taking into account normalization that follows from their biorthonormality, $\delta_{i_1 i_2} = (x_{i_1}^L | x_{i_2}^R) = \mathrm{Tr}\,(x_{i_1}^L)^T x_{i_2}^R$, the entropy in sector a becomes

$$S_2(a) = -\log \sum_b \frac{\tilde s_b^a}{\left(\tilde s_1^a\right)^2} \mathrm{Tr}\left(x_1^L\right)^T x_1^R \left(x_1^L\right)^T x_b^R. \tag{42}$$

The trace is a trace of the tensor network in Fig. 4(b). It is a trace of L_vth power of a transfer matrix times a layer of impurities $\mathbb{X}_b^{L,R}$. The transfer matrix is the same as in Fig. 4(a). For large enough cylinder width L_v the sum is dominated by indices b such that $\Lambda_b = \Lambda$, where Λ is the same maximal leading eigenvalue of the transfer matrices:

$$S_2(a) = \alpha L_v - \widetilde{\gamma}_a. \tag{43}$$

Here $\alpha = -\log \Lambda$ is the same as for vertical projectors and independent of anyon flux a. The topological entropy is

$$\widetilde{\gamma}_a = \log \widetilde{\sum_b} \frac{\tilde s_b^a}{\left(\tilde s_1^a\right)^2} \sum_{m=1}^{G_b} X_{b,m}^a. \tag{44}$$

Here

$$X_{b,m}^a = \left(U_{b,m}\middle|\mathrm{Tr}\left(\mathbb{X}_1^L\right)^T \mathbb{X}_1^R \left(\mathbb{X}_1^L\right)^T \mathbb{X}_1^R \middle| D_{\{b_i\},m}\right) \tag{45}$$

is a form factor where $(U_{1,m}|$ and $|D_{1,m})$ are the up and down leading eigenvectors of the transfer matrix in Fig. 4(b), numbered by $m = 1 \ldots G_b$ where G_b is the degeneracy of the leading eigenvalue, and $\mathrm{Tr}(\mathbb{X}_1^L)^T \mathbb{X}_1^R (\mathbb{X}_1^L)^T \mathbb{X}_b^R$ is the MPO equal to the horizontal layer of impurities $\mathbb{X}_b^{L,R}$ in the same figure. The numerical procedure was applied in the following examples.

A. Toric code

The impurity projectors $\tilde P_\pm$ together with IMPO fusion rules (23) determine the coefficients $\tilde s_{\pm 1} = 1/2$ and $\tilde s_{\pm 2} = \pm 1/2$. As for vertical projectors, the truncated sum runs over $b = 1$ only with degeneracy $G_1 = 1$. The topological entropies are

$$\widetilde{\gamma}_\pm = \log 2 X_{1,1}^a = \log 2 \tag{46}$$

within numerical precision. This number is obtained after numerical evaluation of the form factors and is consistent with the identification $\widetilde{P}_+ = \widetilde{P}_{\mathrm{m}}$ and $\widetilde{P}_- = \widetilde{P}_\epsilon$.

B. Fibonacci string net

Numerical evaluation of coefficients $\tilde s_b^a$ and the form factors yields

$$\widetilde{\gamma}_1 = \log \frac{\mathcal{D}}{d_\tau}, \quad \widetilde{\gamma}_2 = \log \frac{\mathcal{D}}{d_{\bar\tau}}, \quad \gamma_- = \log \frac{\mathcal{D}}{d_\tau d_{\bar\tau}} \tag{47}$$

with numerical precision. Here $\mathcal{D} = 2 + \phi$ is the total quantum dimension and $d_\tau = d_{\bar\tau} = \phi$. These numbers are consistent with the identifications: $\widetilde{P}_1 = \widetilde{P}_\tau$, $\widetilde{P}_2 = \widetilde{P}_{\bar\tau}$, and $\widetilde{P}_3 = \widetilde{P}_{\tau\bar\tau}$.

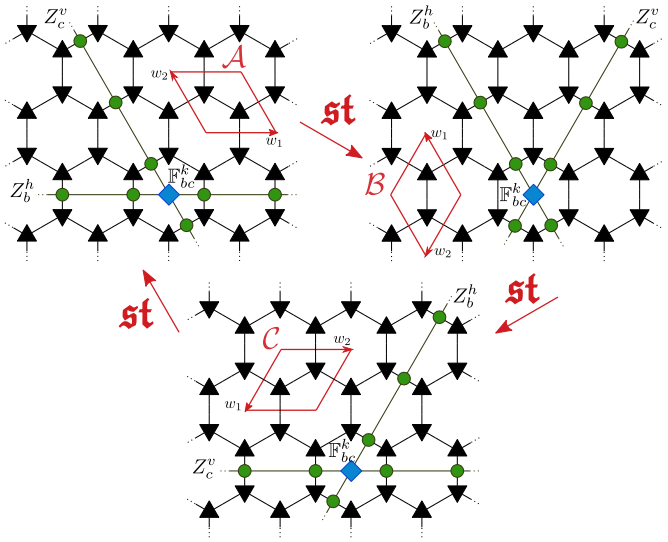

FIG. 5. Basic state. The object $\mathbb{F}_{bc}^k$, includes the lines of Z_b^h and Z_c^v and a tensor at their intersection. When $b = 1$ ($c = 1$) then $\mathbb{F}$ is just vertical MPO symmetry Z_c^v (horizontal Z_b^h). When $b > 1$ then $\mathbb{F}_{bc}^k$ is one of the IMPO symmetries. Inserted into an iPEPS wrapped on an infinite torus it yields state $|\mathbb{F}_{bc}^k\rangle$. The same set of states (for each b, c, k) can be found on each of the tori related by modular $\mathfrak{st}$ transformation, where $(\mathfrak{st})^3 = \mathbb{I}$, which corresponds to 120° counterclockwise rotation on the honeycomb lattice with the chosen tori defined by a pair of unit vectors (w_1, w_2).

C. Ising string net

Similar numerical evaluation as for Fibonacci model yields

$$\widetilde{\gamma}_\sigma = \log\frac{\mathcal{D}}{d_\sigma}, \quad \widetilde{\gamma}_{\bar{\sigma}} = \log\frac{\mathcal{D}}{d_{\bar{\sigma}}}, \tag{48}$$

$$\widetilde{\gamma}_{\sigma\bar{\psi}} = \log\frac{\mathcal{D}}{d_\sigma d_{\bar{\psi}}}, \quad \widetilde{\gamma}_{\psi\bar{\sigma}} = \log\frac{\mathcal{D}}{d_\psi d_{\bar{\sigma}}}, \tag{49}$$

$$\widetilde{\gamma}_\psi = \log\frac{\mathcal{D}}{d_\psi}, \quad \widetilde{\gamma}_{\bar{\psi}} = \log\frac{\mathcal{D}}{d_{\bar{\psi}}}, \tag{50}$$

$$\widetilde{\gamma}_{\sigma\bar{\sigma}} = \log\frac{\mathcal{D}}{d_\sigma d_{\bar{\sigma}}} \tag{51}$$

within numerical precision. Here the total quantum dimension is $\mathcal{D} = 4$ while $d_\sigma = d_{\bar{\sigma}} = \sqrt{2}$ and $d_\psi = d_{\bar{\psi}} = 1$. The numbers are consistent with the anticipated identification of the projectors.

VIII. TOPOLOGICAL S AND T MATRICES

For pedagogical reasons, up to this point we distinguished between vertical projectors, with a trivial $Z_1^h = 1^h$, and impurity projectors. For the present purpose of calculating topological S and T matrices it may be more convenient to treat them all on equal footing. We number MPO symmetries as $Z_a^{h,v}$ with $a = 1, ..., n$, where $a = 1$ labels the trivial identities $1^{h,v}$. A basic building block for the projectors is $\mathbb{F}_{bc}^k$, shown in Fig. 5, including the lines of Z_b^h and Z_c^v and a tensor at their intersection. When $b = 1$ ($c = 1$) then $\mathbb{F}$ is just vertical MPO symmetry Z_c^v (horizontal Z_b^h). When $b > 1$ then $\mathbb{F}_{bc}^k$ is one of the IMPO symmetries. Therefore, in this unified notation each (vertical or impurity) projector on anyon flux a can be expressed as a linear combination

$$P_a = \sum_{bc}\sum_k c_{kbc}^a \mathbb{F}_{bc}^k, \tag{52}$$

where the range of k depends on bc. When inserted into iPEPS wrapped on an infinite torus, the projector yields the ground state with anyon flux a in the horizontal direction:

$$|\Psi^a\rangle = \sum_{ab}\sum_k c_{kab}^a |\mathbb{F}_{ab}^k\rangle. \tag{53}$$

Here the last ket is the iPEPS inserted with $\mathbb{F}_{\alpha\beta}^k$. Up to this point there is nothing essentially new in this paragraph except for fixing notation.

States $|\Psi^a\rangle$ are used to calculate topological S and T matrices. Diagonal T matrix encodes self-statistics, while S matrix stands for mutual statistics. Together they form a representation of a modular group $SL(2, \mathbb{Z})$, by which they are related to the modular transformations of a torus generated by $\mathfrak{s}$ and $\mathfrak{t}$ transformations [61]. It follows that the matrix elements of a combination of the topological S and T matrices are given by the overlaps between $|\Psi^a\rangle$ transformed by a combination of corresponding modular matrices $\mathfrak{s}$ and $\mathfrak{t}$.

Here we work with states on a hexagonal lattice with 120° rotational symmetry and we start by defining torus $\mathcal{A}$ in Fig. 5 with unit vectors w_1, w_2 and corresponding transfer

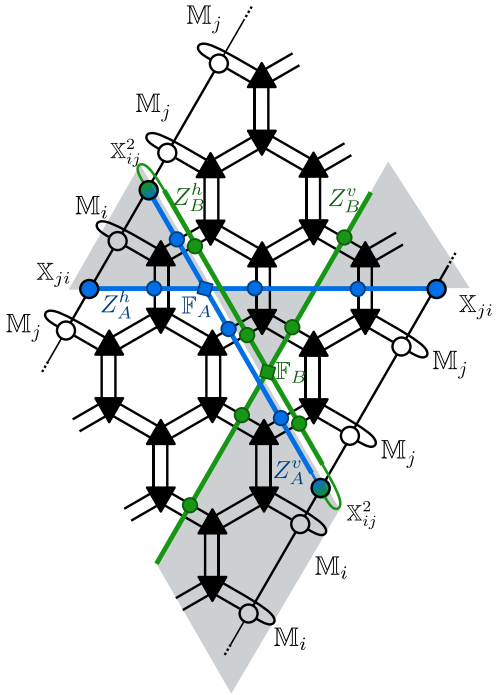

FIG. 6. The overlap in Eq. (55) between iPEPS' on infinite tori $\mathcal{A}$ and $\mathcal{B}$ calculated on torus $\mathcal{B}$, using its vertical boundary MPS. It involves a new class of impurity transfer matrices and their eigenvectors, where a nontrivial MPO symmetry is in only one layer of the PEPS (either bra or ket) or there are two nontrivial MPO symmetries in both layers but they are of a different type. Inserting an MPO symmetry may in general change the boundaries, hence the change of indices $\mathbb{M}_i \to \mathbb{M}_j$ and the gray shaded regions denoting these sector changes.

matrices: vertical $(w_1, L_v w_2)$ and horizontal $(L_h w_1, w_2)$ with $L_{h,v} \to \infty$, see Fig. 2(b) for comparison. Next, we consider all transformations of the unit cell by $\mathfrak{st}$ matrix, which generates 120° counterclockwise rotation, see Fig. 5. This results in tori $\mathcal{B}$ and $\mathcal{C}$ together with their corresponding transfer matrices as shown in Fig. 5. This construction, however, is general and can be applied to lattices with other symmetries as well.

Our method requires finding three complete sets of ground states

$$\{|\Psi^a_{\mathcal{A}}\rangle\}, \quad \{|\Psi^a_{\mathcal{B}}\rangle\}, \quad \{|\Psi^a_{\mathcal{C}}\rangle\}, \tag{54}$$

with well-defined anyon fluxes corresponding to three different tori: $\mathcal{A}$, $\mathcal{B}$, $\mathcal{C}$. Topological S and T matrices are extracted from all possible overlaps between states in (54). This algorithm is presented in Ref. [62] and slightly generalized in the Appendix of Ref. [48].

The core of the calculation is an overlap

$$\langle (\mathbb{F}^k_{ab})_{\mathcal{A}} | (\mathbb{F}^{k'}_{a'b'})_{\mathcal{B}} \rangle, \tag{55}$$

shown in Fig. 6, between two iPEPS's on infinite tori $\mathcal{A}$ and $\mathcal{B}$. It involves a new class of impurity transfer matrices and their eigenvectors, where a nontrivial MPO symmetry is in only one layer of the PEPS (either bra or ket) or there are two nontrivial MPO symmetries in both layers but they are of a different type. This type of overlap was encountered already in the Abelian case in Ref. [48] where they are explained in more detail. In the Abelian case the nontrivial MPO symmetry inserted in just one layer of the PEPS changes the boundary MPS $|v_i\rangle \to |v_j\rangle$, where $i \neq j$. However in the non-Abelian case, all changes of the boundary MPS have to be considered including $i = j$. The possible change of the boundary conditions is denoted in Fig. 6 by shaded gray regions. Once the overlaps are found, we follow the algebra in Appendix B of Ref. [48] to obtain the following topological matrices S and T.

A. Toric code

For analytic tensors with $D = 4$ we obtain the exact matrices up to numerical precision:

$$S_{\mathrm{TC}} = \frac{1}{2}\begin{pmatrix} 1 & 1 & 1 & 1 \\ 1 & 1 & -1 & -1 \\ 1 & -1 & 1 & -1 \\ 1 & -1 & -1 & 1 \end{pmatrix},$$

$$T_{\mathrm{TC}} = \begin{pmatrix} 1 & 0 & 0 & 0 \\ 0 & 1 & 0 & 0 \\ 0 & 0 & 1 & 0 \\ 0 & 0 & 0 & -1 \end{pmatrix}.$$

Here consecutive columns and rows correspond to projectors that were labeled as $1, e, m, \epsilon$. These matrices confirm correctness of this labeling up to possible interchange of e and m that is a matter of convention.

B. Fibonacci string net

For the five states obtained with projectors P_{vac}, $P_{\tau\bar{\tau}}$, $\widetilde{P}_{\tau\bar{\tau}}$, $\widetilde{P}_{\tau}$, $\widetilde{P}_{\bar{\tau}}$ we obtain the matrices:

$$S_{\mathrm{Fib}} = \tfrac{1}{D}\begin{pmatrix} 1 & \varphi^2 & \varphi^2 & \varphi & \varphi \\ \varphi^2 & 1 & 1 & -\varphi & -\varphi \\ \varphi^2 & 1 & 1 & -\varphi & -\varphi \\ \varphi & -\varphi & -\varphi & -1 & \varphi^2 \\ \varphi & -\varphi & -\varphi & \varphi^2 & -1 \end{pmatrix}, \qquad T_{\mathrm{Fib}} = \begin{pmatrix} 1 & 0 & 0 & 0 & 0 \\ 0 & 1 & 0 & 0 & 0 \\ 0 & 0 & 1 & 0 & 0 \\ 0 & 0 & 0 & \mathrm{e}^{4i\pi/5} & 0 \\ 0 & 0 & 0 & 0 & \mathrm{e}^{-4i\pi/5} \end{pmatrix}.$$

For brevity matrix S_{Fib} is shown exact with $\varphi = d_\tau = \frac{1}{2}(1+\sqrt{5})$ although we obtain it with numerical accuracy $\mathcal{O}(10^{-10})$. It is clear that we can remove either second or third row and column because they both correspond to two equivalent ways of obtaining flux $\tau\bar{\tau}$.

C. Ising string net

For the ten states obtained with projectors $P_{\mathrm{vac}}, P_{\psi\bar{\psi}}, P_{\sigma\bar{\sigma}}, \widetilde{P}_{\sigma\bar{\sigma}}, \widetilde{P}_{\bar{\psi}}, \widetilde{P}_{\psi}, \widetilde{P}_{\sigma}, \widetilde{P}_{\sigma\bar{\psi}}, \widetilde{P}_{\bar{\sigma}}, \widetilde{P}_{\psi\bar{\sigma}}$ we obtain the matrices with numerical accuracy $\mathcal{O}(10^{-13})$:

$$S_{\mathrm{Is}} = \tfrac{1}{4}\begin{pmatrix} 1 & 1 & 2 & 2 & 1 & 1 & \sqrt{2} & \sqrt{2} & \sqrt{2} & \sqrt{2} \\ 1 & 1 & 2 & 2 & 1 & 1 & -\sqrt{2} & -\sqrt{2} & -\sqrt{2} & -\sqrt{2} \\ 2 & 2 & 0 & 0 & -2 & -2 & 0 & 0 & 0 & 0 \\ 2 & 2 & 0 & 0 & -2 & -2 & 0 & 0 & 0 & 0 \\ 1 & 1 & -2 & -2 & 1 & 1 & \sqrt{2} & \sqrt{2} & -\sqrt{2} & -\sqrt{2} \\ 1 & 1 & -2 & -2 & 1 & 1 & -\sqrt{2} & -\sqrt{2} & \sqrt{2} & \sqrt{2} \\ \sqrt{2} & -\sqrt{2} & 0 & 0 & \sqrt{2} & -\sqrt{2} & 0 & 0 & 2 & -2 \\ \sqrt{2} & -\sqrt{2} & 0 & 0 & \sqrt{2} & -\sqrt{2} & 0 & 0 & -2 & 2 \\ \sqrt{2} & -\sqrt{2} & 0 & 0 & -\sqrt{2} & \sqrt{2} & 2 & -2 & 0 & 0 \\ \sqrt{2} & -\sqrt{2} & 0 & 0 & -\sqrt{2} & \sqrt{2} & -2 & 2 & 0 & 0 \end{pmatrix},$$

$$T_{\mathrm{Is}} = \begin{pmatrix} 1 & 0 & 0 & 0 & 0 & 0 & 0 & 0 & 0 & 0 \\ 0 & 1 & 0 & 0 & 0 & 0 & 0 & 0 & 0 & 0 \\ 0 & 0 & 1 & 0 & 0 & 0 & 0 & 0 & 0 & 0 \\ 0 & 0 & 0 & 1 & 0 & 0 & 0 & 0 & 0 & 0 \\ 0 & 0 & 0 & 0 & -1 & 0 & 0 & 0 & 0 & 0 \\ 0 & 0 & 0 & 0 & 0 & -1 & 0 & 0 & 0 & 0 \\ 0 & 0 & 0 & 0 & 0 & 0 & e^{i\pi/8} & 0 & 0 & 0 \\ 0 & 0 & 0 & 0 & 0 & 0 & 0 & -e^{i\pi/8} & 0 & 0 \\ 0 & 0 & 0 & 0 & 0 & 0 & 0 & 0 & e^{-i\pi/8} & 0 \\ 0 & 0 & 0 & 0 & 0 & 0 & 0 & 0 & 0 & -e^{-i\pi/8} \end{pmatrix}.$$

It is clear that we can remove either the third or fourth row and column because they both correspond to two equivalent ways of obtaining flux $\sigma\bar{\sigma}$.

IX. SUMMARY

We presented numerical method to determine non-Abelian topological order in iPEPS representing the unique ground state on infinite two-dimensional lattice. The method is based on finding consecutively the following elements:

(1) All of the boundary fixed points of PEPS transfer matrices in the form of matrix product operators v_i;

(2) All MPO symmetries Z_a mapping between the boundaries and their fusion rules;

(3) All impurity eigenvectors x_a of vertical impurity transfer matrices of PEPS inserted with horizontal MPO symmetries Z^h;

(4) All impurity MPO symmetries $\widetilde{Z}$ mapping between the impurity eigenvectors;

(5) All projectors on states with well defined anyon flux along horizontal direction. They are linear combinations of either vertical MPO symmetries or vertical impurity MPO symmetries: $P_a = \sum_{bc}\sum_k c^a_{kbc}\mathbb{F}^k_{bc}$;

(6) All overlaps between states with definite anyon flux on different infinite tori related by modular transformations.

The topological charges and mutual statistics in the form of topological S and T matrices are recovered from the overlaps. They provide full topological characterization of string net models.

A byproduct of the linear ansatz for a projector is an efficient algorithm to obtain the second Renyi topological entanglement entropy directly in the thermodynamic limit. In addition to tests for the string net models, we found nonzero TEE in the variational ansatz of Ref. [46] for the Kitaev model in magnetic field [3], see Appendix E.

ACKNOWLEDGMENTS

We are indebted to Lukasz Cincio and Guifre Vidal, the coauthors of our common Ref. [48], for laying foundations for the present generalization. Special thanks to Lukasz for helpful comments on the present paper. We would also like to thank Hyun-Yong Lee for very useful feedback on the ansatz in Ref. [46]. A.F. would like to thank Bram Vanhecke for explaining the VUMPS algorithm. Numerical calculations were performed in MATLAB with the help of `ncon` function [63] for tensor contractions. A.F. acknowledges financial support by Polish Ministry of Science and Education, Project No. DI2015 021345, from the budget funds for science in 2016–2020 under the Diamond Grant program. This research was supported by Narodowe Centrum Nauki (NCN) under Grant No. 2019/35/B/ST3/01028 (A.F., J.D.) and Etiuda Grant No. 2020/36/T/ST3/00451 (A.F.).

APPENDIX A: FUSION RULES

Fusion rules are encoded in F symbols which have to satisfy the Pentagon equation:

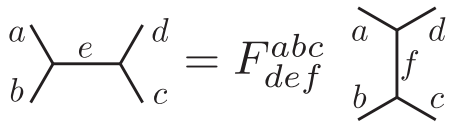

F symbols of both non-Abelian models are mostly given by the allowed fusions: N^c_{ab} describing $a \times b \to c$ with all its (allowed) permutations:

(i) for Fibonacci: $N^1_{11} = N^1_{\tau\tau} = N^\tau_{\tau\tau} = 1$

(ii) for Ising: $N^1_{11} = N^1_{\sigma\sigma} = N^1_{\psi\psi} = N^\sigma_{\psi\psi} = 1$.

Then $F^{abc}_{def} = N^e_{ab}N^e_{cd}N^f_{ad}N^f_{bc}$ unless they are overwritten by additional special rules:

(i) for Fibonacci: $F^{\tau\tau\tau}_{\tau 11} = -F^{\tau\tau\tau}_{\tau\tau\tau} = \frac{1}{d_\tau}$ and $F^{\tau\tau\tau}_{\tau\tau 1} = F^{\tau\tau\tau}_{\tau 1\tau} = \frac{1}{\sqrt{d_\tau}}$.

(ii) for Ising: $F^{\sigma\sigma\sigma}_{\sigma 11} = F^{\sigma\sigma\sigma}_{\sigma 1\psi} = F^{\sigma\sigma\sigma}_{\sigma\psi 1} = -F^{\sigma\sigma\sigma}_{\sigma\psi\psi} = \frac{1}{\sqrt{2}}$ and $F^{\psi\sigma\psi}_{\sigma\sigma\sigma} = F^{\sigma\psi\sigma}_{\psi\sigma\sigma} = -1$.

APPENDIX B: iPEPS TENSORS

iPEPS tensors, shown in Fig. 7, are given by the following combination of F symbols and quantum dimensions d_i:

$$A^i_{\alpha\beta\gamma} = \left(\frac{d_a d_b}{d_c}\right)^{1/4} F^{dab}_{fec}\delta_{aa'}\delta_{bb'}\delta_{cc'}\delta_{dd'}\delta_{ee'}\delta_{ff'} \quad \text{(B1)}$$

$$B^i_{\alpha\beta\gamma} = \left(\frac{d_a d_b}{d_c}\right)^{1/4} F^{dab}_{fec}\delta_{aa'}\delta_{bb'}\delta_{cc'}\delta_{dd'}\delta_{ee'}\delta_{ff'}. \quad \text{(B2)}$$

By construction each tensor has a triple of bond indices along each of the three bonds towards NN lattice sites. We concatenate each triple into a single bond index, e.g., $\alpha = (a, e, d')$. The physical index is also a triple index $i = (a', b', c')$. These basic tensors are forming the topological state after proper contraction of bond indices with respect to their triplet structure. For the toric code and double Fibonacci string nets the bond dimension $D = 2^3 = 8$ is redundantly large and can be reduced to $D = 4$ and $D = 5$ after applying projectors on the bond indices, namely the only nonzero

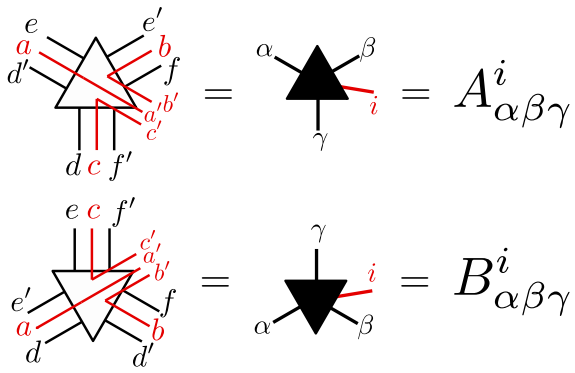

FIG. 7. Tensors forming the iPEPS are defined via combination of F-symbols and corresponding quantum dimensions d_i. All bond indices and the physical index are in fact a triple index. The bond dimension can be reduced by applying projectors on the non zero bond indices.

combinations of bond indices (i, j, k) are those in which the fusion product $i \times j \times k = 1 + \cdots$ contains the trivial anyon. For the double Ising string net, on the other hand, the original bond dimension $D = 3^3 = 27$ can be reduced to $D = 10$.

APPENDIX C: PERTURBATION OF TENSOR SYMMETRY

In Ref. [48] we demonstrated that with our method it is possible to obtain accurate results for topological S and T matrices from a numerically optimized iPEPS ground state of the Kitaev honeycomb model for a wide range of coupling parameters. In the case of Fibonacci and Ising string nets, whose parent Hamiltonians are far more complex, the same test would go far beyond the scope of the present paper.

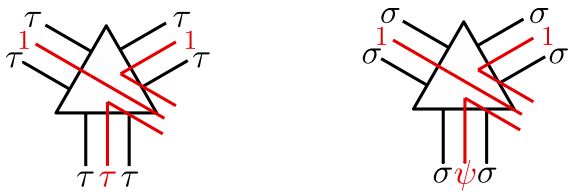

FIG. 8. Symmetry breaking perturbations in Fibonacci (left) and Ising (right) string nets.

However, as most concerns about stability arise from Ref. [64], we can introduce their perturbation at the virtual level of the tensor network—which violates the exact MPO symmetries—to see how our algorithm performs under this crash test.

The vertex violating terms [64], T_p, which are allowed in the stand-alone space but do not represent the physical ground state, are shown in Fig. 8. Additionally we allow all three rotations of the red indices. The fixed-point tensors T are perturbed by adding a vertex violating term T_p controlled by a small parameter ϵ:

$$T \;\rightarrow\; T + \epsilon\, T_p. \tag{C1}$$

For the Fibonacci string-net model perturbed with a strong $\epsilon = 0.1$ we obtained the following topological entanglement entropies:

$$\begin{pmatrix} 1.2847 \\ 0.3235 \\ 0.3235 \\ 0.8047 \\ 0.8047 \end{pmatrix}, \tag{C2}$$

and the following topological matrices:

$$S_{\mathrm{Fib}} = \begin{pmatrix} 0.2771 & 0.7251 & 0.7252 & 0.4484 & 0.4484 \\ 0.7251 & 0.2735 & 0.2749 & -0.4486 & -0.4486 \\ 0.7252 & 0.2749 & 0.2764 & -0.4472 & -0.4472 \\ 0.4484 & -0.4486 & -0.4472 & -0.2764 & 0.7236 \\ 0.4484 & -0.4486 & -0.4472 & 0.7236 & -0.2764 \end{pmatrix}$$

and

$$\mathrm{diag}(T_{\mathrm{Fib}}) = \begin{pmatrix} 1.0000 - 0.0000i \\ 1.0000 + 0.0000i \\ 1.0000 - 0.0000i \\ -0.8090 - 0.5878i \\ -0.8090 + 0.5878i \end{pmatrix}.$$

When compared to the exact numbers, their maximal error is of the order of 10^{-3}. Although there are four anyon fluxes in the Fibonacci model, here as in the main text we keep both $\mathcal{P}_{\tau\bar{\tau}}$ and $\tilde{\mathcal{P}}_{\tau\bar{\tau}}$ which project on the same flux $\tau\bar{\tau}$.

For the Ising string-net model we added a perturbation shown in Fig. 8 with strength $\epsilon = 0.5$, which lead to even more accurate results. We obtained topological entanglement entropy and topological S and T matrices with accuracy $\mathcal{O}(10^{-6})$.

In order to complete the discussion about random perturbations that may arise during numerical optimization of iPEPS we calculated the topological data for a completely random, real perturbation in the Fibonacci string-net model:

$$T \;\rightarrow\; T + \epsilon\, T_{\mathrm{random}}. \tag{C3}$$

For $\epsilon = 0.01$ we recovered the topological entanglement entropies and topological matrices with accuracy of the order of $\mathcal{O}(10^{-4})$.

APPENDIX D: INTRODUCING FINITE CORRELATION LENGTH

In order to see how the algorithm performs when the iPEPS tensors are driven away from the fixed point by introducing a finite correlation length, we apply the local filtering introduced in Refs. [65–67] to the fixed point of the Fibonacci string-net model. The perturbation has the following form:

$$|\Psi\rangle \;\rightarrow\; \prod_i e^{\beta\sigma_i^z}|\Psi\rangle, \tag{D1}$$

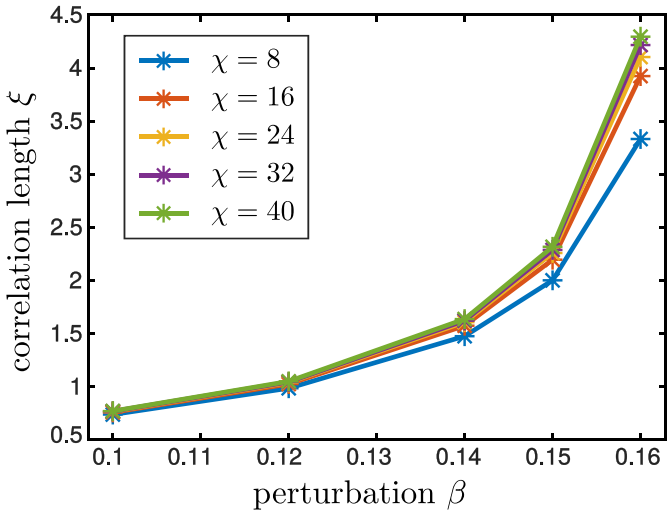

FIG. 9. The correlation length ξ in the Fibonacci string net model in function of the perturbation parameter β in Eq. (D1). Different colors correspond to different bond dimensions χ of the boundary MPS v_i.

where the index i runs over all physical indices and σ^z is the third Pauli matrix. In Ref. [48], by considering a similar perturbation to the toric code, we demonstrated that with our algorithm it is possible to obtain topological S and T matrices for states with correlation length much longer than achievable by the state of the art 2D DMRG techniques.

Figure 9 shows how the correlation length grows with parameter β for the perturbed Fibonacci string-net model. In the Fibonacci model, for parameters $\beta = 0.14, 0.15, 0.16$ such that the correlation length $\xi > 1$, we obtained the topological entanglement entropies and the topological S and T matrices. Their maximal errors are listed in Table I.

APPENDIX E: VARIATIONAL ANSATZ FOR THE KITAEV MODEL IN (1,1,1) MAGNETIC FIELD

We investigate the ansatz proposed in the Supplemental Material of Ref. [46]. Although it satisfies all desired symmetries and has competitive energy, the ansatz was not demonstrated to possess the expected chiral Ising universality class [3]. We show that at least it has nontrivial topological entanglement entropy.

TABLE I. For different values of the perturbation parameter β in Eq. (D1), the table lists corresponding correlation lengths, ξ, and maximal errors of the entries of the list of topological entanglement entropies, ϵ_γ, and the S and T matrices, ϵ_S and ϵ_T.

β	ξ	ϵ_γ	ϵ_S	ϵ_T
0	0	$\mathcal{O}(10^{-10})$	$\mathcal{O}(10^{-10})$	$\mathcal{O}(10^{-10})$
0.14	1.64	$\mathcal{O}(10^{-3})$	$\mathcal{O}(10^{-4})$	$\mathcal{O}(10^{-6})$
0.15	2.32	$\mathcal{O}(10^{-2})$	$\mathcal{O}(10^{-3})$	$\mathcal{O}(10^{-7})$
0.16	4.3	$\mathcal{O}(10^{-2})$	$\mathcal{O}(10^{-3})$	$\mathcal{O}(10^{-4})$

Each TM has two boundary fixed points. They have large bond dimension χ necessary to accommodate a long correlation length. For $\chi = 150$ the correlation length saturates at $\xi \simeq 15.4$. However, when it comes to calculating the topological entanglement entropy, whose cost is much steeper in χ, we will be satisfied with $\chi = 50$, corresponding to $\xi \simeq 10.3$, that is sufficient to recover exact symmetries. There is one nontrivial $\mathcal{Z}_2$ symmetry such that $v_1^L \cdot Z_2^v = v_2^L$ and $v_2^L \cdot Z_2^v = v_1^L$ and, consequently,

$$Z_2^v \cdot Z_2^v = 1^v. \tag{E1}$$

This is the algebra of the $\mathcal{Z}_2$ gauge field that was implemented in the ansatz by construction.

Like in the toric code, the $\mathcal{Z}_2$ algebra (E1) allows for two vertical projectors:

$$P_\pm = \tfrac{1}{2}(1^v \pm Z^v). \tag{E2}$$

They project on ± 1 horizontal flux of the $\mathcal{Z}_2$ gauge field, see Ref. [46]. In this model, when the horizontal cylinder is closed into a torus, the vertical flux also becomes a good quantum number. For an iPEPS wrapped on a torus (without horizontal line Z_2^h) the state is a superposition of both ± 1 vertical fluxes with equal amplitudes.

We also find nontrivial IMPO symmetry $\widetilde{Z}_2^v$ satisfying the $\mathcal{Z}_2$ algebra. It allows for two projectors:

$$\widetilde{P}_\pm = \tfrac{1}{2}\big(\widetilde{1}^v \pm \widetilde{Z}_2^v\big). \tag{E3}$$

Like the vertical projectors, they project on ± 1 horizontal flux of the $\mathcal{Z}_2$ gauge field but with a superposition of vertical fluxes with opposite amplitudes. Therefore, unlike the Fibonacci and Ising string net, neither of these two impurity projectors can be identified with any of the two vertical projectors $P_\pm$.

For vertical projectors we obtain topological entanglement entropy

$$\gamma_\pm = \log 2 \tag{E4}$$

in the vacuum and vortex sector, respectively. This demonstrates topological order in the variational iPEPS of Ref. [46]. The impurity projectors also yield

$$\tilde{\gamma}_\pm = \log 2 \tag{E5}$$

but here the minimally entangled states $\pm$ are different combinations of the vertical $\mathcal{Z}_2$ flux than in Eq. (E4).

[1] X. G. Wen, Topological orders in rigid states, Int. J. Mod. Phys. B **4**, 239 (1990).

[2] A. Kitaev, Fault-tolerant quantum computation by anyons, Ann. Phys. **303**, 2 (2003).

[3] A. Kitaev, Anyons in an exactly solved model and beyond, Ann. Phys. **321**, 2 (2006).

[4] M. A. Levin and X.-G. Wen, String-net condensation: A physical mechanism for topological phases, Phys. Rev. B **71**, 045110 (2005).

[5] Y. Kasahara, T. Ohnishi, Y. Mizukami, O. Tanaka, S. Ma, K. Sugii, N. Kurita, H. Tanaka, J. Nasu, Y. Motome, T. Shibauchi, and Y. Matsuda, Majorana quantization and half-integer thermal quantum Hall effect in a Kitaev spin liquid, Nature (London) **559**, 227 (2018).

[6] S. R. White, Density Matrix Formulation for Quantum Renormalization Groups, Phys. Rev. Lett. **69**, 2863 (1992).

[7] S. R. White, Density-matrix algorithms for quantum renormalization groups, Phys. Rev. B **48**, 10345 (1993).

[8] S. Yan, D. A. Huse, and S. R. White, Spin-liquid ground state of the $S = 1/2$ Kagome Heisenberg antiferromagnet, Science **332**, 1173 (2011).

[9] H.-C. Jiang, Z. Wang, and L. Balents, Identifying topological order by entanglement entropy, Nat. Phys. **8**, 902 (2012).

[10] S.-S. Gong, D. N. Sheng, O. I. Motrunich, and M. P. A. Fisher, Phase diagram of the spin-1/2 $J_1 - J_2$ Heisenberg model on a honeycomb lattice, Phys. Rev. B **88**, 165138 (2013).

[11] Z. Zhu, D. A. Huse, and S. R. White, Weak Plaquette Valence Bond Order in the $S = 1/2$ Honeycomb $J_1 - J_2$ Heisenberg Model, Phys. Rev. Lett. **110**, 127205 (2013).

[12] S.-S. Gong, W. Zhu, and D. N. Sheng, Emergent chiral spin liquid: Fractional quantum Hall effect in a Kagome Heisenberg model, Sci. Rep. **4**, 6317 (2014).

[13] Z. Zhu and S. R. White, Quantum phases of the frustrated XY models on the honeycomb lattice, Mod. Phys. Lett. B **28**, 1430016 (2014).

[14] S.-S. Gong, W. Zhu, L. Balents, and D. N. Sheng, Global phase diagram of competing ordered and quantum spin-liquid phases on the kagome lattice, Phys. Rev. B **91**, 075112 (2015).

[15] W.-J. Hu, S.-S. Gong, W. Zhu, and D. N. Sheng, Competing spin-liquid states in the spin-1/2 Heisenberg model on the triangular lattice, Phys. Rev. B **92** 140403(R) (2015).

[16] W. Zhu, S. S. Gong, D. N. Sheng, and L. Sheng, Possible non-Abelian Moore-Read state in double-layer bosonic fractional quantum Hall system, Phys. Rev. B **91**, 245126 (2015).

[17] Z. Zhu and S. R. White, Spin liquid phase of the $S = 1/2$ $J_1 - J_2$ Heisenberg model on the triangular lattice, Phys. Rev. B **92**, 041105(R) (2015).

[18] M. P. Zaletel, Z. Zhu, Y.-M. Lu, A. Vishwanath, and S. R. White, Space Group Symmetry Fractionalization in a Chiral Kagome Heisenberg Antiferromagnet, Phys. Rev. Lett. **116**, 197203 (2016).

[19] T.-S. Zeng, W. Zhu, J.-X. Zhu, and D. N. Sheng, Nature of continuous phase transitions in interacting topological insulators, Phys. Rev. B **96**, 195118 (2017).

[20] M.-S. Vaezi and A. Vaezi, Numerical observation of parafermion zero modes and their stability in 2D topological states, arXiv:1706.01192.

[21] Z. Zhu, I. Kimchi, D. N. Sheng, and L. Fu, Robust non-Abelian spin liquid and a possible intermediate phase in the antiferromagnetic Kitaev model with magnetic field, Phys. Rev. B **97**, 241110(R) (2018).

[22] M. Gohlke, G. Wachtel, Y. Yamaji, F. Pollmann, and Y. B. Kim, Quantum spin liquid signatures in Kitaev-like frustrated magnets, Phys. Rev. B **97**, 075126 (2018).

[23] M. Gohlke, R. Moessner, and F. Pollmann, Dynamical and topological properties of the Kitaev model in a [111] magnetic field, Phys. Rev. B **98**, 014418 (2018).

[24] L. Cincio and G. Vidal, Characterizing Topological Order by Studying the Ground States on an Infinite Cylinder, Phys. Rev. Lett. **110**, 067208 (2013).

[25] Y.-C. He, D. N. Sheng, and Y. Chen, Chiral Spin Liquid in a Frustrated Anisotropic Kagome Heisenberg Model, Phys. Rev. Lett. **112**, 137202 (2014).

[26] W. Zhu, S. S. Gong, F. D. M. Haldane, and D. N. Sheng, Topological characterization of the non-Abelian Moore-Read state using density-matrix renormalization group, Phys. Rev. B **92**, 165106 (2015).

[27] W. Zhu, S. S. Gong, and D. N. Sheng, Chiral and critical spin liquids in a spin-1/2 kagome antiferromagnet, Phys. Rev. B **92**, 014424 (2015).

[28] B. Bauer, L. Cincio, B. P. Keller, M. Dolfi, G. Vidal, S. Trebst, and A. W. W. Ludwig, Chiral spin liquid and emergent anyons in a Kagome lattice Mott insulator, Nat. Commun. **5**, 5137 (2014).

[29] W. Zhu, S. S. Gong, F. D. M. Haldane, and D. N. Sheng, Fractional Quantum Hall States at $\nu = 13/5$ and $12/5$ and Their Non-Abelian Nature, Phys. Rev. Lett. **115**, 126805 (2015).

[30] A. G. Grushin, J. Motruk, M. P. Zaletel, and F. Pollmann, Characterization and stability of a fermionic $\nu = 1/3$ fractional Chern insulator, Phys. Rev. B **91**, 035136 (2015).

[31] Y.-C. He, S. Bhattacharjee, F. Pollmann, and R. Moessner, Kagome Chiral Spin Liquid as a Gauged $U(1)$ Symmetry Protected Topological Phase, Phys. Rev. Lett. **115**, 267209 (2015).

[32] Y.-C. He and Y. Chen, Distinct Spin Liquids and Their Transitions in Spin-1/2 XXZ Kagome Antiferromagnets, Phys. Rev. Lett. **114**, 037201 (2015).

[33] Y.-C. He, S. Bhattacharjee, R. Moessner, and F. Pollmann, Bosonic Integer Quantum Hall Effect in an Interacting Lattice Model, Phys. Rev. Lett. **115**, 116803 (2015).

[34] S. Geraedts, M. P. Zaletel, Z. Papić, and R. S. K. Mong, Competing Abelian and non-Abelian topological orders in $\nu = 1/3 + 1/3$ quantum Hall bilayers, Phys. Rev. B **91**, 205139 (2015).

[35] R. S. K. Mong, M. P. Zaletel, F. Pollmann, and Z. Papić, Fibonacci anyons and charge density order in the 12/5 and 13/5 quantum Hall plateaus, Phys. Rev. B **95**, 115136 (2017).

[36] Y.-C. He, F. Grusdt, A. Kaufman, M. Greiner, and A. Vishwanath, Realizing and adiabatically preparing bosonic integer and fractional quantum Hall states in optical lattices, Phys. Rev. B **96**, 201103(R) (2017).

[37] E. M. Stoudenmire, D. J. Clarke, R. S. K. Mong, and J. Alicea, Assembling Fibonacci anyons from a Z_3 parafermion lattice model, Phys. Rev. B **91**, 235112 (2015).

[38] Y.-C. He, M. P. Zaletel, M. Oshikawa, and F. Pollmann, Signatures of Dirac Cones in a DMRG Study of the Kagome Heisenberg Model, Phys. Rev. X **7**, 031020 (2017).

[39] S. N. Saadatmand and I. P. McCulloch, Symmetry fractionalization in the topological phase of the spin-1/2 $J_1 - J_2$

triangular Heisenberg model, Phys. Rev. B **94**, 121111(R) (2016).
[40] C. Hickey, L. Cincio, Z. Papić, and A. Paramekanti, Haldane-Hubbard Mott Insulator: From Tetrahedral Spin Crystal to Chiral Spin Liquid, Phys. Rev. Lett. **116**, 137202 (2016).
[41] M. P. Zaletel, Y.-M. Lu, and A. Vishwanath, Measuring space-group symmetry fractionalization in Z_2 spin liquids, Phys. Rev. B **96**, 195164 (2017).
[42] T.-S. Zeng, W. Zhu, and D. Sheng, Tuning topological phase and quantum anomalous Hall effect by interaction in quadratic band touching systems, npj Quantum Mater. **3**, 49 (2018).
[43] F. Verstraete and J. I. Cirac, Renormalization algorithms for Quantum-Many Body Systems in two and higher dimensions, arXiv:cond-mat/0407066.
[44] V. Murg, F. Verstraete, and J. I. Cirac, Variational study of hard-core bosons in a two-dimensional optical lattice using projected entangled pair states, Phys. Rev. A **75**, 033605 (2007).
[45] F. Verstraete, V. Murg, and J. I. Cirac, Matrix product states, projected entangled pair states, and variational renormalization group methods for quantum spin systems, Adv. Phys. **57**, 143 (2008).
[46] H.-Y. Lee, R. Kaneko, T. Okubo, and N. Kawashima, Gapless Kitaev Spin Liquid to Classical String Gas Through Tensor Networks, Phys. Rev. Lett. **123**, 087203 (2019).
[47] P. Corboz, Variational optimization with infinite projected entangled-pair states, Phys. Rev. B **94**, 035133 (2016).
[48] A. Francuz, J. Dziarmaga, G. Vidal, and L. Cincio, Determining topological order from infinite projected entangled pair states, Phys. Rev. B **101**, 041108(R) (2020).
[49] M. B. Şahinoğlu, D. Williamson, N. Bultinck, M. Mariën, J. Haegeman, N. Schuch, and F. Verstraete, Characterizing topological order with matrix product operators, arXiv:1409.2150.
[50] N. Bultinck, M. Mariën, D. J. Williamson, M. B. Şahinoğlu, J. Haegeman, and F. Verstraete, Anyons and matrix product operator algebras, Ann. Phys. **378**, 183 (2017).
[51] M. Iqbal, K. Duivenvoorden, and N. Schuch, Study of anyon condensation and topological phase transitions from a Z_4 topological phase using the projected entangled pair states approach, Phys. Rev. B **97**, 195124 (2018).
[52] C. Fernández-González, R. S. K. Mong, O. Landon-Cardinal, D. Pérez-García, and N. Schuch, Constructing topological models by symmetrization: A projected entangled pair states study, Phys. Rev. B **94**, 155106 (2016).
[53] S. P. G. Crone and P. Corboz, Detecting a Z_2 topologically ordered phase from unbiased infinite projected entangled-pair state simulations, Phys. Rev. B **101**, 115143 (2020).
[54] H. He, H. Moradi, and X.-G. Wen, Modular matrices as topological order parameter by a gauge-symmetry-preserved tensor renormalization approach, Phys. Rev. B **90**, 205114 (2014).
[55] V. Zauner-Stauber, L. Vanderstraeten, M. T. Fishman, F. Verstraete, and J. Haegeman, Variational optimization algorithms for uniform matrix product states, Phys. Rev. B **97**, 045145 (2018).
[56] M. T. Fishman, L. Vanderstraeten, V. Zauner-Stauber, J. Haegeman, and F. Verstraete, Faster methods for contracting infinite two-dimensional tensor networks, Phys. Rev. B **98**, 235148 (2018).
[57] G. De las Cuevas, J. I. Cirac, N. Schuch, and D. Perez-Garcia, Irreducible forms of matrix product states: Theory and applications, J. Math. Phys. **58**, 121901 (2017).
[58] A. Kitaev and J. Preskill, Topological Entanglement Entropy, Phys. Rev. Lett. **96**, 110404 (2006).
[59] J. I. Cirac, D. Poilblanc, N. Schuch, and F. Verstraete, Entanglement spectrum and boundary theories with projected entangled-pair states, Phys. Rev. B **83**, 245134 (2011).
[60] S. T. Flammia, A. Hamma, T. L. Hughes, and X.-G. Wen, Topological Entanglement Rényi Entropy and Reduced Density Matrix Structure, Phys. Rev. Lett. **103**, 261601 (2009).
[61] X.-G. Wen, A theory of 2+1D bosonic topological orders, Nat. Sci. Rev. **3**, 68 (2015).
[62] Y. Zhang, T. Grover, and A. Vishwanath, General procedure for determining braiding and statistics of anyons using entanglement interferometry, Phys. Rev. B **91**, 035127 (2015).
[63] R. N. C. Pfeifer, G. Evenbly, S. Singh, and G. Vidal, NCON: A tensor network contractor for MATLAB, arXiv:1402.0939.
[64] S. K. Shukla, M. B. Şahinoğlu, F. Pollmann, and X. Chen, Boson condensation and instability in the tensor network representation of string-net states, Phys. Rev. B **98**, 125112 (2018).
[65] J. Haegeman, K. Van Acoleyen, N. Schuch, J. I. Cirac, and F. Verstraete, Gauging Quantum States: From Global to Local Symmetries in Many-Body Systems, Phys. Rev. X **5**, 011024 (2015).
[66] J. Haegeman, V. Zauner, N. Schuch, and F. Verstraete, Shadows of anyons and the entanglement structure of topological phases, Nat. Commun. **6**, 8284 (2015).
[67] G.-Y. Zhu and G.-M. Zhang, Gapless Coulomb State Emerging from a Self-Dual Topological Tensor-Network State, Phys. Rev. Lett. **122**, 176401 (2019).

Variational methods for characterizing matrix product operator symmetries

Anna Francuz,[1,*] Laurens Lootens,[2] Frank Verstraete,[2] and Jacek Dziarmaga[1]

[1] *Jagiellonian University, Institute of Theoretical Physics, Łojasiewicza 11, PL-30348 Kraków, Poland*
[2] *Department of Physics and Astronomy, Ghent University, Krijgslaan 281, S9, B-9000 Ghent, Belgium*

(Dated: November 14, 2021)

We present a method of extracting information about topological order from the ground state of a strongly correlated two-dimensional system represented by an infinite projected entangled pair state (iPEPS). As in Phys. Rev. B 101, 041108 (2020) and 102, 235112 (2020) we begin by determining symmetries of the iPEPS represented by infinite matrix product operators (iMPO) that map between the different iPEPS transfer matrix fixed points, to which we apply the fundamental theorem of MPS to find zipper tensors between products of iMPO's that encode fusion properties of the anyons. The zippers can be combined to extract topological F-symbols of the underlying fusion category, which unequivocally identifies the topological order of the ground state. We bring the F-symbols to the canonical gauge, and also compute the Drinfeld center of this unitary fusion category to extract the topological S and T matrices encoding mutual- and self-statistics of the emergent anyons. The algorithm is applied to Abelian toric code, Kitaev model, double semion and twisted quantum double of Z_3, as well as to non-Abelian double Fibonacci, double Ising, and quantum double of S_3 and Rep(S_3) string net models.

I. INTRODUCTION

Topologically ordered phases[1] support anyonic excitations that open the possibility of realizing fault-tolerant quantum computation[2] by braiding of non-Abelian anyons. Besides the class of exactly solvable models[2–4], verifying if a more general microscopic Hamiltonian has a topologically ordered ground state was traditionally regarded to be an extremely hard task. Recently, observation of quantized Hall effect in Kitaev-like ruthenium chloride α-$RuCl_3$ in magnetic field[5] granted the problem with urgent experimental relevance. Intensive experimental search for other Kitaev-like materials is under way[6].

The density matrix renormalization group (DMRG)[7,8] on a long cylinder used to be the numerical method of choice[9–24]. In the limit of infinitely long cylinders, DMRG naturally produces ground states with well-defined anyonic flux from which one can obtain characterization of a topological order via so-called topological S and T matrices[25]. Since the proposal of Ref. 25, this approach has become a common practice[26–43].

Unfortunately, the cost of a DMRG simulation grows exponentially with the circumference of cylinder, limiting this approach to thin cylinders (up to a circumference of $\simeq 14$ sites) and thus to short correlation lengths (up to $\xi = 1 \sim 2$ sites), since the circumference has to be at least $\approx 6\xi$ to reach convergence in the cylinder width. Instead, infinite projected entangled pair states (iPEPS) in principle allow for much longer correlation lengths[44–46]. A unique ground state on an infinite lattice can be represented by an iPEPS that is either a variational ansatz[47] or a result of numerical optimization[48–51].

When wrapped on a cylinder the iPEPS becomes a superposition of degenerate ground states with definite anyonic fluxes. In the realm of the string-net models it is possible[49,52] to produce a PEPS-like tensor network for each ground state with well-defined flux, see Fig. 1.

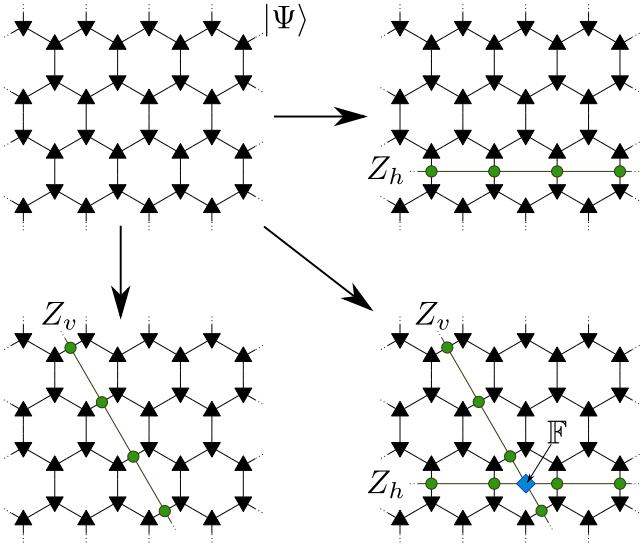

FIG. 1. **The method of Refs. 49 and 52.** From the unique ground state on an infinite lattice – represented by an iPEPS $|\Psi\rangle$ – various states inserted with infinite MPO symmetries, Z_h and Z_v, are constructed. Their linear combinations, whose coefficients are determined by fusion rules of the iMPO symmetries (corresponding to anyonic fusion rules), become a basis of states with well defined anyonic flux. Overlaps of these infinite states determine the topological matrices S and T. Here physical indices are not shown for simplicity.

Such tensor networks are suitable for extracting topological S and T matrices by computing overlaps between the ground states. Furthermore, they allow for computation of topological second Renyi entropy directly in the limit of infinite cylinder's width. The approach of Refs. 49 and 52 does not assume clean realization of certain symmetries on the bond indices, in contrast to[53–56]. This has been demonstrated in Ref. 49 by examples of toric code and double semions perturbed away from a fixed

point towards a ferromagnetic phase as well as for the numerical iPEPS representing the ground state of the Kitaev model in the gapped phase. The same approach was generalized to non-Abelian topological order in Ref. 52. The method does not require restoring the symmetries by suitable gauge transformations of a numerical iPEPS, a feat that was accomplished in Ref. 57 for the toric code with a perturbation. It is also not necessary to optimize symmetry-constrained iPEPS tensors as in Ref. 58. Finally, it also has much lower numerical cost than methods based on the tensor renormalization group[59].

In this work we reconsider the string-net models. Similarly as in Refs. 49 and 52, for a given iPEPS we numerically obtain its infinite matrix product operator (iMPO) symmetries. Products of the iMPO-symmetries realize fusion rules of the corresponding anyons of a unitary fusion category (UFC) $\mathcal{C}$. We use the fundamental theorem of *matrix product states* (MPS)[60,61] and apply it to the iMPO products in order to classify topological order through its related fusion categories. The fundamental theorem of MPS has already been widely used in characterization of phases of both 1D and 2D gapped systems[62,63] as well as the construction of exact renormalization fixed point representations of string-nets with iPEPS[53,54]. The theorem allows us to construct gauge transformations (zippers) between products of iMPO's and their fusion outcomes. The zippers encode information on fusion properties of the corresponding anyons, and they can be combined in order to extract the F-symbols of the underlying UFC $\mathcal{C}$ describing the topological order unequivocally. The different ground states and possible anyonic excitations of the string-net model are actually described by the Drinfeld center $Z(\mathcal{C})$, and different UFCs $\mathcal{C}$ associated to the iMPO symmetries can give the same topological order if their centers are isomorphic[64]. To deal with this redundancy, we compute the center by constructing idempotents of the tube algebra and compute invariants such as the topological S and T matrices which encode mutual- and self-statistics of the emergent anyons. While the S and T matrices provide a useful characterization of the type of topological order, in general they do not uniquely specify the modular category $Z(\mathcal{C})$[65]. By explicitly constructing $Z(\mathcal{C})$, our approach does not suffer from this problem.

The method we use has similarities with previous approaches where one looks for string-like operators on the physical level that commute with the Hamiltonian called ribbon operators[66]. An important fact is that in these approaches, when moving away from the fixed point, these ribbon operators get dressed[67] and their width is proportional to the correlation length. In contrast, in our approach, the iMPO symmetries are not fattened when perturbing the system away from the fixed point since they act purely on the virtual level.

The paper is organized in sections II to IX where we gradually introduce subsequent elements of the algorithm. In Sec. II we give a brief review of 2+1d topological order in PEPS and virtual MPO symmetries, the properties of which are governed by the F-symbols of a UFC $\mathcal{C}$ that we aim to numerically determine for a generic iPEPS. In Sec. III we define fixed points of the iPEPS transfer matrix in the form of iMPS and introduce iMPO symmetries that map between different fixed points. We also identify fusion rules of the iMPO symmetries that are isomorphic with the fusion rules of some input category $\mathcal{C}$. In Sec. IV we introduce X zippers that are gauge transformations between products of two iMPO symmetries acting on a trivial fixed point of the transfer matrix and a single iMPO symmetry applied to the same trivial fixed point. We distinguish between up and down X zippers for, respectively, up and down fixed points. In Sec. V we introduce and construct more elementary Y zippers. Each Y zipper is a gauge transformation between a product of an iMPO symmetry and a fixed point of the transfer matrix and the resulting fixed point. X zippers can be constructed out of the elementary Y zippers. In Sec. VI pairs of complementary left and right X zippers are normalized to become pairs of gauge and inverse gauge transformations. In particular, a non-trivial normalization between up and down zippers is imposed. In Sec. VII we construct F symbols out of the normalized up and down X zippers. The fusion symbols have arbitrary/random numerical gauge. In Sec. VIII we parameterize the gauge freedom and outline how the F symbols can be brought to some canonical gauge that allows to identify the topological order. In Sec. IX we algebraically construct the gauge-invariant central idempotents of the tube algebra made of the zippers, which when inserted into iPEPS – as in Fig. 1 – can be thought of as projectors onto minimally entangled states (MES). However, here we do not construct the MES but use the central idempotents of the tube algebra to directly extract topological S and T matrices[54,68]. Unlike the F symbols, the S and T matrices are gauge-invariant observables with a physical interpretation of statistics of the emergent anyons. In contrast to Ref. 49 and 52, here they are obtained by algebraic manipulation from the F-symbols, the calculation of which is a purely 1D problem, which significantly reduces the complexity of the numerical algorithms. The route via F-symbols therefore provides an alternative that is potentially more stable numerically. The paper is closed with a brief summary of the algorithm in section X and an outlook towards future applications.

II. MPO SYMMETRIES IN PEPS

A necessary condition for a tensor network to exhibit topological order is the existence of string-like operators on the virtual level that can be freely moved through the lattice. These operators are represented as MPO symmetries, that at the level of the local PEPS tensors satisfy

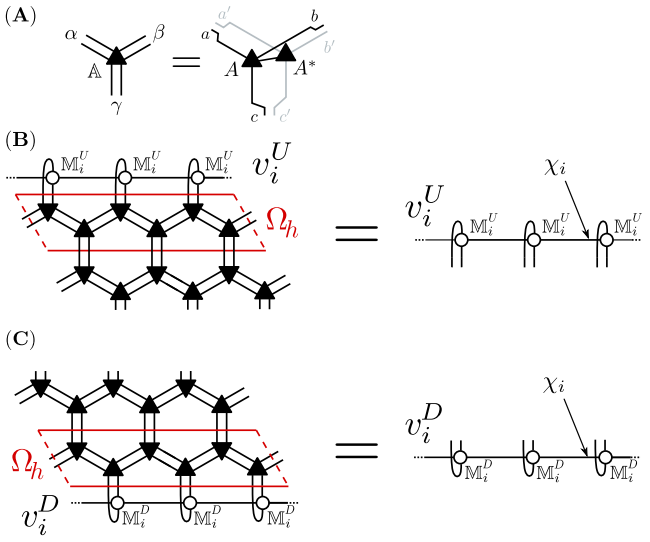

FIG. 2. **Transfer matrix.** In (A), graphical representation of a double iPEPS tensor $\mathbb{A}$ that is made out of an iPEPS tensor A contracted through a physical index with its complex conjugate A^*. In (B) and (C), a horizontal row of $\mathbb{A}$ makes a horizontal transfer matrix Ω_h. Its leading up-eigenvectors, $\left(v_i^U\right|$ and down-eigenvectors, $\left(v_i^D\right|$, with the leading degenerate eigenvalue 1, can be obtained with the VUMPS algorithm[69,70]. The eigenvector can be reshaped into an iMPO form v_i^U. The uniform v_i^U is made of tensors $\mathbb{M}_i^U$ with bond dimension χ_i.

the pulling-through condition:

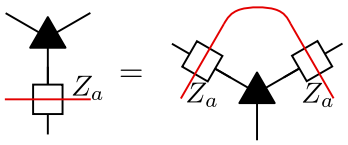

(1)

With periodic boundary conditions these MPO symmetries, which we denote as Z_a, form a representation of a fusion ring

$$Z_a Z_b = \sum_c N_{ab}^c Z_c, \tag{2}$$

where, for the remainder, we will restrict to the multiplicity-free case, i.e. $N_{ab}^c = 0, 1$. Locally this implies the existence of a fusion tensor X_{ab}^c that satisfies the zipper condition

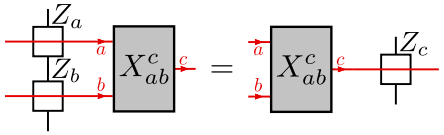

(3)

Multiplication of these MPO symmetries is associative, which imposes the following condition on the fusion tensors:

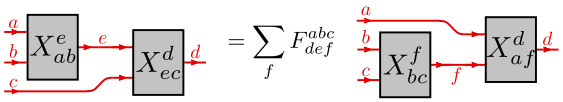

(4)

where $F_{def}^{abc} = (F_d^{abc})_e^f$ is a unitary matrix from e to f. These F-symbols satisfy a consistency condition known as the pentagon equation:

$$\sum_f F_{def}^{abc} \cdot F_{hfj}^{bci} \cdot F_{gdh}^{afi} = F_{geh}^{abj} \cdot F_{gdj}^{eci}, \tag{5}$$

which turns the data N_{ab}^c and F_{def}^{abc} into consistent a unitary fusion category (UFC) $\mathcal{C}$. This UFC completely determines the topological order of the PEPS, and it is the goal of this work to numerically determine its data for an arbitrary PEPS tensor.

III. NUMERICAL MPO SYMMETRIES

The iPEPS representing the ground state on an infinite lattice, $|\psi\rangle$, is assumed to be normalized: $\langle\psi|\psi\rangle = n$. Its norm, which is a contraction between the iPEPS (ket) and its complex conjugate (bra), is a 2D tensor network made of double iPEPS tensors shown in Fig. 2(A). Each row of the network is a horizontal transfer matrix Ω_h in Fig. 2(B). The transfer matrix has several leading up-eigenvectors, $|v_i^U)$ numbered by i, whose degenerate leading eigenvalue is 1 (hence the double iPEPS with n leading eigenvectors is normalized to n). These *boundary fixed points* can be reshaped as iMPO's, v_i^U, acting between virtual bra and ket indices. Together with their corresponding biorthonormal down-eigenvectors, $\left(v_i^D\right|$, that can be also reshaped as iMPO, v_i^D, they satisfy:

$$\Omega_h \approx 1 \sum_{i=1}^{n} |v_i^U)\left(v_i^D\right|, \tag{6}$$

$$\delta_{ij} = \left(v_i^U|v_j^D\right) = \mathrm{Tr}\ \left(v_i^U\right)^T v_j^D. \tag{7}$$

The first and the most important step to identify the topological order is finding the virtual iMPO symmetries of the iPEPS as their existence is a necessary condition for the iPEPS to exhibit topological order. As described in Ref. 49 and 52, the iMPO symmetries Z_a are found numerically as operators mapping between different iMPO boundary fixed points v_i:

$$v_i^U \cdot Z_a = \sum_k \delta_{iak} v_k^U,$$
$$v_i^D \cdot Z_a^T = \sum_k \bar{\delta}_{iak} v_k^D. \tag{8}$$

Here δ_{iak} and $\bar{\delta}_{iak}$ take values either 0 or 1 and in general they do not have to be the same. A trivial $v_1^{U,D}$ can be identified such that its trace with all the iMPO symmetries is equal 1: $\mathrm{Tr}(v_1^U \cdot Z_a \cdot v_1^D \cdot Z_a^\dagger) = 1$. In particular for the up-eigenvector v_1^U all other $v_{i>1}^U$ are obtained from it by the action of corresponding iMPO symmetries:

$$v_1^U \cdot Z_a = v_a^U, \tag{9}$$

while at the same time for the down-eigenvectors:

$$v_1^D \cdot Z_a^T = v_{\bar{a}}^D. \tag{10}$$

Each symmetry Z_a, including the trivial $Z_1 = \mathbb{I}$, represents certain anyon type a. Here $\bar{a}$ is an inverse of anyon type a that in general can be different than a. We note that these numerical iMPO symmetries defined in this way are only required to be symmetries of the iPEPS in the sense that they can be pushed through an entire row/column of the network, and in general will not satisfy the local pulling through condition of (1).

The iMPO symmetries can be obtained by variational minimization of a cost function that follows from Eqs. (9) and (10):

$$|v_1^U \cdot Z_a - v_a^U|^2 + |v_1^D \cdot Z_a^T - v_{\bar{a}}^D|^2, \tag{11}$$

Here Z_a is made of tensors z_a and v_a of $\mathbb{M}_a^U$. The cost function is quadratic in the infinite MPO symmetry Z_a but highly non-linear in its tensor z_a. The minimization is performed with respect to z_a in a quasi-local manner. Namely, we choose one tensor z_a in the infinite Z_a and minimize with respect to it as if it were independent of all other tensors z_a. As the cost function is quadratic in the chosen tensor, its derivative with respect to $z_a^\dagger$ yields a linear equation for z_a. Its solution is a candidate to be substituted in place of all tensors z_a. In practice we substitute its linear combination with the previous z_a with coefficients optimized to minimize the global cost function. This optimization is done in the same way as in Ref. 48. This quasi-local procedure is iterated until convergence of the cost function. In order to avoid local minima, the whole minimization is repeated several times, with different random initial conditions.

In order to minimize the effect of the unnecessary modes in the nullspace of an iMPO symmetry acting on the up and down boundary eigenvectors the bond dimension of Z_a, χ_a, has to be the minimal one that still allows the cost function to be nullified. By definition, this cost function guarantees the correct action of the symmetries on the boundary fixed points but not the "abstract" fusion ring (2). However, the algebra is satisfied in a weaker sense:

$$v_i^U Z_a \cdot Z_b = \sum_c N_{ab}^c \; v_i^U Z_c, \tag{12}$$

$$v_i^D Z_a^T \cdot Z_b^T = \sum_d N_{ba}^d \; v_i^D Z_d^T, \tag{13}$$

i.e., when applied to any boundary fixed point. This is all that we need in the following construction.

Just as (2) is replaced by (12,13), in the realm of numerical iMPO symmetries, the definition of the F-symbol is replaced by

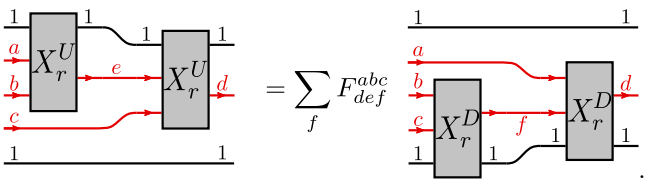

(14)

This diagram includes up and down boundary fixed points in order to execute the weaker "numerical" algebra (12,13). Accordingly, we introduce more general up and down zippers, X^U and X^D, that realize the fusions in (12,13). Their construction is the subject of the following sections IV, V, and VI.

Before proceeding to the X zippers in Sec. IV., we first illustrate this numerical procedure for iMPO symmetries in the following models. Some of the examples are the same as in Ref. 52 but notice that here the symmetries have to be recalculated because the cost function in (11) is in principle more demanding as it has two terms instead of just one. Indeed, in Refs. 49 and 52 it was enough for an iMPO symmetry to satisfy only one of conditions (9,10) because the iMPO symmetries were inserted in an iPEPS as in Fig. 1 and, therefore, it was enough that they acted properly on either the up or the down boundary of the iPEPS. In the present method we use them in the diagrammatic equation 14 where on the left hand side they act on the up boundary and on the right hand side on the down one. Therefore, for the equation to make sense both their up and down action has to be correct.

Finally, as a last remark before we proceed to the examples, numerically there is a freedom of the global phase of the eigenvectors, $v_i^{U,D}$, which can be partially eliminated (up to minus sign) by requiring their Hermiticity (when applicable). In general the random global phases change the fusion rules, so that only their magnitudes are 0 or 1, $|N_{ab}^c| = 0{,}1$. However, in all the examples below the random global phases are adjusted so that all N_{ab}^c are real, either 0 or 1.

A. Toric code and double semions

For analytic fixed point tensors defined in appendix A transfer matrix Ω_h has 2 numerical boundary fixed points $v_{1,2}^{U,D}$ and one non-trivial numerical iMPO symmetry Z_2 which fulfils the Z_2 algebra:

$$\left.\begin{array}{l} v_1^U \cdot Z_2 = v_2^U \\ v_2^U \cdot Z_2 = v_1^U \end{array}\right\} \;\Rightarrow\; Z_2 \cdot Z_2 = \mathbb{I}. \tag{15}$$

The cost function (11) was minimized to zero within machine precision. The fusion rules can be summarized as

$$N_{11}^1 = N_{22}^1 = 1 \tag{16}$$

with all possible permutation of indices. It has to be strongly emphasized that in general the numerical Z_2 iMPO symmetry is not necessarily nullified outside the support subspace of the boundary eigenvectors, therefore the ring on the right of (15) is valid only in the sense of the equalities on the left. The same reservation applies to all fusion rules to be identified numerically in the rest of this paper.

B. Kitaev model

As a realistic example of the toric code universality class we consider the Kitaev model on a honeycomb lattice defined by the following Hamiltonian,

$$\mathcal{H} = -\sum_{\alpha=x,y,z} J_\alpha \sum_{\alpha \text{ links}} \sigma_i^\alpha \sigma_j^\alpha. \tag{17}$$

Here, σ_i^α, $\alpha = x, y, z$ are Pauli matrices acting on site i. We set $J_z = 1$ and study the model along the line $J = J_x = J_y \in (0, 0.5)$. The iPEPS ground state was obtained in Ref. 49 by variational optimization. For iPEPS bond dimension $D = 4$ we find that the bond dimension $\chi = 4$ of boundary iMPO's $v_{1,2}^{U,D}$ suffices to faithfully capture the entanglement properties of the phase. An accurate iMPO symmetry Z_2 is found with the minimal non-trivial bond dimension $\chi_Z = 2$. Its error can be quantified by two numbers:

$$\begin{aligned} \epsilon_Z^U &= \left|1 - \Lambda[\langle v_1^U \cdot Z_2 | v_2^U\rangle]\right|, \\ \epsilon_Z^D &= \left|1 - \Lambda[\langle v_1^D \cdot Z_2^T | v_2^D\rangle]\right|. \end{aligned} \tag{18}$$

Here $\Lambda(x)$ is the leading eigenvalue of a transfer matrix of overlap x. The errors are listed in the following table I. Even though the numerical iPEPS tensors do not assume any symmetry or any special gauge, and their bond dimension is small, the iMPO symmetries turn out to be very accurate.

J	ξ	ϵ_Z^U	ϵ_Z^D
0.4	0.21	$\mathcal{O}(10^{-3})$	$\mathcal{O}(10^{-3})$
0.42	0.22	$\mathcal{O}(10^{-2})$	$\mathcal{O}(10^{-2})$
0.44	0.23	$\mathcal{O}(10^{-4})$	$\mathcal{O}(10^{-4})$
0.46	0.25	$\mathcal{O}(10^{-2})$	$\mathcal{O}(10^{-2})$
0.48	0.26	$\mathcal{O}(10^{-3})$	$\mathcal{O}(10^{-3})$

TABLE I. The errors (18) of the fusion ring of the numerical iMPO symmetry Z_2 with the corresponding up- and down-eigenvectors $v_1^{U,D}$. Here $J = J_x = J_y$ is the coupling constant in the Kitaev model with $J_z = 1$ (17). The iPEPS approximating its ground state with bond dimension $D = 4$ was obtained by variational optimization[49]. Here ξ is the correlation length calculated from the second leading eigenvalue of the iPEPS transfer matrix in the environment of the boundary eigenvectors.

C. Twisted quantum double of $\mathbb{Z}_3$

For this example, the transfer matrix Ω_h has 3 boundary fixed points $v_{1,2,3}^{U,D}$, out of which only one, v_1^U and corresponding v_1^D, is Hermitian and it plays the role of the trivial boundary. The other two boundary fixed points are their own Hermitian conjugates : $v_2^{U,D} = (v_3^{U,D})^\dagger$. Here the labels in eq.11 are not self-inverse, i.e. $a \neq \bar{a}$ for $a = 2, 3$. The iMPO symmetry has bond dimension $\chi = 2$ and it fulfils:

$$\left.\begin{array}{ll} v_1^U \cdot Z_q = v_2^U & v_1^U \cdot Z_{q^*} = v_3^U \\ v_2^U \cdot Z_q = v_3^U\,, & v_2^U \cdot Z_{q^*} = v_1^U \\ v_3^U \cdot Z_q = v_1^U & v_3^U \cdot Z_{q^*} = v_2^U \end{array}\right\} \Rightarrow Z_q Z_{q^*} = \mathbb{I}, \tag{19}$$

$$\left.\begin{array}{ll} v_1^D \cdot Z_q^T = v_3^D & v_1^D \cdot Z_{q^*}^T = v_2^D \\ v_2^D \cdot Z_q^T = v_1^D\,, & v_2^D \cdot Z_{q^*}^T = v_3^D \\ v_3^D \cdot Z_q^T = v_2^D & v_3^D \cdot Z_{q^*}^T = v_1^D \end{array}\right\} \Rightarrow Z_{q^*} Z_q = \mathbb{I}. \tag{20}$$

The two iMPO symmetries Z_q, Z_{q^*}, are denoted with the subscripts $q, q^* = \mathrm{e}^{\pm 2i\pi/3}$. Despite different fusions with the eigenvectors $\delta_{iak} \neq \bar{\delta}_{iak}$ the fusion rules of the iMPO symmetries are given by the following non-zero elements of the fusion tensor

$$\begin{aligned} \forall_{i=1,q,q^*}\ N_{1i}^i = N_{i1}^i = 1, \\ N_{qq^*}^1 = N_{q^*q}^1 = N_{qq}^{q^*} = N_{q^*q^*}^q = 1. \end{aligned} \tag{21}$$

In this case the anyon types q and q^* are the inverses of each other, which justifies the labeling.

D. Fibonacci string-net

Here we employed the iPEPS tensors for a fixed point Fibonacci string net model presented in appendix A. The transfer matrix Ω_h has 2 numerical boundary fixed points, $v_{1,2}^{U,D}$, and one non-trivial numerical iMPO symmetry Z_τ which fulfills:

$$\left.\begin{array}{l} v_1^U \cdot Z_\tau = v_2^U \\ v_2^U \cdot Z_\tau = v_1^U + v_2^U \end{array}\right\} \Rightarrow Z_\tau \cdot Z_\tau = \mathbb{I} + Z_\tau. \tag{22}$$

Again, the cost function (11) was minimized to vanish up to machine precision and the fusion on the right holds only in the sense of the equalities on the left. The fusion algebra on the right of (22) allows us to label the iMPO symmetry with a non-Abelian Fibonacci anyon τ. The fusion rules can be summarized as

$$N_{11}^1 = N_{\tau\tau}^1 = N_{\tau\tau}^\tau = 1. \tag{23}$$

with all possible permutation of indices.

E. Fibonacci string-net with local filtering

In order to drive the iPEPS away from a fixed point and introduce a finite correlation length we apply the local filtering[71–73] to the fixed point of the Fibonacci string-net model. The modification has the following form:

$$|\Psi\rangle \;\rightarrow\; \prod_i \mathrm{e}^{\beta\sigma_i^z} |\Psi\rangle, \tag{24}$$

where i runs over all physical indices, σ^z is the Pauli matrix, and β is a parameter. Correlation lengths ξ are listed in table II. In the table we also present errors (18)

of the two terms appearing in the cost function. The difference between errors of ϵ_Z^U, ϵ_Z^D arises from the fact that with growing correlation length it becomes harder to nullify both errors at the same time, therefore, in order to ensure convergence, in the step where we find an optimal update of tensor z_a we use only one of the conditions (18), namely ϵ_Z^U.

β	ξ	ϵ_Z^U	ϵ_Z^D
0.01	0.23	$\mathcal{O}(10^{-7})$	$\mathcal{O}(10^{-7})$
0.05	0.42	$\mathcal{O}(10^{-4})$	$\mathcal{O}(10^{-3})$
0.12	1.04	$\mathcal{O}(10^{-4})$	$\mathcal{O}(10^{-2})$
0.15	2.32	$\mathcal{O}(10^{-2})$	0.05

TABLE II. The errors (18) of the fusion ring of the the numerical iMPO symmetry with the corresponding up- and down-eigenvectors $v_1^{U,D}$. Parameter β represents the perturbation strength from Eq. (24), while ξ is the corresponding correlation length calculated from the second leading eigenvalue of the iPEPS transfer matrix in the environment of the boundary eigenvectors.

F. Ising string net

Here again we employed the iPEPS tensors for a fixed point Ising string net model presented in appendix A. This time each TM has 3 numerical boundary fixed points, $v_{1,2,3}^{U,D}$, corresponding to 3 anyon types of the input category: $1, \sigma, \psi$. We found two non-trivial iMPO symmetries, labelled as Z_σ and Z_ψ. The fixed points and the symmetries are related by the following set of equations:

$$\left.\begin{aligned} v_1^U \cdot Z_\psi &= v_2^U \\ v_2^U \cdot Z_\psi &= v_1^U \\ v_3^U \cdot Z_\psi &= v_3^U \end{aligned}\right\} \Rightarrow Z_\psi \cdot Z_\psi = \mathbb{I}, \tag{25}$$

$$\left.\begin{aligned} v_1^U \cdot Z_\sigma &= v_3^U \\ v_2^U \cdot Z_\sigma &= v_3^U \\ v_3^U \cdot Z_\sigma &= v_1^U + v_2^U \end{aligned}\right\} \Rightarrow Z_\sigma \cdot Z_\sigma = \mathbb{I} + Z_\psi. \tag{26}$$

The cost function (11) was minimized to machine precision. Furthermore, we verified that with machine precision the symmetries satisfy:

$$v_i^U Z_\sigma \cdot Z_\psi = v_i^U Z_\sigma \;\Rightarrow\; Z_\sigma \cdot Z_\psi = Z_\sigma \tag{27}$$

The equations justify labelling of the symmetries. The fusion rules can be summarized as

$$N_{11}^1 = N_{\sigma\sigma}^1 = N_{\psi\psi}^1 = N_{\psi\psi}^\sigma = 1 \tag{28}$$

with all possible permutation of indices.

G. Quantum double of S_3 and Rep(S_3) string-net

In this section we analyze two different iPEPS representations from Ref. 64 for the quantum double S_3 and the Rep(S_3) string-net model, with MPO symmetries respectively given by UFCs $\mathcal{C}_1 = \mathrm{Rep}(S_3)$ and $\mathcal{C}_2 = \mathrm{Vec}_{S_3}$. These two iPEPS representations describe the same topologically ordered phase since $Z(\mathrm{Rep}(S_3)) = Z(\mathrm{Vec}_{S_3})$.

Rep(S_3) MPO symmetries

In this representation iPEPS tensor has virtual bond dimension $D = 6$ and its related transfer matrix Ω_h has 3 leading eigenvectors $v_{1,2,3}^{U,D}$ corresponding to 3 anyon types $1, \pi, \psi$. There are two non-trivial iMPO symmetries, with corresponding labels π, ψ and they fulfill the following fusion rules with the eigenvectors:

$$\left.\begin{aligned} v_1^U \cdot Z_\psi &= v_3^U \\ v_2^U \cdot Z_\psi &= v_2^U + v_3^U \\ v_3^U \cdot Z_\psi &= v_1^U \end{aligned}\right\} \Rightarrow Z_\psi \cdot Z_\psi = \mathbb{I}, \tag{29}$$

$$\left.\begin{aligned} v_1^U \cdot Z_\pi &= v_3^U \\ v_2^U \cdot Z_\pi &= v_1^U + v_2^U + v_3^U \\ v_3^U \cdot Z_\pi &= v_1^U \end{aligned}\right\} \Rightarrow Z_\sigma \cdot Z_\sigma = \mathbb{I} + Z_\psi + Z_\pi. \tag{30}$$

The same set of equations can be written for the down-eigenvectors. Moreover we observe that:

$$v_i^U Z_\pi \cdot Z_\psi = v_i^U Z_\pi \Rightarrow Z_\pi \cdot Z_\psi = Z_\pi, \tag{31}$$

which enables identification of all allowed fusion rules:

$$N_{11}^1 = N_{\pi\pi}^1 = N_{\psi\psi}^1 = N_{\psi\psi}^\sigma = N_{\pi\pi}^\pi = 1 \tag{32}$$

with all possible permutation of indices.

Vec$_{S_3}$ MPO symmetries

In this representation the iPEPS tensor has bond dimension that is just $D = 4$ while its related transfer matrix Ω_h has degeneracy 6 corresponding to 6 leading eigenvectors $v_{1,2,3,4,5,6}^{U,D}$. There are 5 non-trivial iMPO symmetries Z_a, which are all product iMPOs. There is only one eigenvector, which we label as identity, for which $\mathrm{Tr}(v_1^U \cdot Z_a \cdot v_1^D \cdot (Z_a)^\dagger) = 1$ for all $a = 1, ..., 6$. All the remaining up and down eigenvectors can be obtained from $v_1^{U,D}$ by proper action of the iMPO symmetries:

$$\begin{aligned} &v_1^U \cdot Z_a = v_a^U, \ \forall a = 1,2,3,4,5,6 \\ &v_1^D \cdot Z_a^T = v_a^D, \ \forall a = 1,2,3,4, \\ &v_1^D \cdot Z_5^T = v_6^D, \ v_1^D \cdot Z_6^T = v_5^D \end{aligned} \tag{33}$$

In this case the fusion ring is non-Abelian in the sense that $N_{ab}^c \neq N_{ba}^c$ and apart from trivial fusion rules $N_{1a}^a = N_{a1}^a = 1$, there are 25 non-trivial ones, all equal 1:

$$\begin{aligned} &N_{22}^1, N_{33}^1, N_{44}^1, N_{65}^1, N_{56}^1, N_{63}^2, N_{54}^2, N_{35}^2, N_{46}^2, \\ &N_{52}^3, N_{64}^3, N_{45}^3, N_{26}^3, N_{62}^4, N_{53}^4, N_{25}^4, N_{36}^4, \\ &N_{32}^5, N_{43}^5, N_{24}^5, N_{66}^5, N_{42}^6, N_{23}^6, N_{34}^6, N_{55}^6. \end{aligned} \tag{34}$$

From this we notice that iMPO symmetries Z_a for $a = 1, 2, 3, 4$ are self-inverse, while Z_5 is the inverse of Z_6.

IV. NUMERICAL X ZIPPERS

In this work we employ the fundamental theorem of MPS[60,61] according to which there exist an invertible gauge transformation G_l between two tensors A^i and B^i, where i is the "physical" index, both in a canonical form, generating equal iMPS's such that

$$A^i = G_l \cdot B^i \cdot G_r, \tag{35}$$

where $G_r = G_l^{-1}$. It can be further extended to iMPO and products of iMPO's where, e.g., $A = v_i \cdot Z_a$ and $B = v_k$. In that case the bond dimension of the product $v_i \cdot Z_a$ is usually bigger than the bond dimension of v_k: $\chi_i \cdot \chi_z > \chi_k$. Therefore, the gauge transformation G_l is actually a composition of an isometry U of dimensions $(\chi_i \cdot \chi_z, \chi_k)$ and an invertible $\chi_k \times \chi_k$ matrix g. G_r is a pseudo-inverse of G_l and vice versa.

Due to the algebra of iMPO symmetries (2), which is fulfilled only when acting on the boundary fixed points (13), our goal is to find zipper tensors X^c_{ab} which serve as gauge transformations between products $v_1 \cdot Z_a \cdot Z_b$ and $v_1 \cdot Z_c$:

$$v_1 \cdot Z_a \cdot Z_b \quad \overset{X^c_{ab}}{\longleftrightarrow} \quad v_1 \cdot Z_c \tag{36}$$

Here we consider only the trivial fixed point v_1 to make sure the fusions actually occur only between the iMPO symmetries Z.

This goal can be achieved in two steps, first by obtaining smaller zippers Y^k_{ia} which fuse a product $v_i \cdot Z_a$ into a single MPO v_k. The second step is the proper contraction of zippers Y^k_{ia} to form X^c_{ab} as shown in Fig. 3.

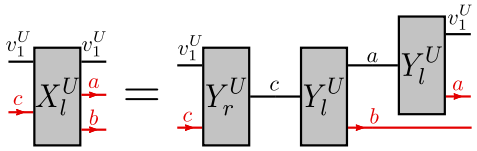

FIG. 3. Contraction of Y zippers that makes an X zipper. Here we show only U-zippers but similar equations hold for their D counterparts. We distinguish between left, l, and right, r, zippers. Contraction of a left zipper with its corresponding right zipper yields an identity. One is a pseudo-inverse of the other.

V. NUMERICAL Y ZIPPERS

The iMPO symmetry algebra, Z_a, includes a trivial symmetry $Z_1 = \mathbb{I}$ corresponding to the trivial anyon type. This identity iMPO is a product of identity matrices and has bond dimension $\chi_1 = 1$. Therefore, all the zippers $(Y_l)^j_{j1}$, together with their r (inverse) counterparts, are trivial identity matrices of dimensions $\chi_j \times \chi_j$. We emphasize again, that Z_1 as a product of identity matrices is sufficient for our construction, because it still acts as the identity on the support subspace of PEPS, but it is not an exact MPO symmetry from Ref.54, where a larger bond dimension is needed to encode the identity action on the relevant subspace only.

From now on we focus the attention on non-trivial zippers between the left and right hand side of the equation $v_j \cdot Z_a = \sum_k \delta_{jak} v_k$ with $a > 1$. The product MPO tensor $M = v_j \cdot Z_a$ is either normal, for which a transfer matrix of $\mathrm{Tr} MM^\dagger$ has only one leading eigenvalue equal 1, or a direct sum of normal tensors, so the transfer matrix has several degenerate leading eigenvalues equal 1. In both cases we proceed by bringing the tensors M into left-canonical form using a repeated QR decomposition. For a fixed point of QR decomposition the relation between the initial tensor and the converged canonical form is:

$$L \cdot M^i = M^i_L \cdot L, \tag{37}$$

which means that the transformation bringing the tensor M^i into its canonical form M^i_L is:

$$L \cdot M^i \cdot \mathrm{pinv}(L) = M^i_L. \tag{38}$$

Here i denotes "physical" indices of tensor M. The pseudo-inverse deals with singularity due to too large bond dimension of M: $\chi_j \cdot \chi_a > \sum_k \chi_k$.

In the next step we reduce the bond dimension for M^i_L and find the gauge transformation relating it with one of the v^i_k tensors. Towards this end we construct a mixed transfer matrix for $\mathrm{Tr} M_L v^\dagger_k$. Its left fixed point, σ_L, is an isometry of dimension $\chi_j \cdot \chi_a \times \chi_k$ truncating the left-canonized product M_L to v_k:

$$\sigma^T_L \cdot M^i_L \cdot \mathrm{pinv}(\sigma^T_L) = v^i_k. \tag{39}$$

Putting the isometry together with the gauge transformation L we can write:

$$(Y_l)^k_{ja} \left(v_j \cdot Z_a\right)^i (Y_r)^k_{ja} = v^i_k, \tag{40}$$

where

$$(Y_l)^k_{ja} = \sigma^T_L \cdot L, \tag{41}$$

$$(Y_r)^k_{ja} = \mathrm{pinv}(L) \cdot \mathrm{pinv}(\sigma^T_L). \tag{42}$$

In diagramatic form equation (40) is:

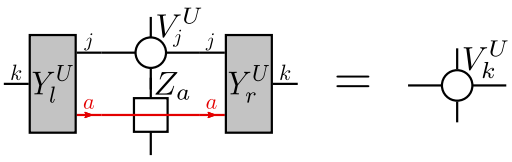

(43)

In all equations above we did not include the labels of the eigenvectors v_i, as there are two sets of them: v^U_i and v^D_i. However, the procedure is the same for both sets with a sole difference that for the down eigenvectors we need to use the transpose Z^T_a in place of Z_a.

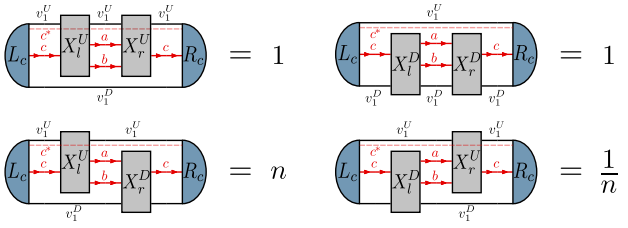

FIG. 4. Normalization conditions for the X_l and X_r zippers. The projectors $X_l^U X_r^U$ and $X_l^D X_r^D$ in the top row act like identities when inserted between the left, L_c, and right, R_c, fixed points of the transfer matrix $Tr(v_1^U \otimes Z_c \otimes v_1^D \otimes Z_c^\dagger)$. Here the $Z_c^\dagger$, which is necessary for the diagram to be non-zero is represented by the dashed line. The mixed products $X_l^U X_r^D$ and $X_l^D X_r^U$ in the bottom row yield n and $1/n$, respectively. The arbitrary n can be brought to 1 by rescaling the right X zippers.

VI. NORMALIZATION OF X ZIPPERS

Having the full set of required Y-zippers $\{Y_l^U, Y_r^U, Y_l^D, Y_r^D\}$, we construct the X-zippers according to Fig. 3. From this construction we get that:

$$\sum_{a,b} (X_l^U)^c_{ab}\ (X_r^U)^c_{ab} = (Y_r^U)^c_{1c}\ (Y_l^U)^c_{1c}, \tag{44}$$

which is not necessarily equal to identity matrix $\mathbb{I}_{\chi_1 \cdot \chi_c}$. However, it is a projector that acts like an identity when inserted between the left, L_c, and right, R_c, fixed points of the transfer matrix $Tr(v_1^U \otimes Z_c \otimes v_1^D \otimes Z_c^\dagger)$, as shown in the top row of Fig. 4 that includes also the complementary X^D case.

A similar normalization between X_l^U and its corresponding X_r^D is not automatic, see the bottom row of Fig. 4. Here the number n depends on somewhat arbitrary normalization of Y zippers making the X zippers. The number can be brought to 1 by rescaling, e.g., $X_l^D \to n X_l^D$ and $X_r^D \to (1/n) X_r^D$. Having thus properly normalized all of the X-zippers we can proceed with the calculation of the F-symbols.

VII. NUMERICAL F SYMBOLS

The last step of the algorithm is to calculate the F-symbols in the equation in Fig. 14. This is a coupled set of equations for F^{abc}_{def} with different index f. In order to decouple them we project both sides onto $\left((X_l^D)^d_{ag} \cdot (X_l^D)^g_{bc}\ \middle|\right.$ from the left. At this point we verify that $\left((X_l^D)^d_{ag} \cdot (X_l^D)^g_{bc}\ \middle|\ (X_r^D)^g_{bc} \cdot (X_r^D)^d_{ag}\right) = \delta_{gf}$ and we obtain an explicit formula:

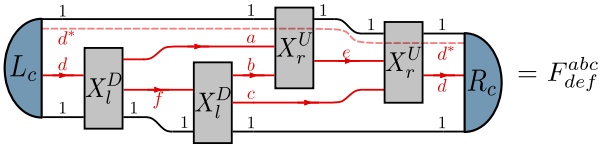

(45)

Here we have immersed the equation in the environment of left L_c and right R_c fixed points of the transfer matrix $Tr(v_1^U \otimes Z_d \otimes v_1^D \otimes Z_d^\dagger)$, the same as was used to find relative normalization of X^U and X^D zippers. The dotted red line denoted by d^* is the trace over indices corresponding to $Z_d^\dagger$.

A similar formula for an inverse of the matrix F is

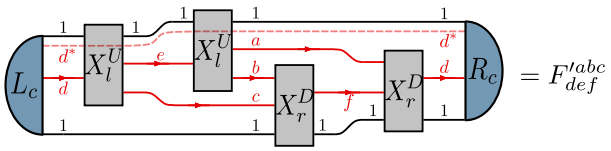

(46)

Both F and F' satisfy the Pentagon equation:

$$\sum_f F^{abc}_{def} \cdot F^{bci}_{hfj} \cdot F^{afi}_{gdh} = F^{abj}_{geh} \cdot F^{eci}_{gdj}, \tag{47}$$

and describe the same topological order, although the value of their elements are in general different. The difference is manifestation of "gauge freedom" of F^{abc}_{def} due to remaining freedom in normalization of X zippers:

$$\{X_l^U, X_r^U, X_l^D, X_r^D\} \ \to\ \{\lambda X_l^U, \frac{1}{\lambda} X_r^U, \lambda X_l^D, \frac{1}{\lambda} X_r^D\}. \tag{48}$$

Here arbitrary $\lambda^c_{ab} \in \mathbb{C}$ depend on the labels of $X = X^c_{ab}$. Their values cannot be fixed by the Pentagon equation. λ^c_{ab} parametrize gauge freedom of the F symbols:

$$F^{abc}_{def} \ \to\ \frac{\lambda^f_{bc}\lambda^d_{af}}{\lambda^e_{ab}\lambda^d_{ec}} F^{abc}_{def}, \quad F'^{abc}_{def} \ \to\ \frac{\lambda^e_{ab}\lambda^d_{ec}}{\lambda^f_{bc}\lambda^d_{af}} F'^{abc}_{def}. \tag{49}$$

A straightforward way to proceed is to look for a gauge λ^c_{ab} that brings the F symbols, within numerical error, to a textbook form characteristic for a given type of topological order. This is what we do in the next section.

It is important to point out that the topological order is given by the monoidal center $Z(\mathcal{C})$, meaning that two fusion categories $\mathcal{C}_1$ and $\mathcal{C}_2$ that a priori look completely different may describe the same topological order[64], in which case $\mathcal{C}_1$ and $\mathcal{C}_2$ are said to be *Morita equivalent*. In order to deal with this redundancy, we compute the monoidal center in section IX, as well as the corresponding S and T matrices.

VIII. F SYMBOLS IN CANONICAL GAUGE

We use the gauge freedom in (49) to bring F symbols to a canonical gauge where, for a unitary fusion category,

the matrices F_d^{abc} are unitary and most elements of F are one, especially if any of a, b, c, d is trivial. To begin we notice that Eq. (49) implies that a product

$$F_{def}^{abc} F'^{abc}_{def}, \tag{50}$$

is gauge invariant. Therefore its square root will be used later to eliminate some of the gauge freedom of the F-symbols.

Additionally, all X_{ab}^c where either $a = 1$ ($b = 1$) are chosen as identities between b and c (a and c). This choice fixes the gauge partially as $\lambda_{1c}^c = 1 = \lambda_{c1}^c$ but we are still left with freedom to choose the λ_{ab}^c where both $a \neq 1$ and $b \neq 1$. This residual gauge freedom leaves invariant all the F_{def}^{abc} where one of a, b, c is equal to 1.

Moreover, when there are only 2 anyon types in the input category, then also the F_{1ef}^{abc} are left invariant by the residual gauge transformation. The only F-symbols that transform in a non-trivial way are:

$$F_{212}^{222} \to \frac{\lambda_{22}^1}{\lambda_{22}^2 \lambda_{22}^2} F_{212}^{222} \equiv \mu F_{212}^{222}, \tag{51}$$

$$F_{221}^{222} \to \frac{\lambda_{22}^2 \lambda_{22}^2}{\lambda_{22}^1} F_{221}^{222} \equiv \frac{1}{\mu} F_{221}^{222}. \tag{52}$$

In the unitary gauge for every fixed set of indices a, b, c, d the matrix F_{def}^{abc} is unitary in indices ef. We can choose $|\mu|$ such that magnitudes of F_{2ef}^{222} become the same as square roots of corresponding products in (50). With a proper phase of μ the matrix F_{2ef}^{222} can be made unitary making manifest that the obtained F symbols describe unitary fusion category.

When there are more than 2 anyon types then there is a freedom:

$$F_{1ef}^{abc} = F_{1ca}^{abc} \to \frac{\lambda_{ab}^c \lambda_{cc}^1}{\lambda_{bc}^a \lambda_{aa}^1} F_{1ca}^{abc} \tag{53}$$

For $a = c$ this freedom is given by a simple ratio:

$$F_{1aa}^{aba} \to \frac{\lambda_{ab}^a}{\lambda_{ba}^a} F_{1aa}^{aba} \equiv \mu(a, b) F_{1aa}^{aba} \tag{54}$$

which allows to determine first non-trivial gauge transformation and eliminate it from all F_{def}^{abc} in which it appears, by a substitution $\lambda_{ab}^a \to \mu(a, b)\lambda_{ba}^a$. The remaining scheme is largely model-dependent, but the general idea is to replace unknown λ's with known ratios μ as we present on the examples below.

A. Toric code and double semions

We obtain the Y and X zipper tensors. For those 2 Abelian models there are 2 trivial Y-zippers: $Y_{11}^1, Y_{21}^2 = \mathbb{I}$ and 2 non-trivial Y-zippers: Y_{12}^2, Y_{22}^1 giving rise to 4 non-zero X-zippers: $X_{11}^1, X_{12}^2, X_{21}^2, X_{22}^1$. For both the toric code and the double semion model all gauges λ in Eq. (48) cancel each other in the expressions for F symbols. We obtain numerically exact F-symbols immediately in the canonical gauge for toric code:

$$F_{def}^{abc} = N_{ab}^e N_{cd}^e N_{ad}^f N_{bc}^f \tag{55}$$

and the same for double semions with the exception for $F_{211}^{222} = -1$.

B. Kitaev model

We obtain the same set of Y and X zippers as for the toric code phase and then use them to find F symbols with an error calculated as the Frobenius norm:

$$\epsilon_F = ||F_{numerical} - F_{canonical}||. \tag{56}$$

Here $F_{canonical}$ are the exact F symbols in (55). Their errors are listed in the following table III. Not quite surprisingly, good accuracy of the iMPO symmetry, see table I, results in accurate F symbols.

J	ϵ_F
0.40	$\mathcal{O}(10^{-3})$
0.42	$\mathcal{O}(10^{-3})$
0.44	$\mathcal{O}(10^{-4})$
0.46	$\mathcal{O}(10^{-2})$
0.48	$\mathcal{O}(10^{-2})$

TABLE III. The error of the numerical F symbols, defined as the Frobenius norm of the difference with respect to the exact ones (56). Here $J = J_x = J_y$ is the coupling in the Kitaev Hamiltonian (17) with $J_z = 1$.

C. Twisted quantum double of Z_3

We find 3 trivial Y zippers with both up and down eigenvectors Y_{i1}^i for $i = 1, q, q^*$ and 6 non-trivial with up-eigenvectors:

$$(Y^U)_{12}^2, (Y^U)_{13}^3, (Y^U)_{23}^1, (Y^U)_{32}^1, (Y^U)_{22}^3, (Y^U)_{33}^2 \tag{57}$$

and with down eigenvectors:

$$(Y^D)_{12}^3, (Y^D)_{13}^2, (Y^D)_{23}^3, (Y^D)_{32}^2, (Y^D)_{22}^1, (Y^D)_{33}^1, \tag{58}$$

which altogether give rise to a unique set of X zippers: trivial X_{1a}^a, X_{a1}^a for $a = 1, q, q^*$ and $X_{22}^3, X_{33}^2, X_{23}^1, X_{32}^1$. Therefore there are 4 random residual gauges: $\lambda_{23}^1, \lambda_{32}^1, \lambda_{22}^3, \lambda_{33}^2$, which appear in only 2 combinations:

$$\rho_1 = \frac{\lambda_{23}^1}{\lambda_{32}^1}, \ \rho_2 = \frac{\lambda_{32}^1}{\lambda_{22}^3 \lambda_{33}^2}, \tag{59}$$

where ρ_1 and its inverse fully fixes $F_{133}^{222}, F_{311}^{323}, F_{211}^{232}, F_{122}^{333}$ while ρ_2 fully fixes $F_{321}^{332}, F_{213}^{322}$ and there are only two remaining F-symbols:

$$F_{231}^{223} \to \rho_1 \rho_2 \ F_{231}^{223}$$
$$F_{312}^{233} \to \frac{1}{\rho_1 \rho_2} \ F_{312}^{233}. \tag{60}$$

This procedure allows us to obtain $F^{abc}_{def} = N^e_{ab}N^e_{cd}N^f_{ad}N^f_{bc}$ with the exception of

$$F^{222}_{133} = F^{333}_{122} = (F^{332}_{321})^* = (F^{223}_{231})^* = \mathrm{e}^{\frac{2i\pi}{3}}. \quad (61)$$

The obtained F-symbols necessarily satisfy the Pentagon equation, both before and after the gauge transformation. This is the only example we present, in which the F-symbols and their inverses F^{-1} are not equal, but actually $(F^{abc}_{def})^{-1} = (F^{abc}_{def})^*$.

D. Fibonacci string net

We obtain 2 trivial Y-zippers: $Y^1_{11}, Y^2_{21} = \mathbb{I}$ and 3 non-trivial Y-zippers: $Y^2_{12}, Y^1_{22}, Y^2_{22}$ giving rise to 5 non-zero X-zippers: $X^1_{11}, X^2_{12}, X^2_{21}, X^1_{22}, X^2_{22}$. With X-zippers we obtain F symbols that satisfy the Pentagon equation within machine precision. However, the obtained F symbols turn out to be in a random non-unitary gauge.

As the double Fibonacci model has 2 anyon types, the residual gauge freedom in Eq. 52 can be employed to adjust both F^{abc}_{def} or F'^{abc}_{def} to the absolute values obtained from a square root of the product (50) and then to fix their phase in such a way that F^{abc}_{def} and F'^{abc}_{def} become unitary in indices e, f within numerical precision. This way we obtain $F^{abc}_{def} = N^e_{ab}N^e_{cd}N^f_{ad}N^f_{bc}$ except for

$$F^{\tau\tau\tau}_{\tau 11} = -F^{\tau\tau\tau}_{\tau\tau\tau} = \frac{1}{d_\tau}, \quad F^{\tau\tau\tau}_{\tau\tau 1} = F^{\tau\tau\tau}_{\tau 1\tau} = \frac{1}{\sqrt{d_\tau}}. \quad (62)$$

Here the quantum dimension $d_\tau = (\sqrt{5}+1)/2$.

E. Fibonacci string net with local filtering

We applied the same algorithm for the local filtering that introduces a finite correlation length ξ and drives the state away from the fixed point. Errors of the obtained F symbols are listed in table IV. The error remains small up to the correlation length $\xi = 2.32$. Better results for longer correlations lengths would require further improvement of the algorithm to obtain iMPO symmetries. We leave this refinement for future work.

β	ξ	ϵ_F
0.01	0.23	$\mathcal{O}(10^{-7})$
0.05	0.42	$\mathcal{O}(10^{-5})$
0.12	1.04	$\mathcal{O}(10^{-2})$
0.15	2.32	$\mathcal{O}(10^{-2})$

TABLE IV. The error (56) of numerical F symbols. Here the first column represents the perturbation strength β.

F. Ising string net

As the double Ising model has 3 anyon types in the input category $\mathcal{C}$ there are 5 random residual gauges: $\lambda^1_{\psi\psi}, \lambda^1_{\sigma\sigma}, \lambda^\sigma_{\psi\sigma}, \lambda^\sigma_{\sigma\psi}, \lambda^\psi_{\sigma\sigma}$. They appear in only 3 combinations:

$$\rho_1 = \frac{\lambda^\sigma_{\psi\sigma}}{\lambda^\sigma_{\sigma\psi}}, \quad \rho_2 = \frac{\lambda^1_{\sigma\sigma}}{\lambda^\sigma_{\sigma\psi}\lambda^\psi_{\sigma\sigma}}, \quad \rho_3 = \frac{\lambda^1_{\psi\psi}}{(\lambda^\sigma_{\sigma\psi})^2}. \quad (63)$$

Starting with ρ_1, which fully fixes $F^{\sigma\psi\sigma}_{1\sigma\sigma}, F^{\sigma\psi\sigma}_{\psi\sigma\sigma}$ and $F^{\sigma\sigma\sigma}_{\sigma\psi\psi}$, we find ρ_2 fixing $F^{\sigma\sigma\psi}_{\psi 1\sigma}, F^{\sigma\sigma\sigma}_{\sigma 1\psi}$, and finally ρ_3 which is fully fixing $F^{\sigma\psi\psi}_{\sigma\sigma 1}$. The remaining F symbols are fixed by proper combinations:

$$\begin{aligned}
F^{\psi\psi\sigma}_{\sigma 1\sigma} &\to \frac{\rho_3}{\rho_1^2}\, F^{\psi\psi\sigma}_{\sigma 1\sigma} \\
F^{\psi\sigma\sigma}_{1\sigma\psi} &\to \frac{\rho_1\cdot\rho_2}{\rho_3}\, F^{\psi\sigma\sigma}_{1\sigma\psi} \\
F^{\psi\sigma\sigma}_{\psi\sigma 1} &\to \frac{\rho_1}{\rho_2}\, F^{\psi\sigma\sigma}_{\psi\sigma 1} \\
F^{\sigma\sigma\sigma}_{\sigma\psi 1} &\to \frac{\rho_1}{\rho_2}\, F^{\sigma\sigma\sigma}_{\sigma\psi 1} \\
F^{\sigma\sigma\psi}_{1\psi\sigma} &\to \frac{\rho_3}{\rho_2}\, F^{\sigma\sigma\psi}_{1\psi\sigma}
\end{aligned} \quad (64)$$

This way we obtain $F^{abc}_{def} = N^e_{ab}N^e_{cd}N^f_{ad}N^f_{bc}$ except for

$$F^{\sigma\sigma\sigma}_{\sigma 11} = F^{\sigma\sigma\sigma}_{\sigma 1\psi} = F^{\sigma\sigma\sigma}_{\sigma\psi 1} = -F^{\sigma\sigma\sigma}_{\sigma\psi\psi} = \frac{1}{\sqrt{2}}, \quad (65)$$

$$F^{\psi\sigma\psi}_{\sigma\sigma\sigma} = F^{\sigma\psi\sigma}_{\psi\sigma\sigma} = -1, \quad (66)$$

all with numerical precision.

G. Quantum double of S_3

Rep(S_3) MPO symmetries

Apart from the trivial X-zippers with an identity symmetry $X^a_{1a} = X^a_{a1} = \mathbb{I}_a$ there are 6 non-trivial ones $X^1_{22}, X^1_{33}, X^2_{22}, X^3_{22}, X^2_{32}, X^2_{23}$, all with its corresponding gauge-freedom λ^c_{ab}. However there are only 4 independent variables:

$$\rho_1 = \frac{\lambda^2_{23}}{\lambda^2_{32}}, \rho_2 = \frac{(\lambda^2_{22})^2}{\lambda^1_{22}}, \rho_3 = \frac{\lambda^1_{22}}{\lambda^3_{22}\lambda^1_{33}}, \rho_4 = \frac{\lambda^1_{33}}{(\lambda^3_{22})^2}. \quad (67)$$

After elimination of the gauge freedom from all possible F-symbols containing the aforementioned ratios we obtain that $F^{abc}_{def} = N^e_{ab}N^e_{cd}N^f_{ad}N^f_{bc}$, except for:

$$\begin{aligned}
F^{322}_{222} = F^{232}_{222} = F^{223}_{222} = F^{222}_{322} &= -1 \\
F^{222}_{211} = F^{222}_{231} = F^{222}_{213} = F^{222}_{223} &= \tfrac{1}{d_\pi} \\
F^{222}_{221} = F^{222}_{212} = -F^{222}_{232} = -F^{222}_{223} &= \tfrac{1}{\sqrt{d_\pi}} \\
F^{222}_{222} &= 0,
\end{aligned} \quad (68)$$

where $d_\pi = 2$ is the quantum dimension of π and the remaining quantum dimensions are $d_1 = d_\psi = 1$.

Vec(S_3) MPO symmetries

There are 25 non-trivial fusion rules N_{ab}^c giving rise to corresponding X zippers X_{ab}^c, hence 25 random gauges λ_{ab}^c, which can be eliminated using only 20 ratios ρ_i. It can be done by subsequent substitution of certain ratios $\rho_i = \frac{\lambda_{ab}^e \lambda_{ec}^d}{\lambda_{bc}^f \lambda_{af}^d}$, so that the final F-symbols are all trivial: $F_{def}^{abc} = N_{ab}^e N_{cd}^e N_{ad}^f N_{bc}^f$, with every index taking up to 6 values. All the quantum dimensions are $d_a = 1$.

At first glance the F-symbols in both examples above may seem to describe completely different topological orders as they describe different unitary fusion categories UFC. However the calculation of the Drinfeld center in the following sections proves that this is not the case.

IX. S AND T MATRICES FROM F SYMBOLS

The topological S and T matrices are gauge invariant quantities, which in principle could be obtained from the F symbols in arbitrary gauge by considering proper gauge-cancelling factors[74]. Here instead, we make use of the F-symbols in canonical gauge, obtained in section VIII, to derive a simpler expression.

An important observation is that the labels of all non-zero elements of both X and Y zippers define the possible fusions N_{ab}^c of the anyons in the category, from which we obtain their quantum dimensions d_a, as the largest magnitude eigenvalue of the N_a matrix. In this sense fusion rules and quantum dimensions are exact independently of the correlations in the models.

In order to obtain all the anyons or definite anyonic sectors (MES) in the tensor network ansatz we need to find central idempotents of the algebra generated by elements $A_{abcd} \propto N_{da}^b N_{cd}^b \propto (X_r)_{da}^b (X_l)_{cd}^b$ (connected through the index b, but not summed over b), where we omit possible multiplicities as they are all equal 1 in our examples. Central idempotents, when inserted into PEPS, can be thought of as projectors onto states with well-defined anyon flux along the torus. The multiplication of the basis elements $e_i := A_{abcd}$ defines some algebra, from which we find both central and simple idempotents as desrcibed in Appendix B. The algebra of A_{abcd} can be used to calculate the action of the Dehn twist on a state with a symmetry Z_a along the torus[68]:

$$\begin{aligned} \tilde{T}(A_{abad}) &= A_{a1a\bar{a}} \cdot A_{abad} \\ &= \sum_{e,c} \sqrt{\frac{d_a d_{\bar{a}} d_c d_d}{d_e d_b}} (F_{d1b}^{\bar{a}ad})^{-1} F_{deb}^{\bar{a}da} F_{d1e}^{a\bar{a}d} A_{acae} \delta_{cd}, \\ e_i &= \sum_j \tilde{T}_{ij} e_j \end{aligned} \tag{69}$$

This formula gives rise to the $\tilde{T}$ matrix in the basis of $e_i \equiv A_{abcd}$. In the eigenbasis (the MES basis) this matrix is diagonal and contains the phases corresponding to topological spins: $T = \mathrm{diag}(\theta_1, ...\theta_N)$. However, at this point we do not posses enough knowledge to assign anyon labels to them and certain topological spins belonging to multidimensional particles in non-Abelian anyon models are repeated (e.g. $\theta_{\tau\bar{\tau}}$ in the double Fibonacci string net and $\theta_{\sigma\bar{\sigma}}$ in the double Ising string net). Therefore we proceed with the calculation of the topological S and T matrices in the MES basis. If we denote central idempotents inserted in PEPS to create a minimally entangled state in y-direction by $\mathcal{P}_i^y$ and similarly in the x-direction by $\mathcal{P}_i^x$, then the transformation between these two basis is actually an S matrix:

$$\mathcal{P}_i^y = \sum_j S_{ij} \mathcal{P}_j^x \tag{70}$$

We can further write this expression in terms of the basis elements $e_k := A_{abcd}$:

$$\mathcal{P}_i^y = \sum_a c_a^i e_a^y = \sum_j S_{ij} \sum_b c_b^j e_b^x, \tag{71}$$

which written in the matrix forms without summations, with $E^{x,y}$ being the basis in x and y respectively, B the basis change between x and y, P - the matrix of coefficients of the central idempotents in the E basis, is:

$$PE^y = PBE^x = SPE^x, \;\; \Rightarrow \;\; S = PBP^{-1} \tag{72}$$

Similarly we obtain the expression for the T matrix in the MES basis:

$$T = P\tilde{T}P^{-1} \tag{73}$$

The $\tilde{T}$ was is given in eq.69 and the basis change B is given by the combination of F-symbols, as shown in[68]:

$$S(A_{abad}) = \sum_e d_a \sqrt{\frac{d_d d_{\bar{d}}}{d_e d_b}} (F_{ab1}^{ad\bar{d}})^* F_{a1e}^{d\bar{d}a} F_{abe}^{da\bar{d}} A_{\bar{d}e\bar{d}a} \tag{74}$$

For non-Abelian anyon models, the inversion P^{-1} for 2 or more dimensional idempotents actually means the sum of inverted simple idempotents. Unlike the matrix of central idempotent, the matrix of simple idempotents P_{simple} in most cases is square and invertible. Technically it means that the matrix P_{simple} is made of rows of all simple idempotents, which makes it block-diagonal with two (or more) rows in different blocks corresponding to the same anyon type. Next we invert the matrix of simple idempotents P_{simple}, so that the columns of P_{simple}^{-1} correspond to the inverses of simple idempotents. In the end we sum up the columns that correspond to the same anyon flux to get P^{-1}. Moreover the rows of P corresponding to anyon types that are supported on this multidimensional spaces have to be normalized (divided by their dimensionality).

A. Toric code, double semion, Fibonacci and Ising string net

For all the RG fixed point wave-functions of toric code, double semion, double Fibonacci and double Ising we ob-

tain correct topological S and T matrices within machine precision. All the results are listed below.

- Toric code

$$S_{\mathrm{TC}} = \frac{1}{2}\begin{pmatrix} 1 & 1 & 1 & 1 \\ 1 & 1 & -1 & -1 \\ 1 & -1 & 1 & -1 \\ 1 & -1 & -1 & 1 \end{pmatrix}, \qquad T_{\mathrm{TC}} = \begin{pmatrix} 1 & 0 & 0 & 0 \\ 0 & 1 & 0 & 0 \\ 0 & 0 & 1 & 0 \\ 0 & 0 & 0 & -1 \end{pmatrix}.$$

- double semion

$$S_{\mathrm{ds}} = \frac{1}{2}\begin{pmatrix} 1 & 1 \\ 1 & -1 \end{pmatrix}^{\otimes 2}, \qquad T_{\mathrm{ds}} = \begin{pmatrix} 1 & 0 \\ 0 & i \end{pmatrix} \otimes \begin{pmatrix} 1 & 0 \\ 0 & -i \end{pmatrix}.$$

- double Fibonacci, with $\varphi = \frac{1+\sqrt{2}}{2}$

$$S_{\mathrm{dFib}} = \frac{1}{\varphi+2}\begin{pmatrix} 1 & \varphi \\ \varphi & -1 \end{pmatrix}^{\otimes 2},$$

$$T_{\mathrm{dFib}} = \begin{pmatrix} 1 & 0 \\ 0 & \mathrm{e}^{\frac{4i\pi}{5}} \end{pmatrix} \otimes \begin{pmatrix} 1 & 0 \\ 0 & \mathrm{e}^{\frac{-4i\pi}{5}} \end{pmatrix}.$$

- double Ising

$$S_{\mathrm{dIs}} = \frac{1}{4}\begin{pmatrix} 1 & \sqrt{2} & 1 \\ \sqrt{2} & 0 & -\sqrt{2} \\ 1 & -\sqrt{2} & 1 \end{pmatrix}^{\otimes 2},$$

$$T_{\mathrm{dIs}} = \begin{pmatrix} 1 & 0 & 0 \\ 0 & \mathrm{e}^{\frac{i\pi}{8}} & 0 \\ 0 & 0 & -1 \end{pmatrix} \otimes \begin{pmatrix} 1 & 0 & 0 \\ 0 & \mathrm{e}^{\frac{-i\pi}{8}} & 0 \\ 0 & 0 & -1 \end{pmatrix}.$$

B. Kitaev model

With the F symbols whose errors are listed in table III we can recover topological S and T matrices. The same matrices were obtained in Ref.[49] by a different method. Interestingly, for $J = 0.44$ where the errors of the iMPO symmetries happen to be the most accurate, see table I, the topological matrices obtained here are one order of magnitude more accurate than those in Ref.[49].

J	ϵ_S	ϵ_T
0.40	$\mathcal{O}(10^{-3})$	$\mathcal{O}(10^{-3})$
0.42	$\mathcal{O}(10^{-4})$	$\mathcal{O}(10^{-3})$
0.44	$\mathcal{O}(10^{-4})$	$\mathcal{O}(10^{-4})$
0.46	$\mathcal{O}(10^{-3})$	$\mathcal{O}(10^{-3})$
0.48	$\mathcal{O}(10^{-3})$	$\mathcal{O}(10^{-2})$

TABLE V. Maximal errors of the elements of the topological S and T matrices in the Kitaev model (17). Here $J = J_x = J_y$ for a fixed $J_z = 1$.

C. Fibonacci string-net with local filtering

By direct application of the described procedure for perturbations $\beta = 0.01,\ 0.05$ we can recover topological modular matrices with satisfying precision as shown in the table VI. For higher β in order to obtain the S_{Fib} and T_{Fib} matrices we need to improve the quality of F^{abc}_{def} to satisfy the Pentagon equation 47 with better accuracy. Here we perform a simple Monte Carlo (MC), where we sweep over all non-zero elements of F tensor, apart from $F^{111}_{111}, F^{211}_{221}, F^{121}_{222}, F^{112}_{212}$, which are all equal 1 by construction. In a single MC move we change an element of F tensor $F'^{abc}_{def} = F^{abc}_{def} + \delta \cdot r_1$, where r_1 is a random complex number and $\delta = 0.01 \cdot \epsilon(F)$ is the MC step with $\epsilon(F)$ being the error of the Pentagon equation. We calculate the new error of the Pentagon equation $\epsilon(F')$ and accept it if $\epsilon(F') < \epsilon(F)$ or check if the ratio $\frac{\epsilon(F)}{\epsilon(F')}$ is smaller than another random real number r_2 and accept the move if this is fulfilled. We perform such sweeps over all aforementioned elements of F tensor, which enables to obtain an error low enough to calculate the topological S and T matrices. We list the new error of F symbols together with the errors for the topological S and T matrices in table VI. For $\beta = 0.15$, where the correlation length is $\xi = 2.32$, we can make a comparison with Ref.[52] and we see that the error of topological S matrix is of the same order while the error of topological T matrix is an order of magnitude bigger though the latter one is still negligible.

D. Twisted quantum double of $\mathbb{Z}_3$

For the twisted quantum double of $\mathbb{Z}_3$ we obtain the following T and S matrices:

$$\mathrm{diag}(T_{\mathbb{Z}_3}) = \left(1, 1, 1, \mathrm{e}^{\frac{4i\pi}{9}}, \mathrm{e}^{\frac{-8i\pi}{9}}, \mathrm{e}^{\frac{-2i\pi}{9}}, \mathrm{e}^{\frac{-2i\pi}{9}}, \mathrm{e}^{\frac{-8i\pi}{9}}, \mathrm{e}^{\frac{4i\pi}{9}}\right),$$

$$\frac{\arg(S_{\mathbb{Z}_3})}{2\pi} = \begin{pmatrix} 0 & 0 & 0 & 0 & 0 & 0 & 0 & 0 & 0 \\ 0 & 0 & 0 & -\frac{1}{3} & -\frac{1}{3} & -\frac{1}{3} & \frac{1}{3} & \frac{1}{3} & \frac{1}{3} \\ 0 & 0 & 0 & \frac{1}{3} & \frac{1}{3} & \frac{1}{3} & -\frac{1}{3} & -\frac{1}{3} & -\frac{1}{3} \\ 0 & -\frac{1}{3} & \frac{1}{3} & -\frac{4}{9} & \frac{2}{9} & -\frac{1}{9} & \frac{1}{9} & -\frac{2}{9} & \frac{4}{9} \\ 0 & -\frac{1}{3} & \frac{1}{3} & \frac{2}{9} & -\frac{1}{9} & -\frac{4}{9} & \frac{4}{9} & \frac{1}{9} & -\frac{2}{9} \\ 0 & -\frac{1}{3} & \frac{1}{3} & -\frac{1}{9} & -\frac{4}{9} & \frac{2}{9} & -\frac{2}{9} & \frac{4}{9} & \frac{1}{9} \\ 0 & \frac{1}{3} & -\frac{1}{3} & \frac{1}{9} & \frac{4}{9} & -\frac{2}{9} & \frac{2}{9} & -\frac{4}{9} & -\frac{1}{9} \\ 0 & \frac{1}{3} & -\frac{1}{3} & -\frac{2}{9} & \frac{1}{9} & \frac{4}{9} & -\frac{4}{9} & -\frac{1}{9} & \frac{2}{9} \\ 0 & \frac{1}{3} & -\frac{1}{3} & \frac{4}{9} & -\frac{2}{9} & \frac{1}{9} & -\frac{1}{9} & \frac{2}{9} & -\frac{4}{9} \end{pmatrix},$$

$$|(S_{\mathbb{Z}_3})_{ij}| = \frac{1}{3}.$$

β	ξ	χ	ϵ_S	ϵ_T	ϵ_F^{MC}
0.01	0.23	8	$\mathcal{O}(10^{-7})$	$\mathcal{O}(10^{-7})$	—
0.05	0.42	12	$\mathcal{O}(10^{-5})$	$\mathcal{O}(10^{-5})$	—
0.12	1.04	16	$\mathcal{O}(10^{-3})$	$\mathcal{O}(10^{-6})$	$\mathcal{O}(10^{-3})$
0.15	2.32	20	$\mathcal{O}(10^{-3})$	$\mathcal{O}(10^{-6})$	$\mathcal{O}(10^{-3})$

TABLE VI. The error of the final S and T matrices, ϵ_S and ϵ_T respectively, calculated as the Frobenius norm of the difference between the numerical and the exact ones for different perturbation strengths β. Here χ is the bond dimension of the boundary eigenvectors $v_i^{U,D}$ used for the calculations. The numerical S and T matrices for bigger perturbations $\beta = 0.12, 0.15$ can be obtained only after the error of the numerical F-symbols is reduced up to the value of ϵ_F^{MC} by simple Monte Carlo minimization of the error of Pentagon equation.

E. Quantum double of S_3

For both iPEPS representations we obtain the topological S and T matrices which agree with machine precision with the exact ones up to the simultaneous permutation of columns and rows.

$$\mathrm{diag}(T_{S_3}) = \left(1, \mathrm{e}^{\frac{-2i\cdot\pi}{3}}, 1, -1, \mathrm{e}^{\frac{2i\cdot\pi}{3}}, 1, 1, 1\right),$$

$$S_{S_3} = \frac{1}{6}\begin{pmatrix} 1 & 3 & 2 & 1 & 2 & 3 & 2 & 2 \\ 3 & 3 & 0 & -3 & 0 & -3 & 0 & 0 \\ 2 & 0 & 4 & 2 & -2 & 0 & -2 & -2 \\ 1 & -3 & 2 & 1 & 2 & -3 & 2 & 2 \\ 2 & 0 & -2 & 2 & -2 & 0 & -2 & 4 \\ 3 & -3 & 0 & -3 & 0 & 3 & 0 & 0 \\ 2 & 0 & -2 & 2 & -2 & 0 & 4 & -2 \\ 2 & 0 & -2 & 2 & 4 & 0 & -2 & -2 \end{pmatrix}.$$

The algorithm we present in Appendix B fails to decompose the two-dimensional central idempotent corresponding to the anyon flux $(1,\pi)$ into simple idempotents, which should be done as shown in[68]:

$$(1,\pi) = (1,\pi)_{00} + (1,\pi)_{11}$$

$$(1,\pi) = \frac{1}{3}\left(2\cdot A_{1111} - A_{1515} - A_{1616}\right) \quad (75)$$

$$(1,\pi)_{00} = \frac{1}{3}\left(A_{1111} + \mathrm{e}^{\frac{-2i\cdot\pi}{3}} A_{1515} + \mathrm{e}^{\frac{2i\cdot\pi}{3}} A_{1616}\right) \quad (76)$$

$$(1,\pi)_{11} = \frac{1}{3}\left(A_{1111} + \mathrm{e}^{\frac{2i\cdot\pi}{3}} A_{1515} + \mathrm{e}^{\frac{-2i\cdot\pi}{3}} A_{1616}\right) \quad (77)$$

However that is a necessary step to do in order to obtain correct modular S and T matrices shown above.

X. CONCLUSION AND OUTLOOK

The numerical method to obtain the F-symbols of the fusion category fully characterizing the topological order can be summarized in the following few steps:

1. Finding all boundary fixed points, both up and down, v_i^U, v_i^D of the double iPEPS horizontal transfer matrix Ω_h.

2. Calculating all iMPO symmetries Z_a mapping between different boundary fixed points: $v_i^U \cdot Z_a = v_j^u$ and $v_j^D \cdot Z_a^T = v_j^D$.

3. Finding the gauge transformations Y_{ia}^k between equal iMPOs $M = v_i \cdot Z_a$ and v_k for both up and down eigenvectors and combining them to yield zippers X_{ab}^c fusing the product of iMPO symmetries $v_1 Z_a \cdot Z_b$ into single iMPO symmetry $v_1 Z_c$.

4. Calculating the F-symbols using the associativity of the fusions of iMPO symmetries Z_a.

5. The numerical F-symbols in the random gauge can be brought into canonical gauge by proper inspection of the freedom in the normalization of X_{ab}^c zipppers. They can also be used to calculate gauge invariant topological data in the form of S and T matrices encoding mutual and self statistics of the emergent anyons of the doubled category.

After slight purification of the F-symbols, by minimizing the error of the pentagon equation, the method proved to give accurate results for states with correlation length up to $\xi = 2.3$. Their accuracy is comparable with those from Refs. 49 and 52. On the other hand, in the realistic case of the numerically optimized iPEPS representing the ground state of the Kitaev model, we were able to obtain topological S and T matrices with accuracy an order of magnitude better than with the previous method[49]. A possible explanation is that the present method consists of significantly less numerical steps, therefore it leaves less room for the accumulation of errors. Apart from the first step of finding the boundary fixed points, all the remaining steps are based on contractions of one-dimensional tensor networks. Finally, it provides not only topological S and T matrices but also F symbols that allow for an unambiguous identification of topological order.

As mentioned in the introduction, by studying the virtual iMPO symmetries rather than the physical Wilson line operators, we avoid the complications that arise due to the broadening of these Wilson lines away from the fixed point. Although we have shown that the method is applicable with nonzero correlation length, the correlation lengths for which the correct results are recovered are still rather small and it is clear there is still much room for improvement in several aspects of the algorithm.

Such improvements would allow us to study the change in topological order when driving a certain state through a phase transition. These phase transitions are characterized by the breaking and emergence of MPO symmetries, which should be reflected in the fixed point structure. This becomes particularly interesting when considering variationally optimized iPEPS, where a specific choice of PEPS representation and corresponding MPO symmetries is not imposed but rather chosen by the algorithm. Close to a phase transition, we expect the algorithm to prefer the PEPS representation that most nat-

urally allows the relevant MPO symmetries to be broken or emerge.

ACKNOWLEDGMENTS

Numerical calculations were performed in MATLAB with the help of `ncon` function[75] for tensor contractions. AF acknowledges financial support by Polish Ministry of Science and Education, project No. DI2015 021345, from the budget funds for science in 2016-2020 under the Diamond Grant program. This research was also supported by Narodowe Centrum Nauki (NCN) under grant 2019/35/B/ST3/01028 (AF, JD) and Etiuda grant 2020/36/T/ST3/00451 (AF). This work has received funding from the European Research Council (ERC) under the European Union's Horizon 2020 research and innovation programme (grant agreement No 647905 (QUTE)). LL is supported by a PhD fellowship from the Research Foundation Flanders (FWO).

* corresponding author: anna.francuz@uj.edu.pl

[1] X. G. Wen, "Topological Orders in Rigid States," Int. J. Mod. Phys. B **4**, 239–271 (1990).
[2] A. Kitaev, "Fault-tolerant quantum computation by anyons," Annals of Physics **303**, 2–30 (2003).
[3] A. Kitaev, "Anyons in an exactly solved model and beyond," Annals of Physics **321**, 2–111 (2006).
[4] M. A. Levin and X.-G. Wen, "String-net condensation: A physical mechanism for topological phases," Phys. Rev. B **71**, 045110 (2005).
[5] Y. Kasahara, T. Ohnishi, Y. Mizukami, O. Tanaka, Sixiao Ma, K. Sugii, N. Kurita, H. Tanaka, J. Nasu, Y. Motome, T. Shibauchi, and Y. Matsuda, "Majorana quantization and half-integer thermal quantum hall effect in a kitaev spin liquid," Nature **559**, 227–231 (2018).
[6] V. Leeb, K. Polyudov, S. Mashhadi, S. Biswas, Roser Valentí, M. Burghard, and J. Knolle, "Anomalous quantum oscillations in a heterostructure of graphene on a proximate quantum spin liquid," Phys. Rev. Lett. **126**, 097201 (2021).
[7] S. R. White, "Density matrix formulation for quantum renormalization groups," Phys. Rev. Lett. **69**, 2863 (1992).
[8] S. R. White, "Density-matrix algorithms for quantum renormalization groups," Phys. Rev. B **48**, 10345 (1993).
[9] S. Yan, D. A. Huse, and S. R. White, "Spin-Liquid Ground State of the $S = 1/2$ Kagome Heisenberg Antiferromagnet," Science **332**, 1173 (2011).
[10] H.-C. Jiang, Z. Wang, and L. Balents, "Identifying topological order by entanglement entropy," Nature Physics **8**, 902–905 (2012).
[11] S.-S. Gong, D. N. Sheng, O. I. Motrunich, and M. P. A. Fisher, "Phase diagram of the spin-1/2 $J_1 - J_2$ Heisenberg model on a honeycomb lattice," Phys. Rev. B **88**, 165138 (2013).
[12] Z. Zhu, D. A. Huse, and S. R. White, "Weak Plaquette Valence Bond Order in the $S = 1/2$ Honeycomb $J_1 - J_2$ Heisenberg Model," Phys. Rev. Lett. **110**, 127205 (2013).
[13] S.-S. Gong, W. Zhu, and D. N. Sheng, "Emergent Chiral Spin Liquid: Fractional Quantum Hall Effect in a Kagome Heisenberg Model," Scientific Reports **4**, 6317 (2014).
[14] Z. Zhu and S. R. White, "Quantum phases of the frustrated XY models on the honeycomb lattice," Modern Physics Letters B **28**, 1430016 (2014).
[15] S.-S. Gong, W. Zhu, L. Balents, and D. N. Sheng, "Global phase diagram of competing ordered and quantum spin-liquid phases on the kagome lattice," Phys. Rev. B **91**, 075112 (2015).
[16] W.-J. Hu, S.-S. Gong, W. Zhu, and D. N. Sheng, "Competing spin-liquid states in the spin-1/2 Heisenberg model on the triangular lattice," Phys. Rev. B **92**, 140403 (2015).
[17] W. Zhu, S. S. Gong, D. N. Sheng, and L. Sheng, "Possible non-Abelian Moore-Read state in double-layer bosonic fractional quantum Hall system," Phys. Rev. B **91**, 245126 (2015).
[18] Z. Zhu and S. R. White, "Spin liquid phase of the $S = 1/2$ $J_1 - J_2$ Heisenberg model on the triangular lattice," Phys. Rev. B **92**, 041105 (2015).
[19] M. P. Zaletel, Z. Zhu, Y.-M. Lu, A. Vishwanath, and S. R. White, "Space Group Symmetry Fractionalization in a Chiral Kagome Heisenberg Antiferromagnet," Phys. Rev. Lett. **116**, 197203 (2016).
[20] T.-S. Zeng, W. Zhu, J.-X. Zhu, and D. N. Sheng, "Nature of continuous phase transitions in interacting topological insulators," Phys. Rev. B **96**, 195118 (2017).
[21] M.-S. Vaezi and A. Vaezi, "Numerical Observation of Parafermion Zero Modes and their Stability in 2D Topological States," (2017), arXiv:1706.01192 [quant-ph].
[22] Z. Zhu, I. Kimchi, D. N. Sheng, and L. Fu, "Robust non-Abelian spin liquid and a possible intermediate phase in the antiferromagnetic Kitaev model with magnetic field," Phys. Rev. B **97**, 241110 (2018).
[23] Matthias Gohlke, Gideon Wachtel, Youhei Yamaji, Frank Pollmann, and Yong Baek Kim, "Quantum spin liquid signatures in kitaev-like frustrated magnets," Phys. Rev. B **97**, 075126 (2018).
[24] Matthias Gohlke, Roderich Moessner, and Frank Pollmann, "Dynamical and topological properties of the kitaev model in a [111] magnetic field," Phys. Rev. B **98**, 014418 (2018).
[25] L. Cincio and G. Vidal, "Characterizing Topological Order by Studying the Ground States on an Infinite Cylinder," Phys. Rev. Lett. **110**, 067208 (2013).
[26] Y.-C. He, D. N. Sheng, and Y. Chen, "Chiral Spin Liquid in a Frustrated Anisotropic Kagome Heisenberg Model," Phys. Rev. Lett. **112**, 137202 (2014).
[27] W. Zhu, S. S. Gong, F. D. M. Haldane, and D. N. Sheng, "Topological characterization of the non-Abelian Moore-Read state using density-matrix renormalization group," Phys. Rev. B **92**, 165106 (2015).
[28] W. Zhu, S. S. Gong, and D. N. Sheng, "Chiral and critical spin liquids in a spin-1/2 kagome antiferromagnet," Phys. Rev. B **92**, 014424 (2015).
[29] B. Bauer, L. Cincio, B. P. Keller, M. Dolfi, G. Vidal, S. Trebst, and A. W. W. Ludwig, "Chiral spin liquid and emergent anyons in a Kagome lattice Mott insulator," Nat.

Commun. **5**, 5137 (2014).
[30] W. Zhu, S. S. Gong, F. D. M. Haldane, and D. N. Sheng, "Fractional Quantum Hall States at $\nu = 13/5$ and 12/5 and Their Non-Abelian Nature," Phys. Rev. Lett. **115**, 126805 (2015).
[31] A. G. Grushin, J. Motruk, M. P. Zaletel, and F. Pollmann, "Characterization and stability of a fermionic $\nu = 1/3$ fractional Chern insulator," Phys. Rev. B **91**, 035136 (2015).
[32] Y.-C. He, S. Bhattacharjee, F. Pollmann, and R. Moessner, "Kagome chiral spin liquid as a gauged $U(1)$ symmetry protected topological phase," Phys. Rev. Lett. **115**, 267209 (2015).
[33] Y.-C. He and Y. Chen, "Distinct Spin Liquids and Their Transitions in Spin-1/2 XXZ Kagome Antiferromagnets," Phys. Rev. Lett. **114**, 037201 (2015).
[34] Y.-C. He, S. Bhattacharjee, R. Moessner, and F. Pollmann, "Bosonic integer quantum hall effect in an interacting lattice model," Phys. Rev. Lett. **115**, 116803 (2015).
[35] S. Geraedts, M. P. Zaletel, Z. Papić, and R. S. K. Mong, "Competing Abelian and non-Abelian topological orders in $\nu = 1/3+1/3$ quantum Hall bilayers," Phys. Rev. B **91**, 205139 (2015).
[36] R. S. K. Mong, M. P. Zaletel, F. Pollmann, and Z. Papić, "Fibonacci anyons and charge density order in the 12/5 and 13/5 quantum Hall plateaus," Phys. Rev. B **95**, 115136 (2017).
[37] Y.-C. He, F. Grusdt, A. Kaufman, M. Greiner, and A. Vishwanath, "Realizing and adiabatically preparing bosonic integer and fractional quantum Hall states in optical lattices," Phys. Rev. B **96**, 201103 (2017).
[38] E. M. Stoudenmire, D. J. Clarke, R. S. K. Mong, and J. Alicea, "Assembling Fibonacci Anyons From a Z_3 Parafermion Lattice Model," Phys. Rev. B **91**, 235112 (2015).
[39] Y.-C. He, M. P. Zaletel, M. Oshikawa, and F. Pollmann, "Signatures of Dirac cones in a DMRG study of the Kagome Heisenberg model," Phys. Rev. X **7**, 031020 (2017).
[40] S. N. Saadatmand and I. P. McCulloch, "Symmetry fractionalization in the topological phase of the spin-1/2 J_1-J_2 triangular Heisenberg model," Phys. Rev. B **94**, 121111 (2016).
[41] C. Hickey, L. Cincio, Z. Papić, and A. Paramekanti, "Haldane-Hubbard Mott Insulator: From Tetrahedral Spin Crystal to Chiral Spin Liquid," Phys. Rev. Lett. **116**, 137202 (2016).
[42] M. P. Zaletel, Y.-M. Lu, and A. Vishwanath, "Measuring space-group symmetry fractionalization in Z_2 spin liquids," Phys. Rev. B **96**, 195164 (2017).
[43] T.-S. Zeng, W. Zhu, and D. Sheng, "Tuning topological phase and quantum anomalous Hall effect by interaction in quadratic band touching systems," npj Quantum Materials **3**, 49 (2018).
[44] F. Verstraete and J. I. Cirac, "Renormalization algorithms for Quantum-Many Body Systems in two and higher dimensions," (2004), arXiv:cond-mat/0407066.
[45] V. Murg, F. Verstraete, and J. I. Cirac, "Variational study of hard-core bosons in a two-dimensional optical lattice using projected entangled pair states," Phys. Rev. A **75**, 033605 (2007).
[46] F. Verstraete, V. Murg, and J. I. Cirac, "Matrix product states, projected entangled pair states, and variational renormalization group methods for quantum spin systems," Advances in Physics **57**, 143–224 (2008).
[47] Hyun-Yong Lee, Ryui Kaneko, Tsuyoshi Okubo, and Naoki Kawashima, "Gapless kitaev spin liquid to classical string gas through tensor networks," Phys. Rev. Lett. **123**, 087203 (2019).
[48] P. Corboz, "Variational optimization with infinite projected entangled-pair states," Phys. Rev. B **94**, 035133 (2016).
[49] Anna Francuz, Jacek Dziarmaga, Guifre Vidal, and Lukasz Cincio, "Determining topological order from infinite projected entangled pair states," Phys. Rev. B **101**, 041108 (2020).
[50] Ji-Yao Chen, Laurens Vanderstraeten, Sylvain Capponi, and Didier Poilblanc, "Non-abelian chiral spin liquid in a quantum antiferromagnet revealed by an ipeps study," Phys. Rev. B **98**, 184409 (2018).
[51] Laurens Vanderstraeten, Jutho Haegeman, Philippe Corboz, and Frank Verstraete, "Gradient methods for variational optimization of projected entangled-pair states," Physical Review B **94**, 155123 (2016).
[52] Anna Francuz and Jacek Dziarmaga, "Determining non-abelian topological order from infinite projected entangled pair states," Phys. Rev. B **102**, 235112 (2020).
[53] Mehmet Burak Şahinoğlu, Dominic Williamson, Nick Bultinck, Michael Mariën, Jutho Haegeman, Norbert Schuch, and Frank Verstraete, "Characterizing Topological Order with Matrix Product Operators," Annales Henri Poincaré **22**, 563–592 (2021), arXiv: 1409.2150.
[54] N. Bultinck, M. Mariën, D. J. Williamson, M. B. Şahinoğlu, J. Haegeman, and F. Verstraete, "Anyons and matrix product operator algebras," Annals of Physics **378**, 183–233 (2017).
[55] M. Iqbal, K. Duivenvoorden, and N. Schuch, "Study of anyon condensation and topological phase transitions from a Z_4 topological phase using the projected entangled pair states approach," Phys. Rev. B **97**, 195124 (2018).
[56] C. Fernández-González, R. S. K. Mong, O. Landon-Cardinal, D. Pérez-García, and N. Schuch, "Constructing topological models by symmetrization: A projected entangled pair states study," Phys. Rev. B **94**, 155106 (2016).
[57] S. P. G. Crone and P. Corboz, "Detecting a Z_2 topologically ordered phase from unbiased infinite projected entangled-pair state simulations," Phys. Rev. B **101**, 115143 (2020).
[58] Mohsin Iqbal and Norbert Schuch, "Order parameters and critical exponents for topological phase transitions through tensor networks," (2020), arXiv:2011.06611 [cond-mat.str-el].
[59] H. He, H. Moradi, and X.-G. Wen, "Modular matrices as topological order parameter by a gauge-symmetry-preserved tensor renormalization approach," Phys. Rev. B **90**, 205114 (2014).
[60] J.I. Cirac, D. Pérez-García, N. Schuch, and F. Verstraete, "Matrix product density operators: Renormalization fixed points and boundary theories," Annals of Physics **378**, 100–149 (2017).
[61] Gemma De las Cuevas, J. Ignacio Cirac, Norbert Schuch, and David Perez-Garcia, "Irreducible forms of matrix product states: Theory and applications," Journal of Mathematical Physics **58**, 121901 (2017), https://doi.org/10.1063/1.5000784.
[62] Xie Chen, Zheng-Cheng Gu, and Xiao-Gang Wen, "Classification of gapped symmetric phases in one-dimensional spin systems," Phys. Rev. B **83**, 035107 (2011).

[63] Norbert Schuch, David Pérez-García, and Ignacio Cirac, "Classifying quantum phases using matrix product states and projected entangled pair states," Phys. Rev. B **84**, 165139 (2011).

[64] Laurens Lootens, Jürgen Fuchs, Jutho Haegeman, Christoph Schweigert, and Frank Verstraete, "Matrix product operator symmetries and intertwiners in string-nets with domain walls," SciPost Physics **10** (2021), 10.21468/scipostphys.10.3.053.

[65] Michaël Mignard and Peter Schauenburg, "Modular categories are not determined by their modular data," Letters in Mathematical Physics **111**, 1–9 (2021).

[66] Jacob C Bridgeman, Steven T Flammia, and David Poulin, "Detecting topological order with ribbon operators," Physical Review B **94**, 205123 (2016).

[67] Sergey Bravyi, Matthew B Hastings, and Spyridon Michalakis, "Topological quantum order: stability under local perturbations," Journal of mathematical physics **51**, 093512 (2010).

[68] Dominic J. Williamson, Nick Bultinck, and Frank Verstraete, "Symmetry-enriched topological order in tensor networks: Defects, gauging and anyon condensation," (2017), arXiv:1711.07982 [quant-ph].

[69] V. Zauner-Stauber, L. Vanderstraeten, M. T. Fishman, F. Verstraete, and J. Haegeman, "Variational optimization algorithms for uniform matrix product states," Phys. Rev. B **97**, 045145 (2018).

[70] M. T. Fishman, L. Vanderstraeten, V. Zauner-Stauber, J. Haegeman, and F. Verstraete, "Faster methods for contracting infinite two-dimensional tensor networks," Physical Review B **98** (2018), 10.1103/physrevb.98.235148.

[71] J. Haegeman, K. Van Acoleyen, N. Schuch, J. I. Cirac, and F. Verstraete, "Gauging quantum states: From global to local symmetries in many-body systems," Phys. Rev. X **5**, 011024 (2015).

[72] J. Haegeman, V. Zauner, N. Schuch, and F. Verstraete, "Shadows of anyons and the entanglement structure of topological phases," Nature Communications **6**, 8284 (2015).

[73] G.-Y. Zhu and G.-M. Zhang, "Gapless coulomb state emerging from a self-dual topological tensor-network state," Phys. Rev. Lett. **122**, 176401 (2019).

[74] Tian Lan and Xiao-Gang Wen, "Topological quasiparticles and the holographic bulk-edge relation in (2 + 1)-dimensional string-net models," Phys. Rev. B **90**, 115119 (2014).

[75] R. N. C. Pfeifer, G. Evenbly, S. Singh, and G. Vidal, "Ncon: A tensor network contractor for matlab," (2014), arXiv:1402.0939 [physics.comp-ph].

[76] Laurens Lootens, Marco Deweirdt, and Frank Verstraete, "Topological excitations in tensor networks (in preparation)," (2021).

Appendix A: iPEPS tensors

iPEPS tensors, shown in Fig. 5 are given by the following combination of F-symbols and quantum dimensions d_i:

$$A^i_{\alpha\beta\gamma} = \left(\frac{d_a d_b}{d_c}\right)^{1/4} F^{dab}_{fec}\delta_{aa'}\delta_{bb'}\delta_{cc'}\delta_{dd'}\delta_{ee'}\delta_{ff'} \quad \text{(A1)}$$

$$B^i_{\alpha\beta\gamma} = \left(\frac{d_a d_b}{d_c}\right)^{1/4} F^{dab}_{fec}\delta_{aa'}\delta_{bb'}\delta_{cc'}\delta_{dd'}\delta_{ee'}\delta_{ff'} \quad \text{(A2)}$$

By construction each tensor has a triple of bond indices along each of the three bonds towards NN lattice sites. We concatenate each triple into a single bond index, e.g., $\alpha = (a, e, d')$. The physical index is also a triple index $i = (a', b', c')$. These basic tensors are forming the topological state after proper contraction of bond indices with respect to their triplet structure. For the toric code and double Fibonacci string nets the bond dimension $D = 2^3 = 8$ is redundantly large and can be reduced to $D = 4$ and $D = 5$ after applying projectors on the bond indices, namely the only non-zero combinations of bond indices (i, j, k) are those, in which the fusion product $i \times j \times k = 1 + ...$ contains the trivial anyon. For the double Ising string net, on the other hand, the original bond dimension $D = 3^3 = 27$ can be reduced to $D = 10$.

Appendix B: Algorithm for central idempotents

In this appendix we present an algorithm for numerical calculation of central idempotents from fusion rules N^i_{jk} and F-symbols in a random gauge. When inserted into iPEPS, central idempotents can be thought of as projectors onto minimally entangled states. Central idempotents are build from elements A_{abcd}, which form an algebra $\mathcal{A}$ (more precisely it is a C* algebra). The algorithm can be divided into several points as follows.

1. In the first step we determine all non-zero elements of the algebra $\mathcal{A}$ generated by A_{abcd}:

$$A_{abcd} \propto N^b_{da} N^b_{cd}, \quad \text{(B1)}$$

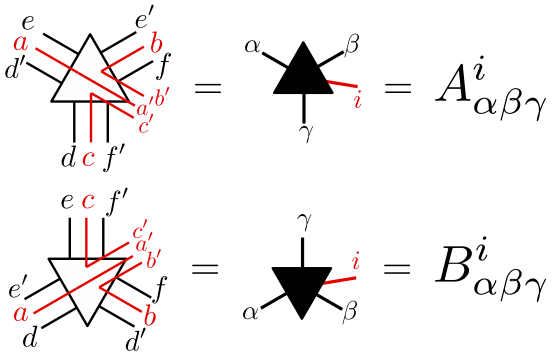

FIG. 5. Tensors forming the iPEPS are defined via combination of F-symbols and corresponding quantum dimensions d_i. All bond indices and the physical index are in fact a triple index. The bond dimension can be reduced by applying projectors on the non zero bond indices.

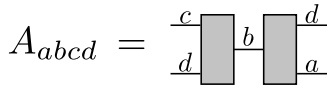

FIG. 6. The tensors A_{abcd} are proportional to $N^b_{da}N^b_{cd}$ and can be represented by the zippers connected by, but not summed over, the index b.

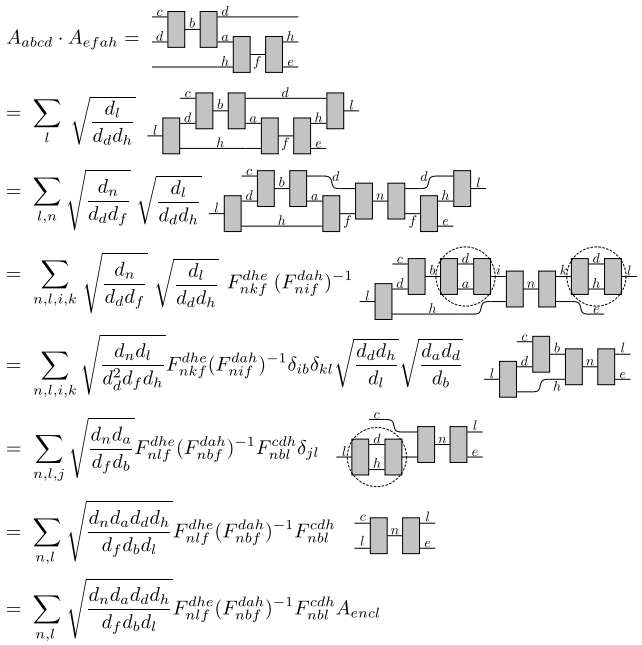

FIG. 7. Derivation of the algebra generated by the tensors A_{abcd} including proper normalization by the quantum dimensions.

as shown in Fig.6. Those non-zero elements are the basis vectors of the algebra $\mathcal{A}$, so we can make assigments $e_i = A_{abcd} \neq 0$ and find their multiplication table.

2. When treated as matrices in the a, c indices, the multiplication of A_{abcd} satisfies:

$$A_{abcd}A_{efah} = e_i e_j = \sum_k f^k_{ij}\ e_k = \sum_k f^k_{ij}\ A_{encl} \qquad \text{(B2)}$$

Using the tensor network diagrammatic expressions, as shown in Fig.7, we can derive the formula for the structure factors f^k_{ij}, which are given by the F-symbols:

$$f^k_{ij} = \sqrt{\frac{d_n d_a d_d d_h}{d_f d_b d_l}} F^{dhe}_{nlf}(F^{dah}_{nbf})^{-1}F^{cdh}_{nbl} \qquad \text{(B3)}$$

3. Now we find the center $\mathcal{Z}(\mathcal{A})$ of the algebra $\mathcal{A}$, i.e. we look for such elements $z = \sum_a\ z_a e_a$ that $\forall b:\ ze_b = e_b z$. We observe that this simplifies to an equation involving only the structure factors:

$$\sum_a z_a(e_a e_b - e_b e_a) = 0\ \Rightarrow\ \forall b, c:\ \sum_a\ (f^c_{ab} - f^c_{ba})z_a = 0. \qquad \text{(B4)}$$

Therefore the vector of coefficients of z in e_a basis belongs to the kernel of the matrix $\mathcal{F}$: $c(z) := (z_1, ..., z_n) \in \mathrm{Ker}(\mathcal{F})$, whose elements are $\mathcal{F}_{b\oplus c,a} = f^c_{ab} - f^c_{ba}$ with $b \oplus c$ index going through all the combinations of b, c indices.

4. From now on we work only with the commutative algebra $\mathcal{Z}(\mathcal{A})$, with elements $Z_k = \sum_a z^k_a e_a$, which are linear combinations of the original basis with coefficients from $c(z) \in \mathrm{Ker}(\mathcal{F})$. We construct its adjoint representation, which is given by the structure factors

$$[ad(Z_k)]_{ab} = \sum_c f^b_{ac} z^k_c \qquad \text{(B5)}$$

5. Due to commutation of the elements of the center $\mathcal{Z}(\mathcal{A})$, if we take random element from the center $Z \in \mathcal{Z}(\mathcal{A}):\ Z = \sum_k c_k ad(Z_k)$ and find the transformation bringing it into the diagonal form: $U^{-1}ZU$, we know that this transformation is diagonalizing all other elements from the center:

$$\forall k:\ U^{-1}ad(Z_k)U = D_k, \qquad \text{(B6)}$$

where D_k is diagonal.

6. We now have to find linear combinations of the matrices D_k to obtain idempotents. Defining d_k as the vectors containing the diagonal elements of D_k, finding idempotents boils down to finding orthogonal linear combinations of the vectors d_k that only contain 1's and 0's. To do this, we build a matrix D with d_k as its row vectors, and compute the row reduced echelon form of the augmented matrix

$$D' = [D\,|\,\mathbb{I}], \quad \mathrm{rref}(D') = [\mathrm{rref}(D)\,|\,M]. \qquad \text{(B7)}$$

7. The central idempotents are now obtained as

$$\mathcal{P}_i = \sum_j M_{ij}Z_j = \sum_{ja} M_{ij}z^j_a e_a. \qquad \text{(B8)}$$

These central idempotents can be further split into simple idempotents by grouping the different e_a according to the $a = c$ string of the associated tube algebra elements A_{abcd}. We note however that this does not always work, as exemplified by the case of Vec_{S_3} in the main text; an alternative general algorithm will be provided in Ref.[76].

Bibliography

[1] Anna Francuz et al. "Determining topological order from infinite projected entangled pair states". In: *Phys. Rev. B* 101 (4 Jan. 2020), p. 041108. DOI: 10.1103/PhysRevB.101.041108. URL: https://link.aps.org/doi/10.1103/PhysRevB.101.041108.

[2] Anna Francuz and Jacek Dziarmaga. "Determining non-Abelian topological order from infinite projected entangled pair states". In: *Phys. Rev. B* 102 (23 Dec. 2020), p. 235112. DOI: 10.1103/PhysRevB.102.235112. URL: https://link.aps.org/doi/10.1103/PhysRevB.102.235112.

[3] Anna Francuz et al. "Variational methods for characterizing matrix product operator symmetries". In: (2021). arXiv: 2107.05265 [cond-mat.str-el].

[4] L. D. Landau. "On the theory of phase transitions". In: *Zh. Eksp. Teor. Fiz.* 7 (1937), pp. 19–32.

[5] V. L. Ginzburg and L. D. Landau. "On the Theory of superconductivity". In: *Zh. Eksp. Teor. Fiz.* 20 (1950), pp. 1064–1082.

[6] D. C. Tsui, H. L. Stormer, and A. C. Gossard. "Two-Dimensional Magnetotransport in the Extreme Quantum Limit". In: *Phys. Rev. Lett.* 48 (22 May 1982), pp. 1559–1562. DOI: 10.1103/PhysRevLett.48.1559. URL: https://link.aps.org/doi/10.1103/PhysRevLett.48.1559.

[7] "The Nobel Prize in Physics 1998". In: *NobelPrize.org* (May 2021). URL: https://www.nobelprize.org/prizes/physics/1998/summary/.

[8] Y. Kasahara et al. "Majorana quantization and half-integer thermal quantum Hall effect in a Kitaev spin liquid". In: *Nature* 559.7713 (July 2018), pp. 227–231. ISSN: 1476-4687. DOI: 10.1038/s41586-018-0274-0. URL: https://doi.org/10.1038/s41586-018-0274-0.

[9] Lucile Savary and Leon Balents. "Quantum spin liquids: a review". In: *Reports on Progress in Physics* 80.1 (Nov. 2016), p. 016502. ISSN: 1361-6633. DOI: 10.1088/0034-4885/80/1/016502. URL: http://dx.doi.org/10.1088/0034-4885/80/1/016502.

[10] Alexei Kitaev. "Anyons in an exactly solved model and beyond". In: *Annals of Physics* 321.1 (2006). January Special Issue, pp. 2–111. ISSN: 0003-4916. DOI: https://doi.org/10.1016/j.aop.2005.10.005. URL: https://www.sciencedirect.com/science/article/pii/S0003491605002381.

[11] Xiao-Gang Wen. "Colloquium: Zoo of quantum-topological phases of matter". In: *Rev. Mod. Phys.* 89 (4 Dec. 2017), p. 041004. DOI: 10.1103/RevModPhys.89.041004. URL: https://link.aps.org/doi/10.1103/RevModPhys.89.041004.

[12] Xie Chen, Zheng-Cheng Gu, and Xiao-Gang Wen. "Local unitary transformation, long-range quantum entanglement, wave function renormalization, and topological order". In: *Phys. Rev. B* 82 (15 Oct. 2010), p. 155138. DOI: 10.1103/PhysRevB.82.155138. URL: https://link.aps.org/doi/10.1103/PhysRevB.82.155138.

[13] Umberto Borla et al. "Gauging the Kitaev chain". In: *SciPost Physics* 10.6 (June 2021). ISSN: 2542-4653. DOI: 10.21468/scipostphys.10.6.148. URL: http://dx.doi.org/10.21468/SciPostPhys.10.6.148.

[14] W. Pauli. "The Connection Between Spin and Statistics". In: *Phys. Rev.* 58 (8 Oct. 1940), pp. 716–722. DOI: 10.1103/PhysRev.58.716. URL: https://link.aps.org/doi/10.1103/PhysRev.58.716.

[15] M. V. Berry. "Quantal Phase Factors Accompanying Adiabatic Changes". In: *Proceedings of the Royal Society of London. Series A, Mathematical and Physical Sciences* 392.1802 (1984), pp. 45–57. ISSN: 00804630. DOI: https://doi.org/10.1098/rspa.1984.0023. URL: https://royalsocietypublishing.org/doi/10.1098/rspa.1984.0023.

[16] Xiao-Gang Wen. "A theory of 2+1D bosonic topological orders". In: *National Science Review* 3.1 (Nov. 2015), pp. 68–106. ISSN: 2053-714X. DOI: 10.1093/nsr/nwv077. URL: http://dx.doi.org/10.1093/nsr/nwv077.

[17] Erik Verlinde. "Fusion rules and modular transformations in 2D conformal field theory". In: *Nuclear Physics B* 300 (1988), pp. 360–376. ISSN: 0550-3213. DOI: https://doi.org/10.1016/0550-3213(88)90603-7. URL: https://www.sciencedirect.com/science/article/pii/0550321388906037.

[18] Xiao-Gang Wen. "Modular transformation and bosonic/fermionic topological orders in Abelian fractional quantum Hall states". In: (2012). arXiv: 1212.5121 [cond-mat.str-el].

[19] X. G. Wen. "Topological Order in Rigid States". In: *Int. J. Mod. Phys. B* 4 (1990), p. 239. DOI: 10.1142/S0217979290000139.

[20] Esko Keski-Vakkuri and Xiao-Gang Wen. "The ground state structure and modular transformations of fractional quantum Hall states on a torus". In: *International Journal of Modern Physics B* 07.25 (Nov. 1993), pp. 4227–4259. ISSN: 1793-6578. DOI: 10.1142/s0217979293003644. URL: http://dx.doi.org/10.1142/S0217979293003644.

[21] Michaël Mignard and Peter Schauenburg. "Modular categories are not determined by their modular data". In: (2017). arXiv: 1708.02796 [math.QA].

[22] Yi Zhang et al. "Quasiparticle statistics and braiding from ground-state entanglement". In: *Phys. Rev. B* 85 (23 June 2012), p. 235151. DOI: 10.1103/PhysRevB.85.235151. URL: https://link.aps.org/doi/10.1103/PhysRevB.85.235151.

[23] Alexei Kitaev and John Preskill. "Topological Entanglement Entropy". In: *Physical Review Letters* 96.11 (Mar. 2006). ISSN: 1079-7114. DOI: 10.1103/physrevlett.96.110404. URL: http://dx.doi.org/10.1103/PhysRevLett.96.110404.

[24] A.Yu. Kitaev. "Fault-tolerant quantum computation by anyons". In: *Annals of Physics* 303.1 (Jan. 2003), pp. 2–30. ISSN: 0003-4916. DOI: 10.1016/s0003-4916(02)00018-0. URL: http://dx.doi.org/10.1016/S0003-4916(02)00018-0.

[25] Michael A. Levin and Xiao-Gang Wen. "String-net condensation: A physical mechanism for topological phases". In: *Physical Review B* 71.4 (Jan. 2005). ISSN: 1550-235X. DOI: 10.1103/physrevb.71.045110. URL: http://dx.doi.org/10.1103/PhysRevB.71.045110.

[26] Parsa Hassan Bonderson. "Non-Abelian Anyons and Interferometry". In: (2007). DOI: 10.7907/5NDZ-W890. URL: https://resolver.caltech.edu/CaltechETD:etd-06042007-101617.

[27] Jacob C. Bridgeman, Steven T. Flammia, and David Poulin. "Detecting topological order with ribbon operators". In: *Physical Review B* 94.20 (Nov. 2016). ISSN: 2469-9969. DOI: 10.1103/physrevb.94.205123. URL: http://dx.doi.org/10.1103/PhysRevB.94.205123.

[28] Steven R. White. "Density matrix formulation for quantum renormalization groups". In: *Phys. Rev. Lett.* 69 (19 Nov. 1992), pp. 2863–2866. DOI: 10.1103/PhysRevLett.69.2863. URL: https://link.aps.org/doi/10.1103/PhysRevLett.69.2863.

[29] Steven R. White. "Density-matrix algorithms for quantum renormalization groups". In: *Phys. Rev. B* 48 (14 Oct. 1993), pp. 10345–10356. DOI: 10.1103/PhysRevB.48.10345. URL: https://link.aps.org/doi/10.1103/PhysRevB.48.10345.

[30] M. Fannes, B. Nachtergaele, and R. F. Werner. "Finitely correlated states on quantum spin chains". In: *Communications in Mathematical Physics* 144.3 (1992), pp. 443–490. DOI: cmp/1104249404. URL: https://doi.org/.

[31] A Klümper, A Schadschneider, and J Zittartz. "Matrix Product Ground States for One-Dimensional Spin-1 Quantum Antiferromagnets". In: *Europhysics Letters (EPL)* 24.4 (Nov. 1993), pp. 293–297. ISSN: 1286-4854. DOI: 10.1209/0295-5075/24/4/010. URL: http://dx.doi.org/10.1209/0295-5075/24/4/010.

[32] M. B. Hastings. "Solving gapped Hamiltonians locally". In: *Phys. Rev. B* 73 (8 Feb. 2006), p. 085115. DOI: 10.1103/PhysRevB.73.085115. URL: https://link.aps.org/doi/10.1103/PhysRevB.73.085115.

[33] M B Hastings. "An area law for one-dimensional quantum systems". In: *Journal of Statistical Mechanics: Theory and Experiment* 2007.08 (Aug. 2007), P08024–P08024. ISSN: 1742-5468. DOI: 10.1088/1742-5468/2007/08/p08024. URL: http://dx.doi.org/10.1088/1742-5468/2007/08/P08024.

[34] F. Verstraete and J. I. Cirac. "Matrix product states represent ground states faithfully". In: *Physical Review B* 73.9 (Mar. 2006). ISSN: 1550-235X. DOI: 10.1103/physrevb.73.094423. URL: http://dx.doi.org/10.1103/PhysRevB.73.094423.

[35] Stellan Östlund and Stefan Rommer. "Thermodynamic Limit of Density Matrix Renormalization". In: *Phys. Rev. Lett.* 75 (19 Nov. 1995), pp. 3537–3540. DOI: 10.1103/PhysRevLett.75.3537. URL: https://link.aps.org/doi/10.1103/PhysRevLett.75.3537.

[36] F. Verstraete and J. I. Cirac. "Renormalization algorithms for Quantum-Many Body Systems in two and higher dimensions". In: (July 2004). URL: arXiv:cond-mat/0407066.

[37] G. Vidal. "Entanglement Renormalization". In: *Phys. Rev. Lett.* 99 (22 Nov. 2007), p. 220405. DOI: 10.1103/PhysRevLett.99.220405. URL: https://link.aps.org/doi/10.1103/PhysRevLett.99.220405.

[38] Philippe Corboz et al. "Simulation of interacting fermions with entanglement renormalization". In: *Physical Review A* 81.1 (Jan. 2010). ISSN: 1094-1622. DOI: 10.1103/physreva.81.010303. URL: http://dx.doi.org/10.1103/PhysRevA.81.010303.

[39] Philippe Corboz and Guifré Vidal. "Fermionic multiscale entanglement renormalization ansatz". In: *Phys. Rev. B* 80 (16 Oct. 2009), p. 165129. DOI: 10.1103/PhysRevB.80.165129. URL: https://link.aps.org/doi/10.1103/PhysRevB.80.165129.

[40] Philippe Corboz et al. "Simulation of strongly correlated fermions in two spatial dimensions with fermionic projected entangled-pair states". In: *Physical Review B* 81.16 (Apr. 2010). ISSN: 1550-235X. DOI: 10.1103/physrevb.81.165104. URL: http://dx.doi.org/10.1103/PhysRevB.81.165104.

[41] Thomas Barthel, Carlos Pineda, and Jens Eisert. "Contraction of fermionic operator circuits and the simulation of strongly correlated fermions". In: *Phys. Rev. A* 80 (4 Oct. 2009), p. 042333. DOI: 10.1103/PhysRevA.80.042333. URL: https://link.aps.org/doi/10.1103/PhysRevA.80.042333.

[42] E. Y. Loh et al. "Sign problem in the numerical simulation of many-electron systems". In: *Phys. Rev. B* 41 (13 May 1990), pp. 9301–9307. DOI: 10.1103/PhysRevB.41.9301. URL: https://link.aps.org/doi/10.1103/PhysRevB.41.9301.

[43] Philippe Corboz. "Improved energy extrapolation with infinite projected entangled-pair states applied to the two-dimensional Hubbard model". In: *Physical Review B* 93.4 (Jan. 2016). ISSN: 2469-9969. DOI: 10.1103/physrevb.93.045116. URL: http://dx.doi.org/10.1103/PhysRevB.93.045116.

[44] Philippe Corboz et al. "Stripes in the two-dimensional $t - J$ model with infinite projected entangled-pair states". In: *Physical Review B* 84.4 (July 2011). ISSN: 1550-235X. DOI: 10.1103/physrevb.84.041108. URL: http://dx.doi.org/10.1103/PhysRevB.84.041108.

[45] Philippe Corboz, T. M. Rice, and Matthias Troyer. "Competing States in the $t - J$ Model: Uniformd-Wave State versus Stripe State". In: *Physical Review Letters* 113.4 (July 2014). ISSN: 1079-7114. DOI: 10.1103/physrevlett.113.046402. URL: http://dx.doi.org/10.1103/PhysRevLett.113.046402.

[46] Alexander Weiße and Holger Fehske. "Exact Diagonalization Techniques". In: *Computational Many-Particle Physics*. Ed. by H. Fehske, R. Schneider, and A. Weiße. Berlin, Heidelberg: Springer Berlin Heidelberg, 2008, pp. 529–544. ISBN: 978-3-540-74686-7. DOI: 10.1007/978-3-540-74686-7_18. URL: https://doi.org/10.1007/978-3-540-74686-7_18.

[47] J.I. Cirac et al. "Matrix product density operators: Renormalization fixed points and boundary theories". In: *Annals of Physics* 378 (2017), pp. 100–149. ISSN: 0003-4916. DOI: https://doi.org/10.1016/j.aop.2016.12.030. URL: https://www.sciencedirect.com/science/article/pii/S0003491616303013.

[48] Gemma De las Cuevas et al. "Irreducible forms of matrix product states: Theory and applications". In: *Journal of Mathematical Physics* 58.12 (2017), p. 121901. DOI: 10.1063/1.5000784. eprint: https://doi.org/10.1063/1.5000784. URL: https://doi.org/10.1063/1.5000784.

[49] F. Verstraete et al. "Criticality, the Area Law, and the Computational Power of Projected Entangled Pair States". In: *Physical Review Letters* 96.22 (June 2006). ISSN: 1079-7114. DOI: 10.1103/physrevlett.96.220601. URL: http://dx.doi.org/10.1103/PhysRevLett.96.220601.

[50] Román Orús. "Tensor networks for complex quantum systems". In: *Nature Reviews Physics* 1.9 (Aug. 2019), pp. 538–550. ISSN: 2522-5820. DOI: 10.1038/s42254-019-0086-7. URL: http://dx.doi.org/10.1038/s42254-019-0086-7.

[51] Ulrich Schollwöck. "The density-matrix renormalization group in the age of matrix product states". In: *Annals of Physics* 326.1 (Jan. 2011), pp. 96–192. ISSN: 0003-4916. DOI: 10.1016/j.aop.2010.09.012. URL: http://dx.doi.org/10.1016/j.aop.2010.09.012.

[52] E.M. Stoudenmire and Steven R. White. "Studying Two-Dimensional Systems with the Density Matrix Renormalization Group". In: *Annual Review of Condensed Matter Physics* 3.1 (Mar. 2012), pp. 111–128. ISSN: 1947-5462. DOI: 10.1146/annurev-conmatphys-020911-125018. URL: http://dx.doi.org/10.1146/annurev-conmatphys-020911-125018.

[53] R. J. Baxter. "Variational approximations for square lattice models in statistical mechanics". In: *Journal of Statistical Physics* 19.5 (Nov. 1978), pp. 461–478. ISSN: 1572-9613. DOI: 10.1007/BF01011693. URL: https://doi.org/10.1007/BF01011693.

[54] R. J. Baxter. In: *Exactly solved models in statistical mechanics* (1982).

[55] Tomotoshi Nishino and Kouichi Okunishi. "Corner Transfer Matrix Renormalization Group Method". In: 65.4 (Apr. 1996), pp. 891–894. DOI: 10.1143/jpsj.65.891. URL: https://doi.org/10.1143/jpsj.65.891.

[56] Román Orús and Guifré Vidal. "Simulation of two-dimensional quantum systems on an infinite lattice revisited: Corner transfer matrix for tensor contraction". In: *Physical Review B* 80.9 (Sept. 2009). ISSN: 1550-235X. DOI: 10.1103/physrevb.80.094403. URL: http://dx.doi.org/10.1103/PhysRevB.80.094403.

[57] Frank Verstraete and Juan Ignacio Cirac. "Renormalization algorithms for Quantum-Many Body Systems in two and higher dimensions". In: (2004). URL: arXiv:cond-mat/0407066.

[58] J. Jordan et al. "Classical Simulation of Infinite-Size Quantum Lattice Systems in Two Spatial Dimensions". In: *Phys. Rev. Lett.* 101 (25 Dec. 2008), p. 250602. DOI: 10.1103/PhysRevLett.101.250602. URL: https://link.aps.org/doi/10.1103/PhysRevLett.101.250602.

[59] Jutho Haegeman, Tobias J. Osborne, and Frank Verstraete. "Post-matrix product state methods: To tangent space and beyond". In: *Physical Review B* 88.7 (Aug. 2013). ISSN: 1550-235X. DOI: 10.1103/physrevb.88.075133. URL: http://dx.doi.org/10.1103/PhysRevB.88.075133.

[60] Jutho Haegeman et al. "Time-Dependent Variational Principle for Quantum Lattices". In: *Physical Review Letters* 107.7 (Aug. 2011). ISSN: 1079-7114. DOI: 10.1103/physrevlett.107.070601. URL: http://dx.doi.org/10.1103/PhysRevLett.107.070601.

[61] V. Zauner-Stauber et al. "Variational optimization algorithms for uniform matrix product states". In: *Phys. Rev. B* 97 (4 Jan. 2018), p. 045145. DOI: 10.1103/PhysRevB.97.045145. URL: https://link.aps.org/doi/10.1103/PhysRevB.97.045145.

[62] Laurens Vanderstraeten, Jutho Haegeman, and Frank Verstraete. "Tangent-space methods for uniform matrix product states". In: *SciPost Physics Lecture Notes* (Jan. 2019). ISSN: 2590-1990. DOI: 10.21468/scipostphyslectnotes.7. URL: http://dx.doi.org/10.21468/SciPostPhysLectNotes.7.

[63] F. Verstraete, V. Murg, and J.I. Cirac. "Matrix product states, projected entangled pair states, and variational renormalization group methods for quantum spin systems". In: *Advances in Physics* 57.2 (Mar. 2008), pp. 143–224. ISSN: 1460-6976. DOI: 10.1080/14789940801912366. URL: http://dx.doi.org/10.1080/14789940801912366.

[64] Philippe Corboz. "Variational optimization with infinite projected entangled-pair states". In: *Phys. Rev. B* 94 (3 July 2016), p. 035133. DOI: 10.1103/PhysRevB.94.035133. URL: https://link.aps.org/doi/10.1103/PhysRevB.94.035133.

[65] Laurens Vanderstraeten et al. "Gradient methods for variational optimization of projected entangled-pair states". In: *Physical Review B* 94.15 (Oct. 2016). ISSN: 2469-9969. DOI: 10.1103/physrevb.94.155123. URL: http://dx.doi.org/10.1103/PhysRevB.94.155123.

[66] H. C. Jiang, Z. Y. Weng, and T. Xiang. "Accurate Determination of Tensor Network State of Quantum Lattice Models in Two Dimensions". In: *Phys. Rev. Lett.* 101 (9 Aug. 2008), p. 090603. DOI: 10.1103/PhysRevLett.101.090603. URL: https://link.aps.org/doi/10.1103/PhysRevLett.101.090603.

[67] Ho N. Phien et al. "Infinite projected entangled pair states algorithm improved: Fast full update and gauge fixing". In: *Phys. Rev. B* 92 (3 July 2015), p. 035142. DOI: 10.1103/PhysRevB.92.035142. URL: https://link.aps.org/doi/10.1103/PhysRevB.92.035142.

[68] Jacek Dziarmaga. "Time evolution of an infinite projected entangled pair state: Neighborhood tensor update". In: *Phys. Rev. B* 104 (9 Sept. 2021), p. 094411. DOI: 10.1103/PhysRevB.104.094411. URL: https://link.aps.org/doi/10.1103/PhysRevB.104.094411.

[69] J. Eisert, M. Cramer, and M. B. Plenio. "Colloquium: Area laws for the entanglement entropy". In: *Reviews of Modern Physics* 82.1 (Feb. 2010), pp. 277–306. ISSN: 1539-0756. DOI: 10.1103/revmodphys.82.277. URL: http://dx.doi.org/10.1103/RevModPhys.82.277.

[70] Christoph Holzhey, Finn Larsen, and Frank Wilczek. "Geometric and renormalized entropy in conformal field theory". In: *Nuclear Physics B* 424.3 (Aug. 1994), pp. 443–467. ISSN: 0550-3213. DOI: 10.1016/0550-3213(94)90402-2. URL: http://dx.doi.org/10.1016/0550-3213(94)90402-2.

[71] M. B. Plenio et al. "Entropy, Entanglement, and Area: Analytical Results for Harmonic Lattice Systems". In: *Phys. Rev. Lett.* 94 (6 Feb. 2005), p. 060503. DOI: 10.1103/PhysRevLett.94.060503. URL: https://link.aps.org/doi/10.1103/PhysRevLett.94.060503.

[72] Dimitri Gioev and Israel Klich. "Entanglement Entropy of Fermions in Any Dimension and the Widom Conjecture". In: *Phys. Rev. Lett.* 96 (10 Mar. 2006), p. 100503. DOI: 10.1103/PhysRevLett.96.100503. URL: https://link.aps.org/doi/10.1103/PhysRevLett.96.100503.

[73] Michael M. Wolf. "Violation of the Entropic Area Law for Fermions". In: *Phys. Rev. Lett.* 96 (1 Jan. 2006), p. 010404. DOI: 10.1103/PhysRevLett.96.010404. URL: https://link.aps.org/doi/10.1103/PhysRevLett.96.010404.

[74] Michael M. Wolf et al. "Area Laws in Quantum Systems: Mutual Information and Correlations". In: *Physical Review Letters* 100.7 (Feb. 2008). ISSN: 1079-7114. DOI: 10.1103/physrevlett.100.070502. URL: http://dx.doi.org/10.1103/PhysRevLett.100.070502.

[75] Ignacio Cirac et al. "Matrix Product States and Projected Entangled Pair States: Concepts, Symmetries, and Theorems". In: (2011). arXiv: 2011.12127 [quant-ph].

[76] Ian Affleck et al. "Rigorous results on valence-bond ground states in antiferromagnets". In: *Phys. Rev. Lett.* 59 (7 Aug. 1987), pp. 799–802. DOI: 10.1103/PhysRevLett.59.799. URL: https://link.aps.org/doi/10.1103/PhysRevLett.59.799.

[77] M. Fannes, B. Nachtergaele, and R. F. Werner. "Finitely correlated states on quantum spin chains". In: 144.3 (Mar. 1992), pp. 443–490. DOI: 10.1007/bf02099178. URL: https://doi.org/10.1007/bf02099178.

[78] Guifré Vidal. "Efficient Classical Simulation of Slightly Entangled Quantum Computations". In: *Physical Review Letters* 91.14 (Oct. 2003). ISSN: 1079-7114. DOI: 10.1103/physrevlett.91.147902. URL: http://dx.doi.org/10.1103/PhysRevLett.91.147902.

[79] Hui Li and F. D. M. Haldane. "Entanglement Spectrum as a Generalization of Entanglement Entropy: Identification of Topological Order in Non-Abelian Fractional Quantum Hall Effect States". In: *Physical Review Letters* 101.1 (July 2008). ISSN: 1079-7114. DOI: 10.1103/physrevlett.101.010504. URL: http://dx.doi.org/10.1103/PhysRevLett.101.010504.

[80] J. Ignacio Cirac et al. "Entanglement spectrum and boundary theories with projected entangled-pair states". In: *Physical Review B* 83.24 (June 2011). ISSN: 1550-235X. DOI: 10.1103/physrevb.83.245134. URL: http://dx.doi.org/10.1103/PhysRevB.83.245134.

[81] Alfréd Rényi. "On measures of information and entropy". In: *In Proc. Symp. on Math., Stat. and Probability* (1961), pp. 547–561.

[82] Xie Chen et al. "Tensor product representation of a topological ordered phase: Necessary symmetry conditions". In: *Physical Review B* 82.16 (Oct. 2010). ISSN: 1550-235X. DOI: 10.1103/physrevb.82.165119. URL: http://dx.doi.org/10.1103/PhysRevB.82.165119.

[83] Sujeet K. Shukla et al. "Boson condensation and instability in the tensor network representation of string-net states". In: *Phys. Rev. B* 98 (12 Sept. 2018), p. 125112. DOI: 10.1103/PhysRevB.98.125112. URL: https://link.aps.org/doi/10.1103/PhysRevB.98.125112.

[84] Andras Molnar et al. "Normal projected entangled pair states generating the same state". In: *New Journal of Physics* 20.11 (Nov. 2018), p. 113017. ISSN: 1367-2630. DOI: 10.1088/1367-2630/aae9fa. URL: http://dx.doi.org/10.1088/1367-2630/aae9fa.

[85] G. Scarpa et al. "Projected Entangled Pair States: Fundamental Analytical and Numerical Limitations". In: *Physical Review Letters* 125.21 (Nov. 2020). ISSN: 1079-7114. DOI: 10.1103/physrevlett.125.210504. URL: http://dx.doi.org/10.1103/PhysRevLett.125.210504.

[86] N. Bultinck et al. "Anyons and matrix product operator algebras". In: *Annals of Physics* 378 (Mar. 2017), pp. 183–233. ISSN: 0003-4916. DOI: 10.1016/j.aop.2017.01.004. URL: http://dx.doi.org/10.1016/j.aop.2017.01.004.

[87] Mehmet Burak Şahinoğlu et al. "Characterizing Topological Order with Matrix Product Operators". In: *Annales Henri Poincaré* 22.2 (Jan. 2021), pp. 563–592. ISSN: 1424-0661. DOI: 10.1007/s00023-020-00992-4. URL: http://dx.doi.org/10.1007/s00023-020-00992-4.

[88] Dominic J. Williamson, Nick Bultinck, and Frank Verstraete. "Symmetry-enriched topological order in tensor networks: Defects, gauging and anyon condensation". In: (2017). arXiv: 1711.07982 [quant-ph].

[89] H. C. Jiang, Z. Y. Weng, and D. N. Sheng. "Density Matrix Renormalization Group Numerical Study of the Kagome Antiferromagnet". In: *Phys. Rev. Lett.* 101 (11 Sept. 2008), p. 117203. DOI: 10.1103/PhysRevLett.101.117203. URL: https://link.aps.org/doi/10.1103/PhysRevLett.101.117203.

[90] Simeng Yan, David A. Huse, and Steven R. White. "Spin-Liquid Ground State of the S = 1/2 Kagome Heisenberg Antiferromagnet". In: *Science* 332.6034 (2011), pp. 1173–1176. ISSN: 0036-8075. DOI: 10.1126/science.1201080. eprint: https://science.sciencemag.org/content/332/6034/1173.full.pdf. URL: https://science.sciencemag.org/content/332/6034/1173.

[91] P. W. Anderson. "The Resonating Valence Bond State in La2CuO4 and Superconductivity". In: *Science* 235.4793 (1987), pp. 1196–1198. ISSN: 0036-8075. DOI: 10.1126/science.235.4793.1196. URL: https://science.sciencemag.org/content/235/4793/1196.

[92] Stefan Depenbrock, Ian P. McCulloch, and Ulrich Schollwöck. "Nature of the Spin-Liquid Ground State of the $S = 1/2$ Heisenberg Model on the Kagome Lattice". In: *Phys. Rev. Lett.* 109 (6 Aug. 2012), p. 067201. DOI: 10.1103/PhysRevLett.109.067201. URL: https://link.aps.org/doi/10.1103/PhysRevLett.109.067201.

[93] Hong-Chen Jiang, Zhenghan Wang, and Leon Balents. "Identifying topological order by entanglement entropy". In: *Nature Physics* 8.12 (Nov. 2012), pp. 902–905. ISSN: 1745-2481. DOI: 10.1038/nphys2465. URL: http://dx.doi.org/10.1038/nphys2465.

[94] H. J. Liao et al. "Gapless Spin-Liquid Ground State in the $S = 1/2$ Kagome Antiferromagnet". In: *Physical Review Letters* 118.13 (Mar. 2017). ISSN: 1079-7114. DOI: 10.1103/physrevlett.118.137202. URL: http://dx.doi.org/10.1103/PhysRevLett.118.137202.

[95] Shou-Shu Gong, Wei Zhu, and D. N. Sheng. "Emergent Chiral Spin Liquid: Fractional Quantum Hall Effect in a Kagome Heisenberg Model". In: *Scientific Reports* 4.1 (Sept. 2014). DOI: 10.1038/srep06317. URL: https://doi.org/10.1038/srep06317.

[96] Shou-Shu Gong et al. "Global phase diagram of competing ordered and quantum spin-liquid phases on the kagome lattice". In: *Phys. Rev. B* 91 (7 Feb. 2015), p. 075112. DOI: 10.1103/PhysRevB.91.075112. URL: https://link.aps.org/doi/10.1103/PhysRevB.91.075112.

[97] Zhenyue Zhu, David A. Huse, and Steven R. White. "Weak Plaquette Valence Bond Order in the S=1/2 Honeycomb J_1-J_2 Heisenberg Model". In: *Phys. Rev. Lett.* 110 (12 Mar. 2013), p. 127205. DOI: 10.1103/PhysRevLett.110.127205. URL: https://link.aps.org/doi/10.1103/PhysRevLett.110.127205.

[98] Zhenyue Zhu and Steven R. White. "Quantum phases of the frustrated XY models on the honeycomb lattice". In: *Modern Physics Letters B* 28.31 (Dec. 2014), p. 1430016. ISSN: 1793-6640. DOI: 10.1142/s0217984914300166. URL: http://dx.doi.org/10.1142/S0217984914300166.

[99] L. Cincio and G. Vidal. "Characterizing Topological Order by Studying the Ground States on an Infinite Cylinder". In: *Phys. Rev. Lett.* 110 (6 Feb. 2013), p. 067208. DOI: 10.1103/PhysRevLett.110.067208. URL: https://link.aps.org/doi/10.1103/PhysRevLett.110.067208.

[100] Yin-Chen He, D. N. Sheng, and Yan Chen. "Obtaining topological degenerate ground states by the density matrix renormalization group". In: *Phys. Rev. B* 89 (7 Feb. 2014), p. 075110. DOI: 10.1103/PhysRevB.89.075110. URL: https://link.aps.org/doi/10.1103/PhysRevB.89.075110.

[101] Yin-Chen He and Yan Chen. "Distinct Spin Liquids and Their Transitions in Spin - 1/2 XXZ Kagome Antiferromagnets". In: *Physical Review Letters* 114.3 (Jan. 2015). ISSN: 1079-7114. DOI: 10.1103/physrevlett.114.037201. URL: http://dx.doi.org/10.1103/PhysRevLett.114.037201.

[102] W. Zhu et al. "Topological characterization of the non-Abelian Moore-Read state using density-matrix renormalization group". In: *Phys. Rev. B* 92 (16 Oct. 2015), p. 165106. DOI: 10.1103/PhysRevB.92.165106. URL: https://link.aps.org/doi/10.1103/PhysRevB.92.165106.

[103] Leon Balents. "Spin liquids in frustrated magnets". In: *Nature* 464.7286 (Mar. 2010), pp. 199–208. DOI: 10.1038/nature08917. URL: https://doi.org/10.1038/nature08917.

[104] Luke J. Sandilands et al. "Scattering Continuum and Possible Fractionalized Excitations in α-$RuCl_3$". In: *Physical Review Letters* 114.14 (Apr. 2015). ISSN: 1079-7114. DOI: 10.1103/physrevlett.114.147201. URL: http://dx.doi.org/10.1103/PhysRevLett.114.147201.

[105] A. Banerjee et al. "Proximate Kitaev quantum spin liquid behaviour in a honeycomb magnet". In: *Nature Materials* 15.7 (Apr. 2016), pp. 733–740. DOI: 10.1038/nmat4604. URL: https://doi.org/10.1038/nmat4604.

[106] Arnab Banerjee et al. "Neutron scattering in the proximate quantum spin liquid α-RuCl3". In: *Science* 356.6342 (June 2017), pp. 1055–1059. DOI: 10.1126/science.aah6015. URL: https://doi.org/10.1126/science.aah6015.

[107] Kejing Ran et al. "Spin-Wave Excitations Evidencing the Kitaev Interaction in Single Crystalline $\alpha-RuCl_3$". In: *Phys. Rev. Lett.* 118 (10 Mar. 2017), p. 107203. DOI: 10.1103/PhysRevLett.118.107203. URL: https://link.aps.org/doi/10.1103/PhysRevLett.118.107203.

[108] Matthias Gohlke et al. "Quantum spin liquid signatures in Kitaev-like frustrated magnets". In: *Physical Review B* 97.7 (Feb. 2018). ISSN: 2469-9969. DOI: 10.1103/physrevb.97.075126. URL: http://dx.doi.org/10.1103/PhysRevB.97.075126.

[109] Zheng Zhu et al. "Robust non-Abelian spin liquid and a possible intermediate phase in the antiferromagnetic Kitaev model with magnetic field". In: *Physical Review B* 97.24 (June 2018). ISSN: 2469-9969. DOI: 10.1103/physrevb.97.241110. URL: http://dx.doi.org/10.1103/PhysRevB.97.241110.

[110] Matthias Gohlke, Roderich Moessner, and Frank Pollmann. "Dynamical and topological properties of the Kitaev model in a [111] magnetic field". In: *Physical Review B* 98.1 (July 2018). ISSN: 2469-9969. DOI: 10.1103/physrevb.98.014418. URL: http://dx.doi.org/10.1103/PhysRevB.98.014418.

[111] S. P. G. Crone and P. Corboz. "Detecting a Z_2 topologically ordered phase from unbiased infinite projected entangled-pair state simulations". In: *Physical Review B* 101.11 (Mar. 2020). ISSN: 2469-9969. DOI: 10.1103/physrevb.101.115143. URL: http://dx.doi.org/10.1103/PhysRevB.101.115143.

[112] Mohsin Iqbal, Kasper Duivenvoorden, and Norbert Schuch. "Study of anyon condensation and topological phase transitions from a $\mathbb{Z}_4$ topological phase using the projected entangled pair states approach". In: *Phys. Rev. B* 97 (19 May 2018), p. 195124. DOI: 10.1103/PhysRevB.97.195124. URL: https://link.aps.org/doi/10.1103/PhysRevB.97.195124.

[113] Carlos Fernández-González et al. "Constructing topological models by symmetrization: A projected entangled pair states study". In: *Phys. Rev. B* 94 (15 Oct. 2016), p. 155106. DOI: 10.1103/PhysRevB.94.155106. URL: https://link.aps.org/doi/10.1103/PhysRevB.94.155106.

[114] Mohsin Iqbal, Didier Poilblanc, and Norbert Schuch. "Gapped Z_2 spin liquid in the breathing kagome Heisenberg antiferromagnet". In: *Physical Review B* 101.15 (Apr. 2020). ISSN: 2469-9969. DOI: 10.1103/physrevb.101.155141. URL: http://dx.doi.org/10.1103/PhysRevB.101.155141.

[115] J. Dubail and N. Read. "Tensor network trial states for chiral topological phases in two dimensions and a no-go theorem in any dimension". In: *Phys. Rev. B* 92 (20 Nov. 2015), p. 205307. DOI: 10.1103/PhysRevB.92.205307. URL: https://link.aps.org/doi/10.1103/PhysRevB.92.205307.

[116] Hyun-Yong Lee et al. "Gapless Kitaev Spin Liquid to Classical String Gas through Tensor Networks". In: *Physical Review Letters* 123.8 (Aug. 2019). ISSN: 1079-7114. DOI: 10.1103/physrevlett.123.087203. URL: http://dx.doi.org/10.1103/PhysRevLett.123.087203.

[117] Hyun-Yong Lee et al. "Abelian and non-Abelian chiral spin liquids in a compact tensor network representation". In: *Physical Review B* 101.3 (Jan. 2020). ISSN: 2469-9969. DOI: 10.1103/physrevb.101.035140. URL: http://dx.doi.org/10.1103/PhysRevB.101.035140.

[118] Sébastien Dusuel et al. "Perturbative study of the Kitaev model with spontaneous time-reversal symmetry breaking". In: *Physical Review B* 78.12 (Sept. 2008). ISSN: 1550-235X. DOI: 10.1103/physrevb.78.125102. URL: http://dx.doi.org/10.1103/PhysRevB.78.125102.

[119] Hyun-Yong Lee et al. "Magnetic field induced quantum phases in a tensor network study of Kitaev magnets". In: 11.1 (Apr. 2020). DOI: 10.1038/s41467-020-15320-x. URL: https://doi.org/10.1038/s41467-020-15320-x.